Phosphorus-Containing Ruthenacycles: Exploring Their Potential in Processes Relevant to Hydrophosphination

by

Krista Maria Elena Morrow
B.Sc., University of Victoria, 2010

A Thesis Submitted in Partial Fulfillment
of the Requirements for the Degree of

MASTER OF SCIENCE

in the Department of Chemistry

Supervisory Committee

Phosphorus-Containing Ruthenacycles:
Exploring Their Potential in Processes Relevant to Hydrophosphination

by

Krista Maria Elena Morrow
B.Sc., University of Victoria, 2010

Supervisory Committee

Dr. Lisa Rosenberg, Department of Chemistry
Supervisor

Dr. Cornelia Bohne, Department of Chemistry
Departmental Member

Abstract

Supervisory Committee
Dr. Lisa Rosenberg, Department of Chemistry
Supervisor
Dr. Cornelia Bohne, Department of Chemistry
Departmental Member

Phosphorus-containing metallacycles formed from the [2+2] cycloaddition of unsaturated substrates at the Ru-P π-bond of $[\mathrm{Ru}(\eta^5\text{-indenyl})(\mathrm{PCy_2})(\mathrm{PPh_3})]$ (**2**) were examined as possible intermediates relevant to hydrophosphination. Reagents, intermediates, products, and by-products involved in the [2+2] cycloaddition were identified and analyzed for reactivity and stability. The products, metallacycles of the form $[\mathrm{Ru}(\eta^5\text{-indenyl})(\kappa^2\text{-}\mathrm{R}\underline{\mathrm{C}}\mathrm{HCH_2}\underline{\mathrm{P}}\mathrm{Cy_2})(\mathrm{PPh_3})]$ (**4**), were found to undergo facile cycloreversion. An ethylene η^2-coordination adduct was directly observed by low temperature $^{31}\mathrm{P}\{^1\mathrm{H}\}$ NMR as an intermediate in the [2+2] cycloaddition mechanism. Steric and electronic effects of alkene substituents on metallacycle formation and selectivity were investigated in detail through rate constant and activation parameter determination, as well as collaborative computational DFT analyses and the construction of a Hammett plot. Preliminary attempts at releasing phosphinated products from ruthenacycle complexes via protonolysis and phosphine substitution were conducted. An unexpected metallacyclic product of one of these attempts, $[\mathrm{Ru}(\eta^5\text{-indenyl})(\kappa^2\text{-}\underline{\mathrm{C}}\mathrm{HCH}\underline{\mathrm{P}}\mathrm{Cy_2})(\mathrm{PPh_3})]$ (**10**), was identified and characterized.

Table of Contents

List of Tables

List of Figures

List of Schemes

List of Abbreviations

Å	Angstrom (1 x 10^{-10} m)
Anal.	analysis
atm	atmosphere
Ar	aryl
br	broad
Bu	butyl group, $-C_4H_9$
°C	degrees Celsius
C*	centroid of η^5-indenyl ring
cal	calorie(s)
Calcd	calculated
cat	catalyst
cm^{-1}	wavenumber
COSY	correlation spectroscopy
Cy	cyclohexyl group, $-C_6H_{11}$
d	doublet *or* day(s)
dd	doublet of doublets
ddd	doublet of doublet of doublets
dec	decomposes
deg (or °)	degrees
Δ	solid state indenyl slip parameter *or* heat
$\Delta\delta(C_{3a,7a})$	solution phase indenyl slip parameter
DEPT	distortionless enhanced polarization transfer
DFT	density functional theory
dm	doublet of multiplets
dt	doublet of triplets
δ	NMR chemical shift in parts per million
EI	electron ionisation
equiv	equivalents
E_s	Taft parameter for steric bulk
Et	ethyl group, $-C_2H_5$
η^n	hapticity
EXSY	exchange spectroscopy
FAB	fast atom bombardment
FPT	freeze-pump-thaw cycle(s)
g	grams
(g)	gas
h	hour(s)
$^1H\{^{31}P\}$	observed proton while decoupling phosphorus
HMBC	homonuclear multiple-bond connectivity
HR	high-resolution
HSQC	heteronuclear single quantum coherence
Hz	hertz

i	iso
IR	infrared
J	joule(s) *or* scalar nuclear spin-spin coupling constant (NMR)
κ^n	denticity
K	Kelvin
K	equilibrium constant
k	rate constant
kcal	kilocalorie(s)
L	litre *or* neutral donor ligand
(l)	liquid
M	molarity *or* metal
M^+	parent ion
m	multiplet (NMR) *or* medium (IR)
Me	methyl, $-CH_3$
mg	milligrams
MHz	megahertz
min	minute(s) *or* minimum
mL	millilitre(s)
mmol	millimole(s)
mM	millimolar
mol	mole(s)
mp	melting point (°C)
MS	mass spectrometry
mw	molecular weight
m/z	mass to charge ratio
μL	microlitre
nm	nanometer
NMR	nuclear magnetic resonance
NOE	nuclear Overhauser effect
NOESY	nuclear Overhauser effect spectroscopy
o	ortho *or* octet (NMR)
om	overlapping multiplets
$^{31}P\{^1H\}$	observed phosphorus while decoupling proton
p	para
Ph	phenyl group, $-C_6H_5$
ppm	parts per million
Pr	propyl group, $-C_3H_7$
py	pyridine
q	quartet
R	alkyl *or* aryl group
RI	relative integration
ROMP	ring-opening metathesis polymerization
RT	room temperature
s	singlet (NMR)
(s)	solid

sept	septet
T	temperature
t	triplet
t	tertiary
θ	Tolman cone angle
Tol	tolyl group, $-C_6H_4CH_3$
VT	variable temperature
w	weak
$\omega_{1/2}$	line width at half height
X	anionic donor ligand

List of Numbered Compounds

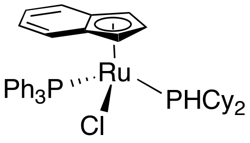

1a

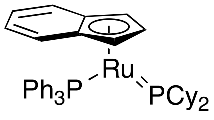

2

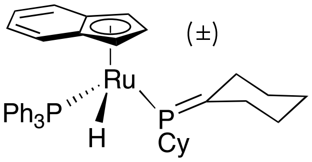

3

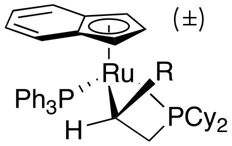

***syn*-4(a-e)**

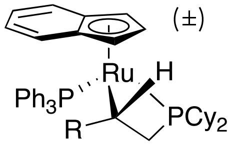

***anti*-4(a-e)**

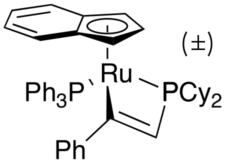

5

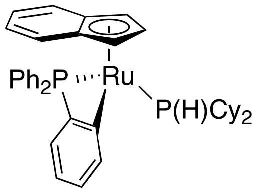

6

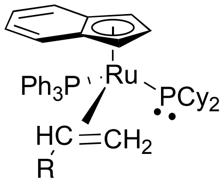

7a-e

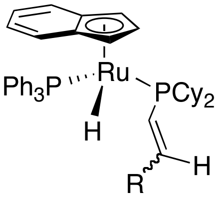

8a-e

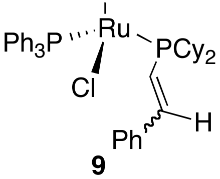

9

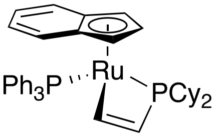

10

Acknowledgements

There are a great number of people to whom I owe my heartfelt thanks for their assistance. First among them is my supervisor, Dr. Lisa Rosenberg. I am extremely grateful for her steady guidance, unfailing enthusiasm, endless patience, and eagerness in sharing knowledge. I have also been fortunate enough to work with some wonderful people in the Rosenberg group who have helped me by participating in discussions, providing suggestions, and preparing starting materials, as well as other contributions that have made this project an enjoyable and memorable one: Marc-André Hoyle, Peter Lee, Michael Jarosz, Miranda Skjel, and Sophie-Langis Barsetti.

I am grateful for the assistance of Dr. Cornelia Bohne, for both helpful discussions and for the use of the Bohne lab UV-Vis spectrophotometer in performing kinetic studies. The training, assistance, and patience provided by Christine Greenwood and Chris Barr made the NMR spectroscopy presented in this thesis possible. Thanks to Dr. Dimitrios Pantazis at the Max Plank Institute for Bioinorganic Chemistry for performing all of the theroretical calculations, and to Dr. Bob McDonald at the University of Alberta for solving the crystal structures presented. Thank you also to everyone at Science Stores as well as the staff, office, and instructors of the Chemistry department for providing help when and wherever it was needed.

I am also very grateful to my family and friends, and most especially to my fiancé, Geoff, for all of their love, encouragement, and support.

Chapter 1 Overview

1.1 Chiral Phosphines: Applications and Approaches

Chiral phosphines have found widespread use as ligands in asymmetric metal-mediated catalysis[1,2]. Mono-[3,4] and bidentate[5] ligands of trivalent phosphorus are the most commonly used forms of these ancillary ligands. They convey chirality to the metal through either a P-stereogenic centre or an element of chirality in a carbon backbone[2,6,7] (Figure 1.1).

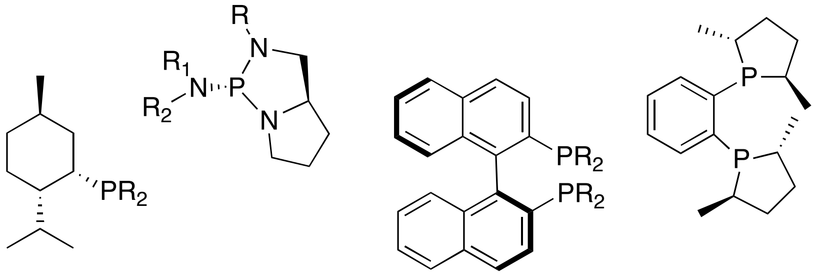

Figure 1.1. Mono- and bidentate chiral phosphines

While enantiomerically pure phosphines are of paramount importance to the catalytic production of other chiral compounds, efficient routes to chiral phosphines themselves are limited. Chiral resolution of racemic mixtures[8], modification of naturally-occurring chiral compounds[5], and asymmetric synthesis by use of stoichiometric chiral auxiliaries[9-11] are all effective, but are fairly inefficient preparatory methods that require expensive, stoichiometric chiral building blocks and multiple synthetic steps.

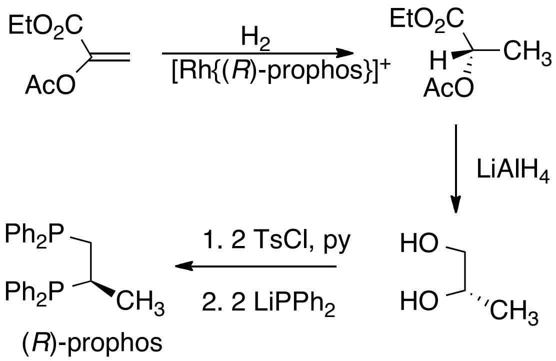

Scheme 1.1. The use of asymmetric catalytic hydrogenation to form chiral precursors in the synthesis of (R)-prophos.

Another method of synthesizing chiral phosphines is by the introduction of chirality through asymmetric catalysis. This method circumvents the requirement for stoichiomeric amounts of expensive chiral starting materials and auxiliaries. Asymmetric catalysis provides a cost-effective route to chiral compounds that can be subsequently converted to chiral phosphines[6,10], as demonstrated by the rhodium-catalyzed synthesis of (*R*)-prophos by Fryzuk and Bosnich[12] (Scheme 1.1). In this synthesis, a chiral metal complex, [Rh{(*R*)-prophos}]$^+$, is used to set the chirality of an organic compound in a catalytic asymmetric hydrogenation step. Further synthetic manipulation of this chiral organic compound then installs phosphine groups to form the final chiral phosphine product. This phosphine group installation, or P-C bond formation, is a crucial step when synthesizing organophosphines from P-H or P-Cl precursors[10]. Similarly, chirality can also be introduced after P-C bond formation, by the catalytic modification of organophosphorus compounds[6,10]. An example of this is the formation of chiral phosphine oxides by asymmetric ring-closing metathesis (ARCM)[10,13] (Scheme 1.2). In this patented process a vinyl phosphine oxide is desymmetrised by ARCM using a chiral version of Schrock's Mo catalyst for olefin metathesis.

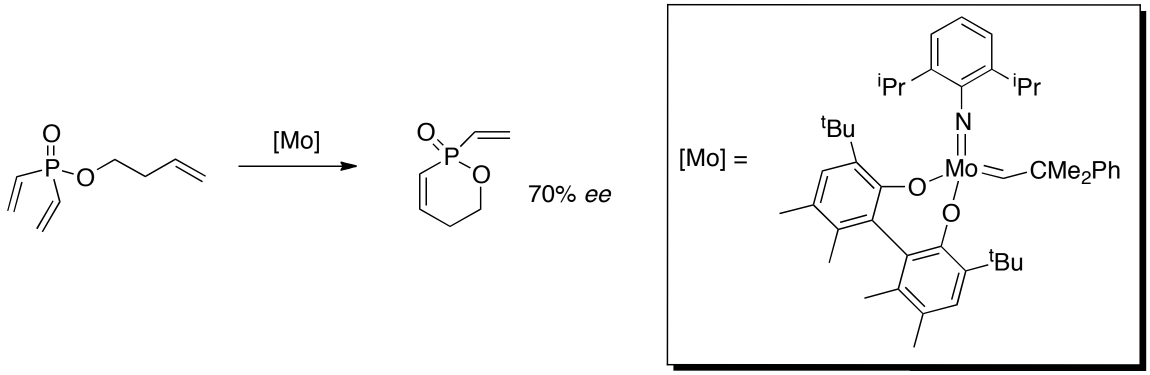

Scheme 1.2. Formation of a chiral phosphine oxide by ARCM.

These synthetic processes have been investigated in great detail[6,10], and offer vast improvements from the traditional, non-catalytic methods previously mentioned. However, introduction of chirality via asymmetric catalysis still requires multiple synthetic steps if it is accomplished either post- or pre- P-C bond formation. Recent advances in chiral phosphine synthesis have focused on asymmetric catalytic P-C bond formation[10,14-16], effectively both introducing chirality and forming the P-C bond in one synthetic step.

1.2 Asymmetric Metal-Catalyzed P-C Bond Formation

Asymmetric, metal-catalyzed P-C bond formation is currently being explored as an efficient, economical route to chiral phosphines[10,16]. The two main routes to P-C bond formation, shown in Figure 1.2, are “phosphination”, resulting from nucleophilic substitution by a phosphine (e.g. PR_2H) or phosphido (e.g. PR_2^-) at an sp^2 or sp^3 carbon with a good leaving group, and “hydrophosphination”, in which P-H bonds in primary and secondary phosphines add across unsaturated C-X bonds (alkenes, alkynes, carbonyls, isocyanides)[16]. In both cases phosphorus-containing substrates act as nucleophiles, either through their inherent nucleophilicity or by activation at a metal centre.

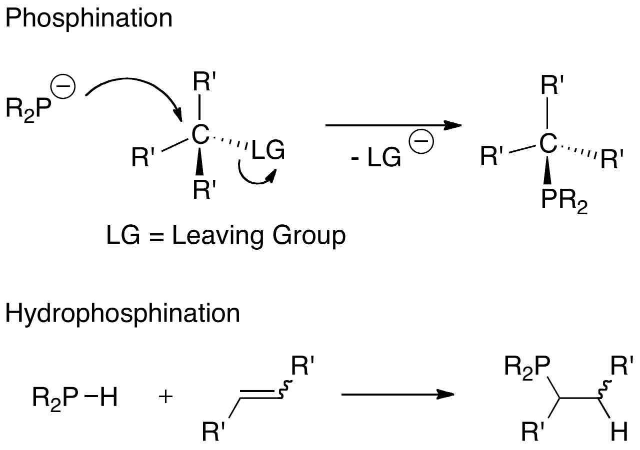

Figure 1.2. General overall reactions of phosphination and hydrophosphination.

1.2.1 Metal-Catalyzed Phosphination

Transition metal-catalyzed cross-coupling of aryl-[17-19] and alkyl-[20,21] halides or triflates with organophosphorus substrates is a relatively popular route to P-stereogenic phosphines[16,22]. These phosphination reactions are applicable to a wide range of organophosphorus substrates[16] including primary and secondary alkyl- or arylphosphines[21,23], phosphine-boranes[24], phosphine oxides[25], H-phosphonates[26], phosphonium salts[27], and silylphosphines[18].

The general mechanism for the Pd-, Pt- or Ni-catalyzed arylation of P-H containing substrates (Figure 1.3) involves initial oxidative addition of the arylhalide (or triflate) (**A** to **B**), phosphine coordination and Pd-P bond formation coupled with proton abstraction from the phosphine by a stoichiometric base (**B** to **C**), and subsequent reductive elimination to form the P-C bond (**C** to **A**)[16]. While commonly catalyzed by Pd, Pt or Ni, recent advances in copper-catalyzed cross-coupling have made it a potential, cost-effective alternative to more expensive catalysts[28-31]. The Cu-catalyzed coupling mechanism is not as well established as for Pd, but could potentially proceed through similar oxidative addition/reductive elimination steps, cycling between Cu(I) and Cu(III) species, as observed for analogous amination reactions[32].

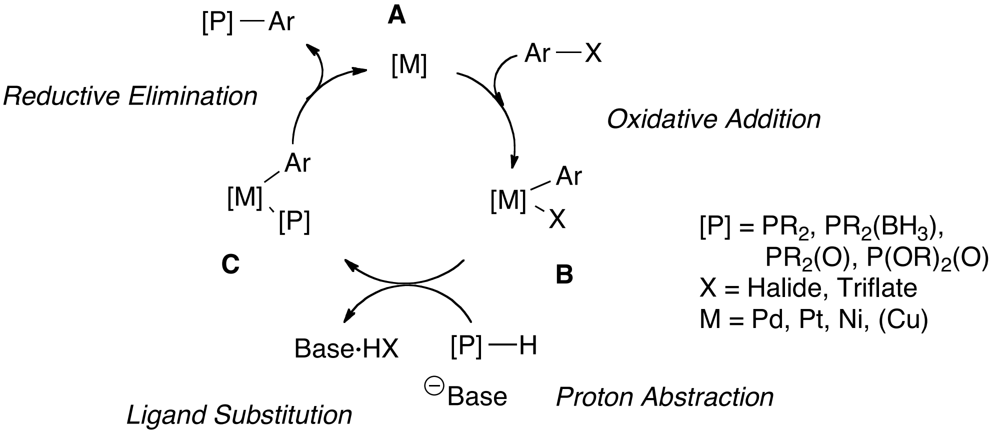

Figure 1.3. Proposed cross-coupling mechanism for metal-catalyzed arylation of P-H containing substrates.

The mechanism for Ru or Pt-catalyzed phosphination of alkyl halides[16], however, is slightly different than that shown in Figure 1.3. The activation of the organophosphorus species is similarly accomplished by either coordination of the phosphine to the metal centre and subsequent proton abstraction by base, or by coordination of the phosphido species after proton abstraction, substituting the coordinated halide or triflate. With either method, the resulting nucleophilic phosphido ligand attacks a free electrophile in an S_N2-type nucleophilic substitution mechanism, as opposed to P-C bond-forming reductive elimination between the coordinated electrophile and activated phosphido nucleophile of structure **C** in Figure 1.3[20,21].

In both the aryl- and alkylation cross-coupling reactions, complex **C** exists in an equilibrium between diastereomers if the terminal phosphido is unsymmetrically substituted[16]. The relative amounts and reactivities of these diastereomers are what determine the enantioselectivity of the overall phosphination reaction and the resulting product distributions, as illustrated by Glueck *et al.* in the asymmetric alkylation of PHMe(Is), catalyzed by the enantiomerically pure [Pt(*R*,*R*)-Me-DuPhos)(Ph)][19,33] (Figure 1.4).

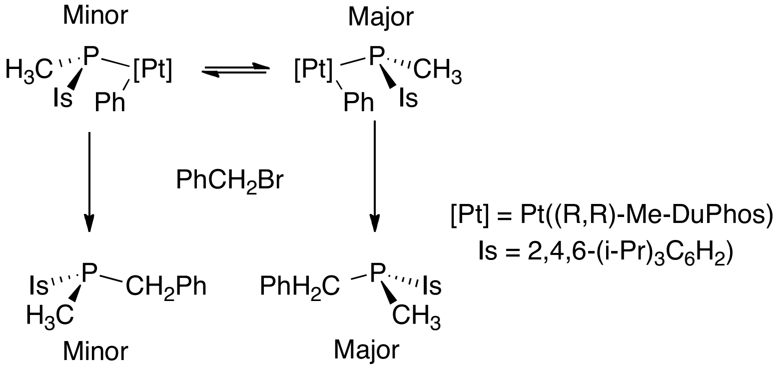

Figure 1.4. Diastereomer interconversion as the source of enantioselectivity in the Pt-catalyzed asymmetric phosphination of benzyl bromide with PHMe(Is).

1.2.2 Metal-Catalyzed Hydrophosphination

Though an effective route to the synthesis of chiral phosphines, phosphination requires the use of relatively costly, highly-functionalized starting materials and/or produces undesirable wastes in the form of inorganic salts [34] [35]. Hydrophosphination, the addition of a P-H group across an unsaturated carbon-carbon bond, is therefore an attractive alternative due to its overall atom-economy (no unwanted co-products formed) and the wide availability of unsaturated substrates. Hydrophosphination itself is a facile reaction, being readily accomplished though simple acidic[36], basic[37-41], radical[42-44] and thermal[34,35,45] activation. Despite these benefits, successful hydrophosphination routes to structurally complex phosphine ligands are not as abundant as their phosphination counterparts, due to difficulties in controlling regio- and stereoselectivity of the P-H addition in current non-catalytic processes[10,46-48]. The use of a metal-mediator to effect hydrophosphination not only offers catalytic activation, but a potentially tuneable and selective route to regio- and stereocontrol.

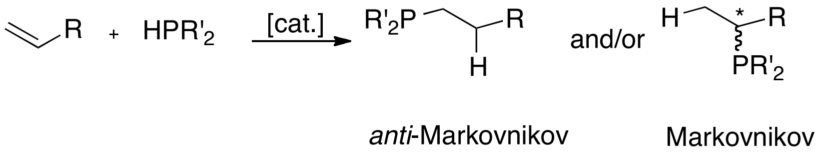

Scheme 1.3. Hydrophosphination of mono-substituted alkenes results in anti-Markovnikov or Markovnikov addition products with potential stereocentres at resulting tertiary carbons.

Current asymmetric, metal-catalyzed hydrophosphination processes occur by a wide variety of proposed mechanistic pathways. As described in the following sections, the formation of the P-C bond may occur by insertion of an unsaturated substrate into an M-P bond, P-C reductive elimination, direct nucleophilic attack of activated phosphorus on a C-electrophile, or via a [2+2] cycloaddition between an unsaturated substrate and an M-P double bond[16].

1.2.2.1 Insertion into an M-P Bond

Phosphorus-carbon bond formation via concerted alkene or alkyne insertion into an M-P bond has been observed for early metal and lanthanide catalysts[16,49] (Figure 1.5). The subsequent C-H bond formation is usually accomplished through σ-bond metathesis with the substrate phosphine P-H bond, which concurrently regenerates the M-PR_2 intermediate. This process is clearly demonstrated by the calcium-catalyzed hydrophosphination of alkenes and alkynes described by Procopiou *et al.*[50] (Figure 1.5).

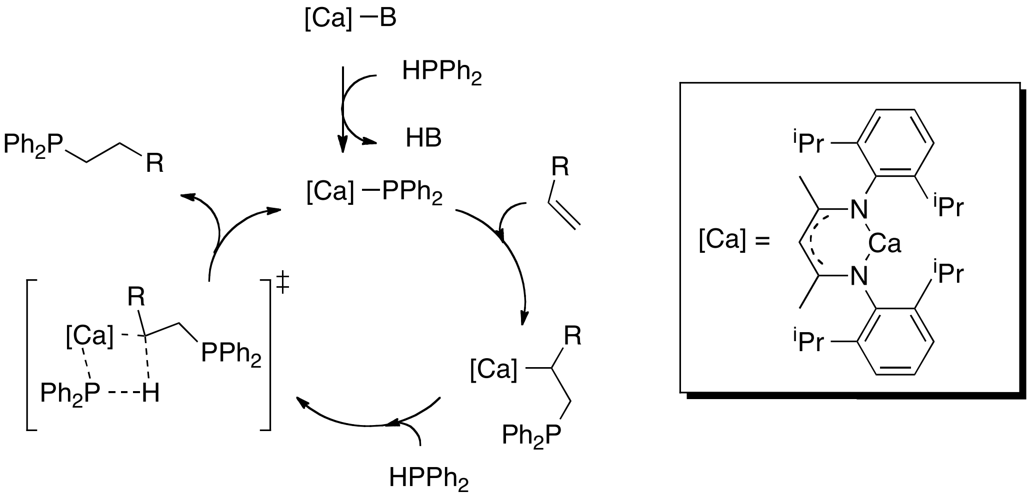

Figure 1.5. Proposed mechanism for calcium-catalyzed alkene hydrophosphination.

Intramolecular hydrophosphination, resulting in cyclic phosphine products, is observed for lanthanide catalysts when primary phosphine and terminal alkene functionalities are part of the same substrate[49,51] (Figure 1.6). As with calcium-catalyzed hydrophosphination, the precatalyst [Cp^*_2LnB] ($Cp^* = \eta^5$-Me_5C_5; Ln = La, Sm, Y, Lu; B = $CH(SiMe_3)_2$, $N(SiMe_3)_2$) is activated by coordination of the phosphine and proton abstraction by a base to form a phosphido-lanthanide complex. Both DFT and experimental studies suggest that the subsequent insertion of the alkene into the P-Ln bond is approximately thermoneutral. Protonolysis (i.e. cleavage of the Ln-C bond via protonation) with the primary alkyl phosphine via σ-bond metathesis then results in product formation and catalyst regeneration[49,51]. The addition is regioselective, invariably giving Markovnikov products, with P-C bond formation occurring at the substituted, β-carbon, instead of the terminal, α-carbon.

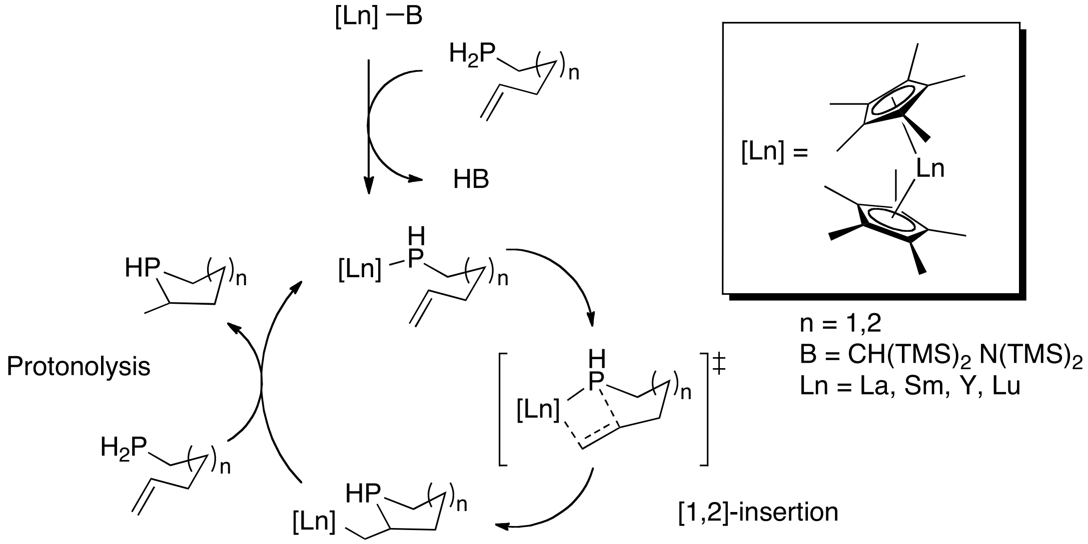

Figure 1.6. Proposed mechanism for lanthanide-catalyzed intramolecular hydrophosphination.

1.2.2.2 P-C Reductive Elimination

Another route to P-H addition across unsaturated substrates is catalyzed by late transition metals (Pd, Pt, Rh, Cu) and involves the reductive elimination of P-C bonds[16]. The rhodium-catalyzed hydrophosphinylation of alkynes (similar to hydrophosphination, but with the addition of a phosphine oxide) is illustrative of this mechanism[52] (Figure 1.7). The precatalyst, $[Rh(cod)Cl]_2$ (cod = 1,5-cyclooctadiene) is activated by coordination and oxidative addition of the P-H substrate. Alkyne insertion into the Rh-H bond results in an activated alkene that reductively eliminates with the coordinated P-ligand to yield the alkylated, *anti*-Markovnikov product. Subsequent oxidative addition of another equivalent of the P-H substrate regenerates the catalyst[52].

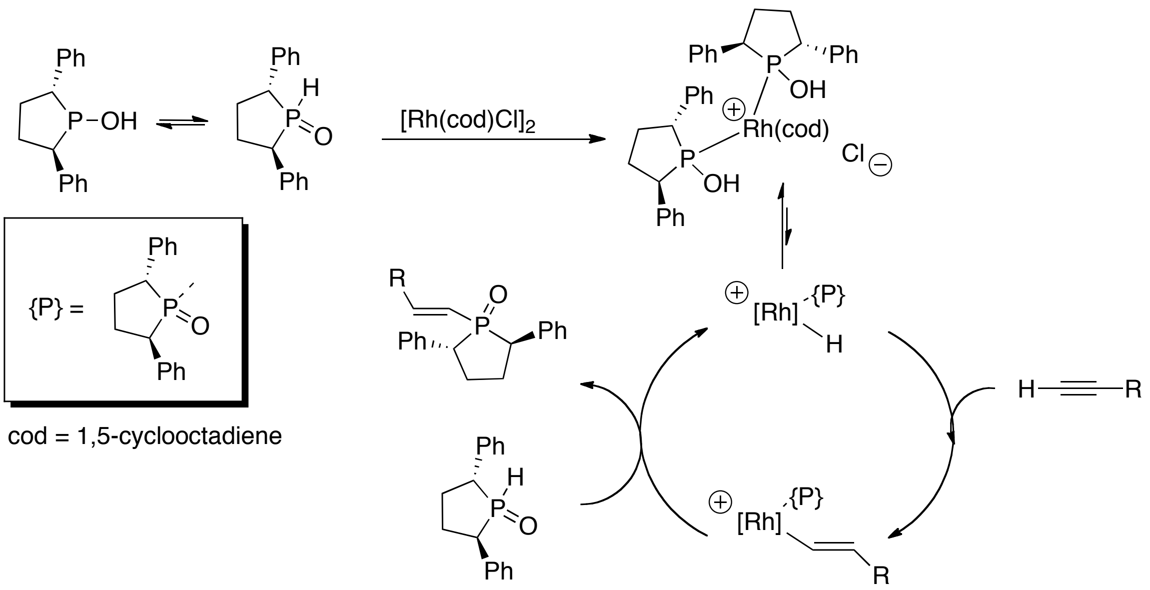

Figure 1.7. Proposed mechanism for Rh-catalyzed alkyne hydrophosphinylation.

Although this reductive elimination mechanism has been observed for hydrophosphination reactions of phosphino-boranes[53] and diphosphines[54], it is more commonly used to effect the addition of phosphine oxides[52,55-58], which must be subsequently reduced to trivalent phosphines for use as ligands.

1.2.2.3 Direct P-Nucleophilic Attack

In addition to promoting classical organometallic processes such as migratory insertion and reductive elimination, metal centres have been used to either activate alkenes as electrophiles for nucleophilic attack by free phosphines, or conversely to activate phosphine substrates to promote direct attack on alkenes[59]. These latter types of nucleophilic addition reactions are applicable mainly to activated, or Michael acceptor-type alkenes[10,16,59].

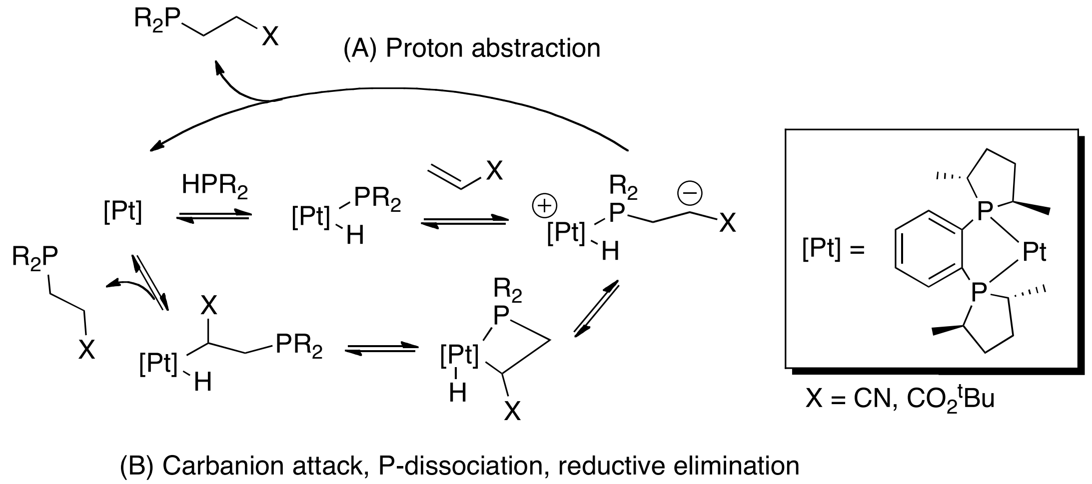

Figure 1.8. Proposed stepwise mechanism for the Pt-catalyzed hydrophosphination of activated alkenes.

For example, the platinum-catalyzed hydrophosphination of acrylonitrile described by Glueck *et al.* begins with an oxidative addition of a secondary phosphine to form a nucleophilic phosphido complex[33,60] (Figure 1.8). A zwitterionic intermediate is produced by nucleophilic attack of the phosphido on the activated alkene. Subsequent protonation of the zwitterion and catalyst regeneration is postulated to occur by two possible pathways: A) proton abstraction by the carbanion from the platinum hydride or B) carbanion attack at Pt, Pt-P dissociation, and reductive elimination of the alkyl hydride. Detailed mechanistic studies, including zwitterion trapping experiments, support this stepwise mechanism[33,60].

1.2.2.4 [2+2] Cycloaddition to an M-P Double Bond

Previous sections have described catalytic hydrophosphination reactions effected by M-P single bonds. The reactivity of M-P double bonds towards hydrophosphination is a promising, though largely unexplored area[16]. Currently, there exists only one example of a successful hydrophosphination reaction using an M-P double bond complex as an intermediate[61]. The titanium-catalyzed hydrophosphination of diphenylacetylene proceeds through a highly reactive phosphinidene complex, formed from a primary phosphine (Figure 1.9). The alkyne, diphenylacetylene, undergoes [2+2] cycloaddition with the phosphinidene to yield a 4-membered, phosphorus-containing metallacycle intermediate. Subsequent protonolysis of the metallacyle with phenylphosphine, followed by abstraction of the coordinated phenylphosphido α-proton, yields the vinyl phosphine product and regenerates the catalyst[61].

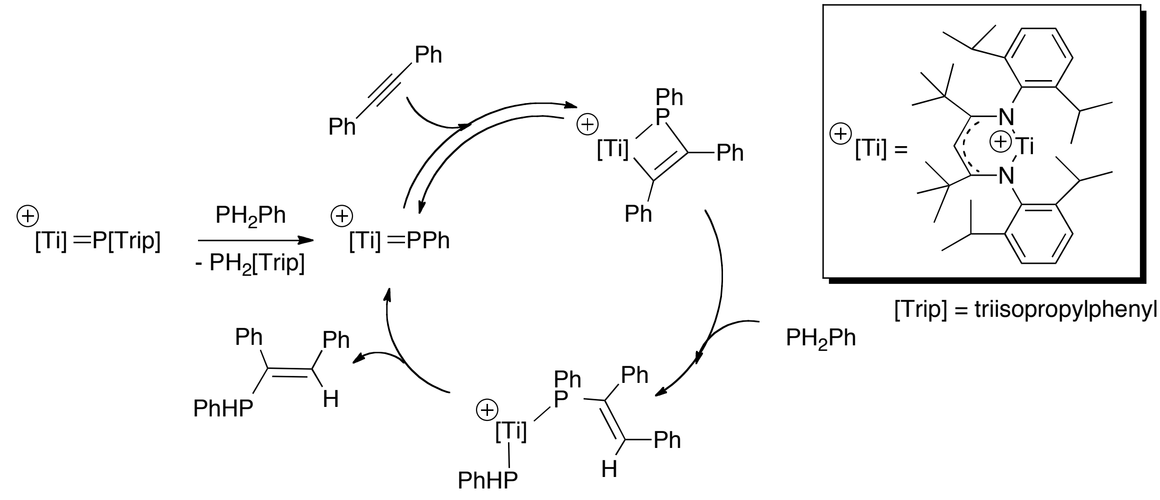

Figure 1.9. Titanium-catalyzed hydrophosphination of diphenylacetylene via [2+2] cycloaddition with a phosphinidene intermediate.

1.2.2.5 Summary of Proposed Hydrophosphination Mechanisms

An overall theme observed in the hydrophosphination of unsaturated C-C bonds is the differing reactivity of late- and early-metal catalyst systems. Early transition-metal and lanthanide systems usually effect hydrophosphination of simple, non-activated substrates via concerted pathways such as σ-bond metathesis[50] and [2+2] cycloaddition[61]. Late transition-metal systems are mostly observed to catalyze hydrophosphination by more step-wise processes[19,59], typically involving a phosphine nucleophile and an alkene or alkyne that is rendered electrophilic, either by an electron-withdrawing substituent or by coordination to a metal centre.

1.3 Research Goals and Rationale

As mentioned previously, only one example of metal-mediated hydrophosphination exists that includes a metal-phosphorus multiple bond as a catalytic intermediate[61]. Further investigation into this area of catalytic hydrophosphination is necessary to exploit the high reactivity of these metal phosphinidene (M=PR) and phosphido (M=PR_2) complexes and to introduce regio- and stereoselectivity in the process.

1.3.1 Highly Reactive Ru=P Complexes as Possible Intermediates in Metal-Mediated P-C Bond Formation

Recent work by the Rosenberg group has led to the characterization of a highly reactive ruthenium-phosphido species containing a ruthenium-phosphorus π-bond[62] (Scheme 1.4). The deprotonation of the coordinated secondary phosphine complex **1a** by potassium *tert*-butoxide and subsequent loss of the chloride ligand in salt form (KCl) yields the five-coordinate species **2**, which exhibits double bond character between ruthenium and phosphorus. Small amounts of the phosphaalkene isomer **3** are also observed in solution in equilibrium with **2**.

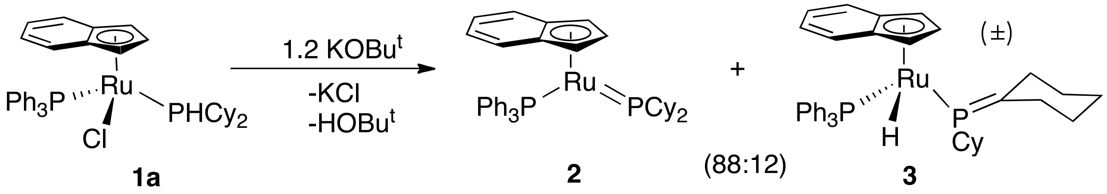

Scheme 1.4. Preparation of a coordinatively-unsaturated ruthenium-phosphido complex containing a ruthenium-phosphorus π-bond. Chirality at Ru gives rise to diastereomers of complex **3**.

Unlike the hydrophosphination catalysts described previously, complex **2** consists of a late metal, Ru, that reacts with *both* simple and activated alkenes and alkynes. Complex **2** undergoes [2+2] cycloaddition with unsaturated substrates to form 4-membered metallacycle species containing phosphorus (Scheme 1.5) [63,64], such as the unsubstituted ethylene adduct, [Ru(η^5-indenyl)(κ^2-$\underline{C}H_2CH_2\underline{P}Cy_2$)($PPh_3$)] (**4a**). Cycloaddition was found to be 100% regioselective for substituted alkenes (R = CN, **4b**; ^{n}Bu, **4c**; OEt, **4d**) and alkynes (R = Ph, **5**), occurring exclusively to yield metallacyclic products with α-carbon substitution.

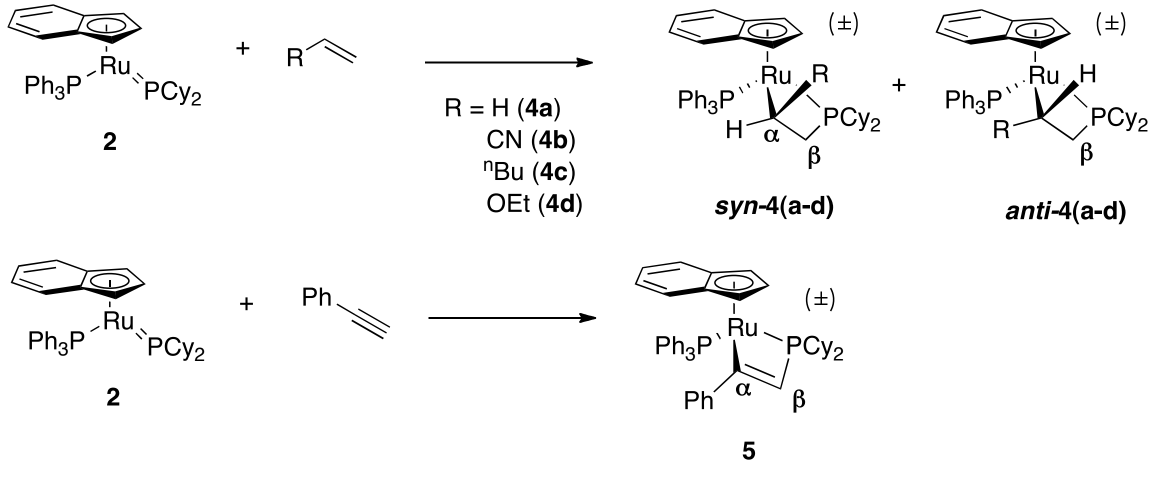

Scheme 1.5. [2+2] cycloaddition of substituted alkenes and alkynes with complex 2.

Reactions with substituted alkenes (R = CN, ^{n}Bu, OEt) resulted in various mixtures of diastereomeric products, ***syn***- and ***anti*-4(b-d)**. Substituent orientation on the α-carbon of the resulting four-membered ring distinguishes these isomers. Isomers are described as having either *syn*- (directed toward) or *anti*- (directed away) substituent orientation with respect to the coordinated indenyl ligand. The activated alkene acrylonitrile adds to complex **2** with complete *syn*-selectivity, with no observable traces of the *anti* isomer in solution. Simple, non-activated alkenes 1-hexene and ethyl vinyl ether were found to give 95:5 and 50:50 *syn*:*anti* isomer distribution ratios, respectively[64].

The P-C bond formation effected by this [2+2] cycloaddition between complex **2** and various alkenes and alkynes is analogous to the first step of the titanium-catalyzed hydrophosphination of diphenylacetylene mentioned previously[61] in section **1.2.2.4**. Further exploration of this analogy is necessary to determine if both the five-coordinate ruthenium complex **2** and the four-membered metallacycle products have potential as intermediates in a catalytic mechanism for the hydrophosphination of alkenes and alkynes. The previously-established regio- and stereoselectivity of the [2+2] cycloaddition, as well as the broad scope of reactivity that complex **2** exhibits toward alkene substitution (reacting with both electron rich and electron deficient alkenes), makes these complexes ideal candidates for further investigation towards incorporation into a hydrophosphination mechanism.

1.4 [2+2] Cycloaddition Metallacycle Products as Catalytic Intermediates

The role of four-membered metallacycles formed by [2+2] cycloaddition as catalytic intermediates is not unknown in metal-mediated transformations. In addition to the titanium-catalyzed P-C bond formation described previously, [2+2] cycloadditions featuring four-membered metallacycles are observed in catalytic cycles resulting in the formation of C-C and other C-heteroatom bonds.

1.4.1 [2+2] Cycloaddition In C-C Bond Formation

Olefin metathesis is perhaps one of the most exploited metal-catalyzed reactions that proceeds via a [2+2] cycloaddition mechanism involving four-membered metallacycles as key intermediates[65,66]. In both ring closing metathesis (RCM) and ring opening metathesis polymerization (ROMP), metallacylobutane intermediates are formed by the [2+2] cycloaddition of alkenes or alkynes to a metal-carbon double bond, commonly described as a metal centre with a carbene ligand. Cycloreversion may occur to regenerate the starting olefins, or proceed via a different pathway to form the new olefin products and regenerate the metal catalyst bearing a new carbene ligand (Figure 1.10). There are many transition metals that catalyze these reactions including Re, W, Mo, Ti, V, Zr, Nb, Ta, Cr, Tc, Ru, Os, Co, Rh, and Ir[65,66].

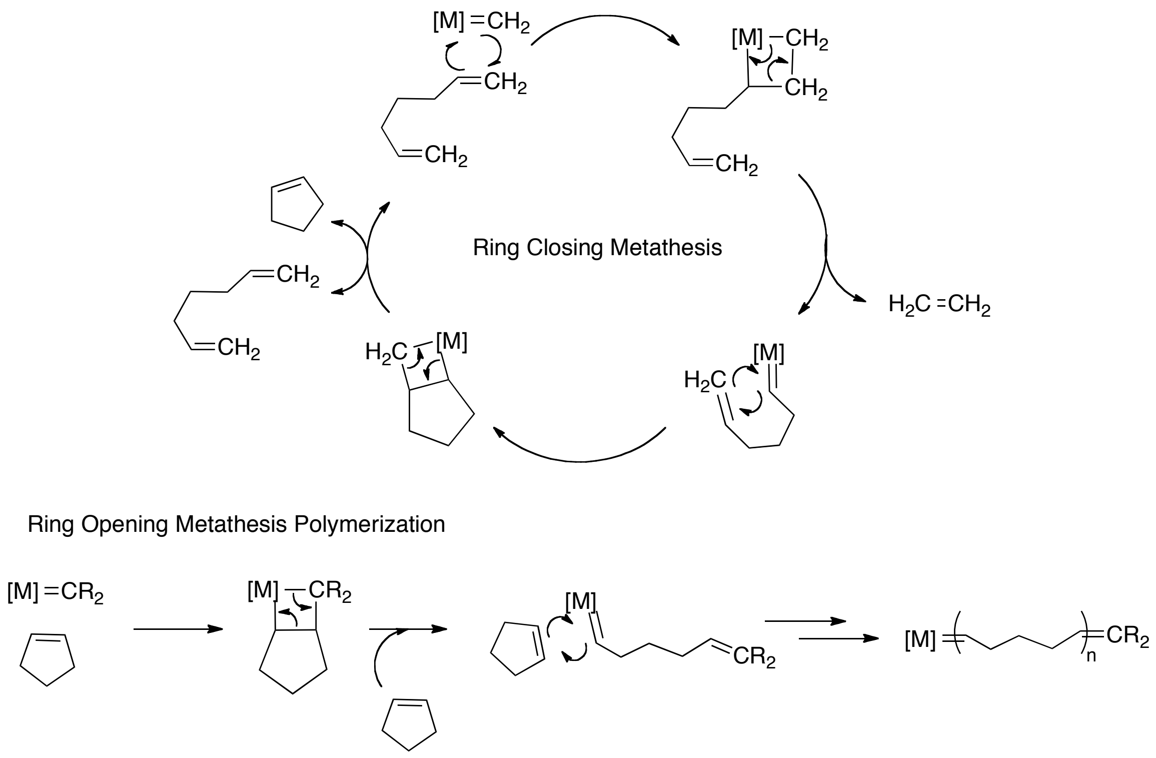

Figure 1.10. Catalytic mechanisms of RCM and ROMP involving metallacyclobutane intermediates.

Of particular relevance to work in this thesis is the series of Ru-based catalysts developed by Grubbs (e.g. $[RuCl_2(CHPh)(PCy_3)_2]$), which proceed through ruthenacyclobutane intermediates. Metallacyclobutane intermediates have been hailed as the potential keys to overall regio- and stereocontrol in olefin metathesis[66,67]. Recent experimental and computational work has focused on ruthenacyclobutanes relevant to Grubbs-type olefin metathesis in order to elucidate structural details and possible handles for stereo- and regiocontrol in the final olefin products[67-73].

1.4.2 [2+2] Cycloaddition In C-O Bond Formation

While research into the mechanism of olefin metathesis has been extensive, there are few concrete examples of C-O bond formation via a [2+2] cycloaddition pathway[74,75].

Although currently a topic of ongoing debate, there is evidence for the formation of metallaoxetanes in a number of early- to mid-transition metal-mediated alkene epoxidation rections[74]. In the mechanism of chromyl chloride epoxidation of olefins proposed by Sharpless *et al.*[76], a metallaoxetane is formed by the [2+2] cycloaddition of the olefin and the Cr=O π-bond (Scheme 1.6). A [1,2] shift then generates the coordinated epoxide.

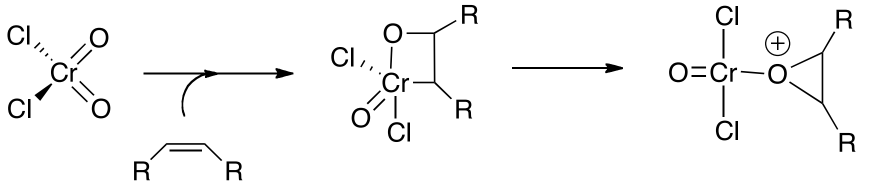

Scheme 1.6. Proposed mechanism for the epoxidation of olefins by chromium chloride.

1.4.3 [2+2] Cycloaddition In C-N Bond Formation

The formation of 4-membered, nitrogen-containing metallacycles by [2+2] cycloadditions to effect C-N bond formation is most prevalent in alkyne hydroamination reactions catalyzed by group 4 metals[75,77]. Hydroamination is analogous to hydrophosphination in that a N-H bond (compared to the P-H bond in hydrophosphination) is added across a C-C unsaturated bond in a typically atom-economical process. For example, in the titanium-catalyzed hydroamination of 1-phenylpropyne the catalytically active metal imido complex undergoes reversible [2+2] cycloaddition to form an azametallacyclobutene intermediate[78,79] (Figure 1.11). Protonolysis of the azametallacyclobutene by a primary amine, followed by subsequent α-elimination releases the hydroamination product and regenerates the active imido species.

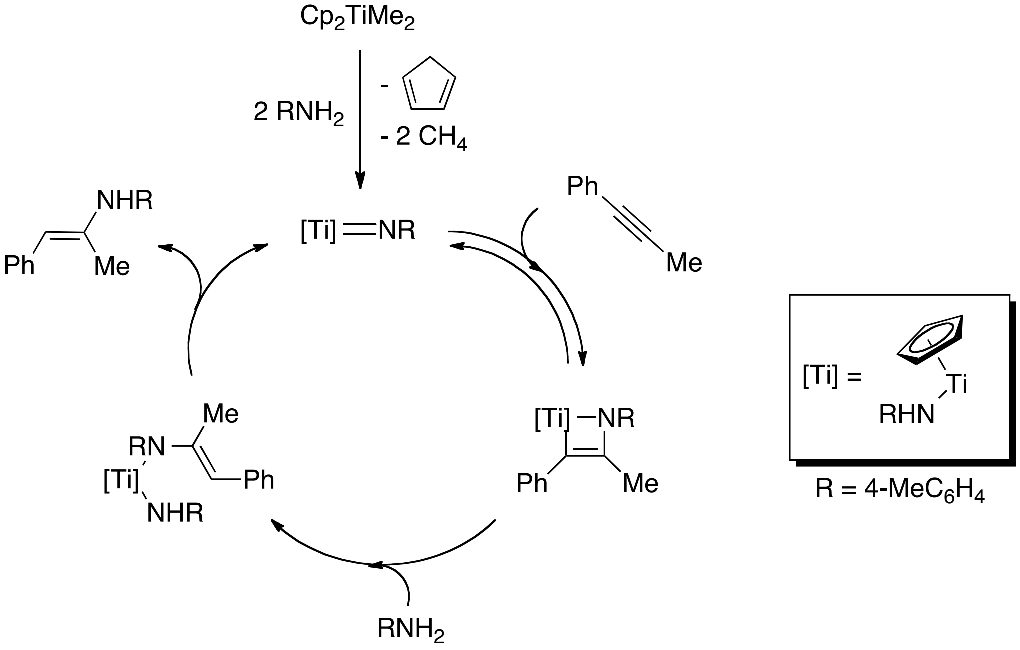

Figure 1.11. Simplified proposed mechanism for the titanium-catalyzed hydroamination of 1-phenylpropylene.

In summary, the mechanism of [2+2] cycloaddition between unsaturated substrates and metal-atom (C, N, O, P) π-bonds has proven valuable in the catalytic syntheses of a wide variety of useful compounds[75]. Olefin metathesis[66], as well as some alkene epoxidations[74] and alkyne hydroaminations[77], all feature four-membered metallacycles as key intermediates in their synthetic catalytic processes. These cases, as well as one example of titanium-catalyzed hydrophosphination involving a four-membered metallacyle[61], highlight the utility of the [2+2] cycloaddition mechanism in catalytic C-C and C-heteroatom bond formation.

1.5 Scope of this Thesis

The overall goal that this thesis addresses is the development of a Ru-mediated asymmetric, catalytic hydrophosphination process (Figure 1.12). The immediate steps taken towards this goal by this research were to examine the potential of the terminal phosphido complex **2**, as well as the resulting metallacycle products (**4**) formed from [2+2] cycloadditions with alkenes, as intermediates in catalytic hydrophosphination reactions.

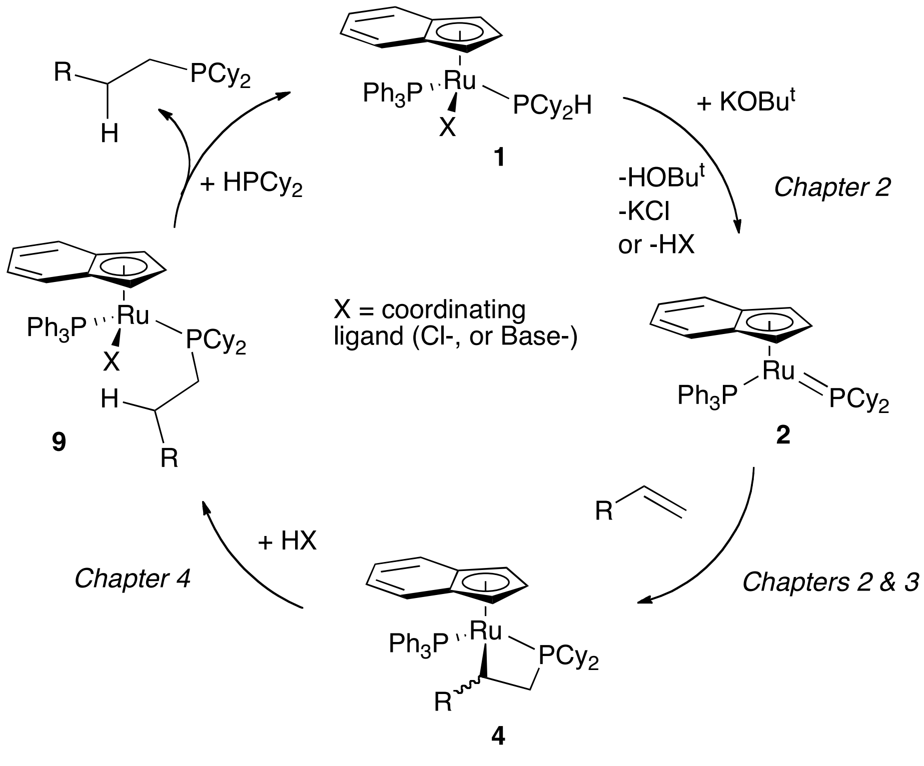

Figure 1.12. Possible cycle for Ru-catalyzed hydrophosphination of alkenes explored by this thesis. Chapters focus on specific aspects of this cycle.

Chapter 2 explores the synthetic aspects of metallacycle formation, including one-pot syntheses of metallacycles from the chloride precursor **1a**, thermal stabilities and unexpected cycloreversion of the metallacycle complexes, and observation of an alkene coordination intermediate in the [2+2] cycloaddition. The effects of alkene substituent steric and electronic factors on metallacycle formation are examined by kinetic studies in Chapter 3, which include rate constant and activation parameter determination as well as analysis by a Hammett study. Chapter 3 also discusses experimentally-observed versus computationally-predicted diastereomer distributions and selectivity in metallacycle formation. Chapter 4 looks ahead to the full potential catalytic cycle (Figure 1.12), in which methods of releasing a phosphinated product from the metallacycle are explored. Possible directions for future work to expand upon the findings of Chapters 2-4 are described in Chapter 5.

1.6 References

(1) Noyori, R. *Asymmetric Catalysis in Organic Synthesis*; Wiley: New York, USA, 1994.

(2) Börner, A. *Phosphorus Ligands in Asymmetric Catalysis: Synthesis and Applications*; Wiley-VCH: Weinheim, Germany, 2008.

(3) Horner, L.; Siegel, H.; Buthe, H. *Angew. Chem.* **1968**, *80*, 1034.

(4) Knowles, W. S.; Sabacky, M. J. *Chem. Commun. (London)* **1968**, 1445.

(5) Kagan, H. B.; Dang Tuan, P. *J. Am. Chem.Soc.* **1972**, *94*, 6429.

(6) Luhr, S.; Holz, J.; Borner, A. *ChemCatChem* **2011**, *3*, 1708.

(7) Barta, K.; Holscher, M.; Francio, G.; Leitner, W. *Eur. J. Org. Chem.* **2009**, *2009*, 4102.

(8) Miyashita, A.; Yasuda, A.; Takaya, H.; Toriumi, K.; Ito, T.; Souchi, T.; Noyori, R. *J. Am. Chem. Soc.* **1980**, *102*, 7932.

(9) Vineyard, B. D.; Knowles, W. S.; Sabacky, M. J.; Bachman, G. L.; Weinkauff, D. J. *J. Am. Chem. Soc.* **1977**, *99*, 5946.

(10) Glueck, D. S. *Chem. - Eur. J.* **2008**, *14*, 7108.

(11) Adams, H.; Collins, R. C.; Jones, S.; Warner, C. J. A. *Org. Lett.* **2011**, *13*, 6576.

(12) Fryzuk, M. D.; Bosnich, B. *J. Am. Chem. Soc.* **1978**, *100*, 5491.

(13) Gouverneur, V.; ISIS Innovation Ltd.: Great Britain, 2007; Vol. WO/2007/057690.

(14) Huang, Y.; Pullarkat, S. A.; Li, Y.; Leung, P.-H. *Chem. Commun.* **2010**, *46*, 6950.

(15) Huang, Y.; Chew, R. J.; Li, Y.; Pullarkat, S. A.; Leung, P.-H. *Org. Lett.* **2011**, *13*, 5862.

(16) Glueck, D. S. *Top. Organomet. Chem.* **2010**, *31*, 65-100. Recent Advances in Metal-Catalyzed C–P Bond Formation. (In *C-X Bond Formation*, Vigalok, A., Ed.)

(17) Blank, N. F.; Moncarz, J. R.; Brunker, T. J.; Scriban, C.; Anderson, B. J.; Amir, O.; Glueck, D. S.; Zakharov, L. N.; Golen, J. A.; Incarvito, C. D.; Rheingold, A. L. *J. Am. Chem. Soc.* **2007**, *129*, 6847.

(18) Chan, V. S.; Bergman, R. G.; Toste, F. D. *J. Am. Chem. Soc.* **2007**, *129*, 15122.

(19) Scriban, C.; Glueck, D. S.; Golen, J. A.; Rheingold, A. L. *Organometallics* **2007**, *26*, 5124.

(20) Chan, V. S.; Stewart, I. C.; Bergman, R. G.; Toste, F. D. *J. Am. Chem. Soc.* **2006**, *128*, 2786.

(21) Chan, V. S.; Chiu, M.; Bergman, R. G.; Toste, F. D. *J. Am. Chem. Soc.* **2009**, *131*, 6021.

(22) Schwan, A. L. *Chem. Soc. Rev.* **2004**, *33*, 218.

(23) Anderson, B. J.; Guino-o, M. A.; Glueck, D. S.; Golen, J. A.; DiPasquale, A. G.; Liable-Sands, L. M.; Rheingold, A. L. *Org. Lett.* **2008**, *10*, 4425.

(24) Vallette, H.; Pican, S.; Boudou, C.; Levillain, J.; Plaquevent, J.-C.; Gaumont, A.-C. *Tetrahedron Lett.* **2006**, *47*, 5191.

(25) Pirat, J.-L.; Monbrun, J.; Virieux, D.; Cristau, H.-J. *Tetrahedron* **2005**, *61*, 7029.

(26) Laven, G.; Stawinski, J. *Synlett.* **2009**, *2009*, 225.

(27) Kwong, F. Y.; Lai, C. W.; Yu, M.; Chan, K. S. *Tetrahedron* **2004**, *60*, 5635.

(28) Gelman, D.; Jiang, L.; Buchwald, S. L. *Org. Lett.* **2003**, *5*, 2315.

(29) Allen, D. V.; Venkataraman, D. *J. Org. Chem.* **2003**, *68*, 4590.

(30) Huang, C.; Tang, X.; Fu, H.; Jiang, Y.; Zhao, Y. *J. Org. Chem.* **2006**, *71*, 5020.

(31) Zhuang, R.; Xu, J.; Cai, Z.; Tang, G.; Fang, M.; Zhao, Y. *Org. Lett.* **2011**, *13*, 2110.

(32) Tye, J. W.; Weng, Z.; Johns, A. M.; Incarvito, C. D.; Hartwig, J. F. *J. Am. Chem. Soc.* **2008**, *130*, 9971.

(33) Scriban, C.; Glueck, D. S.; Zakharov, L. N.; Kassel, W. S.; DiPasquale, A. G.; Golen, J. A.; Rheingold, A. L. *Organometallics* **2006**, *25*, 5757.

(34) Mimeau, D.; Delacroix, O.; Gaumont, A.-C. *Chem. Commun.* **2003**, 2928.

(35) Mimeau, D.; Gaumont, A.-C. *J. Org. Chem.* **2003**, *68*, 7016.

(36) Dombek, B. D. *J. Org. Chem.* **1978**, *43*, 3408.

(37) Bunlaksananusorn, T.; Knochel, P. *J. Org. Chem.* **2004**, *69*, 4595.

(38) Headley, C. E.; Marsden, S. P. *J. Org. Chem.* **2007**, *72*, 7185.

(39) Carlone, A.; Bartoli, G.; Bosco, M.; Sambri, L.; Melchiorre, P. *Angew. Chem. Int. Ed.* **2007**, *46*, 4504.

(40) Ibrahem, I.; Rios, R.; Vesely, J.; Hammar, P.; Eriksson, L.; Himo, F.; Cordova, A. *Angew. Chem., Int. Ed.* **2007**, *46*, 4507.

(41) Perrier, A.; Comte, V.; Moise, C.; Richard, P.; Le Gendre, P. *Eur. J. Org. Chem.* **2010**, *2010*, 1562.

(42) Rauhut, M. M.; Currier, H. A.; Semsel, A. M.; Wystrach, V. P. *J. Org. Chem.* **1961**, *26*, 5138.

(43) Trofimov, B.; Malysheva, S.; Parshina, L.; Gusarova, N.; Belogorlova, N. *Synlett.* **2010**, *2011*, 94.

(44) Daeffler, C. S.; Grubbs, R. H. *Org. Lett.* **2011**, *13*, 6429.

(45) Hoffmann, H.; Diehr, H. J. *Chem. Ber.* **1965**, *98*, 363.

(46) Alonso, F.; Beletskaya, I. P.; Yus, M. *Chem. Rev.* **2004**, *104*, 3079.

(47) Han, L.-B.; Tanaka, M. *Chem. Commun.* **1999**, 395.

(48) Tanaka, M. *Top. Curr. Chem.* **2004**, *232*, 25.

(49) Motta, A.; Fragala, I. L.; Marks, T. J. *Organometallics* **2005**, *24*, 4995.

(50) Crimmin, M. R.; Barrett, A. G. M.; Hill, M. S.; Hitchcock, P. B.; Procopiou, P. A. *Organometallics* **2007**, *26*, 2953.

(51) Douglass, M. R.; Stern, C. L.; Marks, T. J. *J. Am. Chem. Soc.* **2001**, *123*, 10221.

(52) Duraud, A.; Toffano, M.; Fiaud, J.-C. *Eur. J. Org. Chem.* **2009**, *2009*, 4400.

(53) Join, B.; Mimeau, D.; Delacroix, O.; Gaumont, A.-C. *Chem. Commun.* **2006**, 3249.

(54) Nagata, S.; Kawaguchi, S.-I.; Matsumoto, M.; Kamiya, I.; Nomoto, A.; Sonoda, M.; Ogawa, A. *Tetrahedron Lett.* **2007**, *48*, 6637.

(55) Ananikov, V.; Khemchyan, L.; Beletskaya, I. *Synlett.* **2009**, *2009*, 2375.

(56) Niu, M.; Fu, H.; Jiang, Y.; Zhao, Y. *Chem. Commun.* **2006**, 272.

(57) Han, L.-B.; Ono, Y.; Shimada, S. *J. Am. Chem. Soc.* **2008**, *130*, 2752.

(58) Mizuta, T.; Miyaji, C.; Katayama, T.; Ushio, J.-*i*.; Kubo, K.; Miyoshi, K. *Organometallics* **2008**, *28*, 539.

(59) Glueck, D. S. *Dalton Trans.* **2008**, 5276.

(60) Scriban, C.; Kovacik, I.; Glueck, D. S. *Organometallics* **2005**, *24*, 4871.

(61) Zhao, G.; Basuli, F.; Kilgore, U. J.; Fan, H.; Aneetha, H.; Huffman, J. C.; Wu, G.; Mindiola, D. J. *J. Am. Chem. Soc.* **2006**, *128*, 13575.

(62) Derrah, E. J.; Pantazis, D. A.; McDonald, R.; Rosenberg, L. *Organometallics* **2007**, *26*, 1473.

(63) Derrah, E. J.; McDonald, R.; Rosenberg, L. *Chem. Commun.* **2010**, *46*, 4592.

(64) Derrah, E. J.; Pantazis, D. A.; McDonald, R.; Rosenberg, L. *Angew. Chem., Int. Ed.* **2010**, *49*, 3367.

(65) Bielawski, C. W.; Grubbs, R. H. In *Controlled and Living Polymerization: From Mechanisms to Applications*; Muller, A. H. E., Matyjaszewski, K., Eds.; Wiley-VCH Verlag GmbH & Co.: Weinheim, Germany, 2010, p 297.

(66) Ivin, K. J.; Mol, J. C. *Olefin Metathesis and Metathesis Polymerization*; Academic Press: San Diego, USA, 1997.

(67) Romero, P. E.; Piers, W. E. *J. Am. Chem. Soc.* **2005**, *127*, 5032.

(68) Romero, P. E.; Piers, W. E. *J. Am. Chem. Soc.* **2007**, *129*, 1698.

(69) Piers, W. E.; van der Eide, E. F.; Romero, P. E. *J. Am. Chem. Soc.* **2008**, *130*, 4485.

(70) Piers, W. E.; Rowley, C. N.; van der Eide, E. F.; Woo, T. K. *Organometallics* **2008**, *27*, 6043.

(71) Keitz, B. K.; Grubbs, R. H. *J. Am. Chem. Soc.* **2011**, *133*, 16277.

(72) Grubbs, R. H.; Wenzel, A. G.; Blake, G.; VanderVelde, D. G. *J. Am. Chem. Soc.* **2011**, *133*, 6429.

(73) Grubbs, R. H.; Wenzel, A. G. *J. Am. Chem. Soc.* **2006**, *128*, 16048.

(74) Dauth, A.; Love, J. A. *Chem. Rev.* **2011**, *111*, 2010.

(75) Hartwig, J. F. *Nature* **2008**, *455*, 314.

(76) Sharpless, K. B.; Teranishi, A. Y.; Backvall, J. E. *J. Am. Chem. Soc.* **1977**, *99*, 3120.

(77) Muller, T. E.; Hultzsch, K. C.; Yus, M.; Foubelo, F.; Tada, M. *Chem. Rev.* **2008**, *108*, 3795.

(78) Pohlki, F.; Doye, S. *Angew. Chem., Int. Ed.* **2001**, *40*, 2305.

(79) Straub, B. F.; Bergman, R. G. *Angew. Chem., Int. Ed.* **2001**, *40*, 4632.

Chapter 2 Metallacycle Formation in Solution: Identification and Analysis of Species Involved

2.1 Introduction

When investigating a reaction for possible inclusion in a catalytic cycle, it is important to know the extent of reactivity of both the starting materials and products, as well as any intermediates that the reaction may progress through. Understanding the relative stabilities and reactivities of complexes involved allows for predictable manipulation of the reaction progress and outcome, including increasing product yields by reducing the formation of unwanted by-products.

The aim of this chapter is thus the thorough understanding of possible species in solution during both the generation of the reactive species [Ru(η^5-indenyl)(PCy_2)(PPh_3)] (**2**), and in the [2+2] cycloaddition of unsaturated substrates to **2**. To this end, solution isomerization of **2** was investigated kinetically by UV-Vis and NMR spectroscopy. A one-pot synthetic procedure for the formation of metallacycle products from the chloride precursor [RuCl(η^5-indenyl)($PHCy_2$)(PPh_3)] (**1a**) was developed to reduce solution isomerization of **2** and increase synthetic yields. Variable temperature NMR studies were used to observe an alkene coordination intermediate in the proposed [2+2] cycloaddition mechanism, as well as to conduct detailed studies of metallacycle solution stability. In this manner, complexes involved in the [2+2] cycloaddition of unsaturated substrates to [Ru(η^5-indenyl)(PCy_2)(PPh_3)] (**2**) were examined and analyzed to better understand their reactivities in processes relevant to hydrophosphination.

2.2 Isomerization of [Ru(η^5-indenyl)(PCy_2)(PPh_3)] (2) in Solution

The [2+2] cycloaddition of alkenes and alkynes to the ruthenium-phosphido complex [Ru(η^5-indenyl) (PCy_2)(PPh_3)] (**2**) occurs due to the high reactivity of the Ru=P π-bond, which arises from the coordinative unsaturation at Ru and the highy nucleophilicity of the coordinated phosphido[1]. Previously observed[1] isomerization of complex **2** to a phosphaalkene isomer, **3**, as well as a thermodynamically-favoured orthometallated isomer, **6** (Scheme 2.1), could potentially reduce the amount of **2** available to react with olefinic substrates. The thermal stability and availability of **2** in solution is explored in more detail in the following sections in order to determine the extent of its effect on the reactivity of **2**.

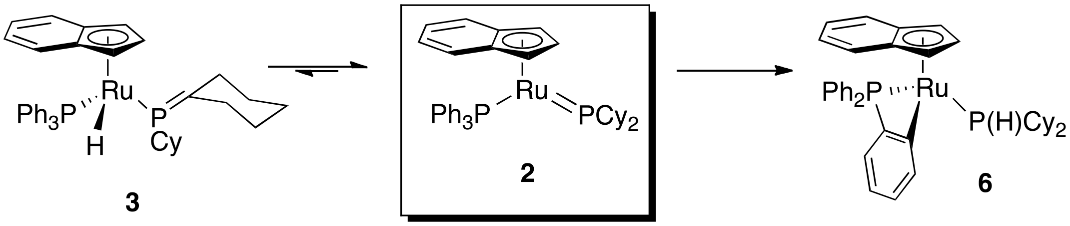

Scheme 2.1. Solution isomerization of **2** to the phosphaalkene **3** and the orthometallated complex **6**.

2.2.1 Equilibrium with Phosphaalkene Isomer 3

In the synthesis of complex **2** from the chloride precursor **1** (Scheme 1.4) reported by Derrah *et al.*[1], the phosphaalkene isomer **3** was observed in a 88:12 (**2** : **3**) ratio with complex **2** at room temperature. Using the equilibrium constant equation [2],

$$K_{eq} = [\text{complex } \mathbf{3}]_{eq}/[\text{complex } \mathbf{2}]_{eq} \quad \ldots\ldots\ldots\ldots (2.1)$$

the equilibrium constant for the isomerization of **2** to **3** at room temperature was determined to be approximately 0.1. The small value for K_{eq} indicates that the equilibrium lies heavily toward the reactive species, complex **2**. Greater accuracy in the determination of the equilibrium constant was not necessary as it was deemed most useful as a descriptive, comparative value.

As the isomerization of the phosphaalkene isomer **3** is reversible, the full amount of starting material **2** is eventually recovered and converted to product in any synthetic reaction that occurs at a greater rate than that of isomerization of **2** to **3**. As **2** is removed from the system by reaction with another substrate, **3** will isomerize to **2** to maintain the weighted equilibrium, as long as **3** remains non-reactive with the substrate present. Studies conducted by previous graduate student, Eric Derrah[3] indicate that the phosphaalkene isomer **3** has low reactivity relative to **2** and is eventually siphoned off by the reaction between substrates and **2**. Further experimental details describing these findings can be found in the 2010 published work[3]. In the numerous reactions with **2** that have been conducted by either Derrah[1,3-5] or me, none have resulted in any product formation that is attributable to the participation of **3**.

2.2.2 Rate Constant of Orthometallation

The irreversible isomerization of complex **2** to orthometallated species **6** presents a greater problem than the equilibrium with the phosphaalkene **3** to reactions involving complex **2** as a starting material (Scheme 2.1). Removal of complex **2** by irreversible isomerization will reduce overall yields of any synthetic process using it as a substrate. In order to determine how this background reaction might compete with the [2+2] cycloaddition, the rate constant of solution isomerization of **2** to **6** at room temperature,

k_{OM}, was determined by monitoring the thermal decomposition of **2** in solution by UV-Vis spectroscopy (Figure 2.1). In solution, the phosphido complex **2** is dark blue, absorbing strongly at 590 nm. As the orthometallated complex **6** is bright yellow in solution, the decomposition of **2** to **6** could be easily monitored by UV-Vis spectroscopy by observing the decrease in solution absorbance at 590 nm. The equation used for the first order rate law[2] is as follows,

$$\ln(\mathrm{abs}) = \ln(\mathrm{abs})_0 - kt \qquad \text{. . . . . (2.2)}$$

where $(\mathrm{abs})_0$ is the initial absorbance of the solution at 590 nm. Therefore, in a relationship between t (time) and ln(abs) (Figure 2.1), the intercept value, m1, is equal to $\ln(\mathrm{abs})_0$ and the slope, m2, is equal to the first order rate constant, k.

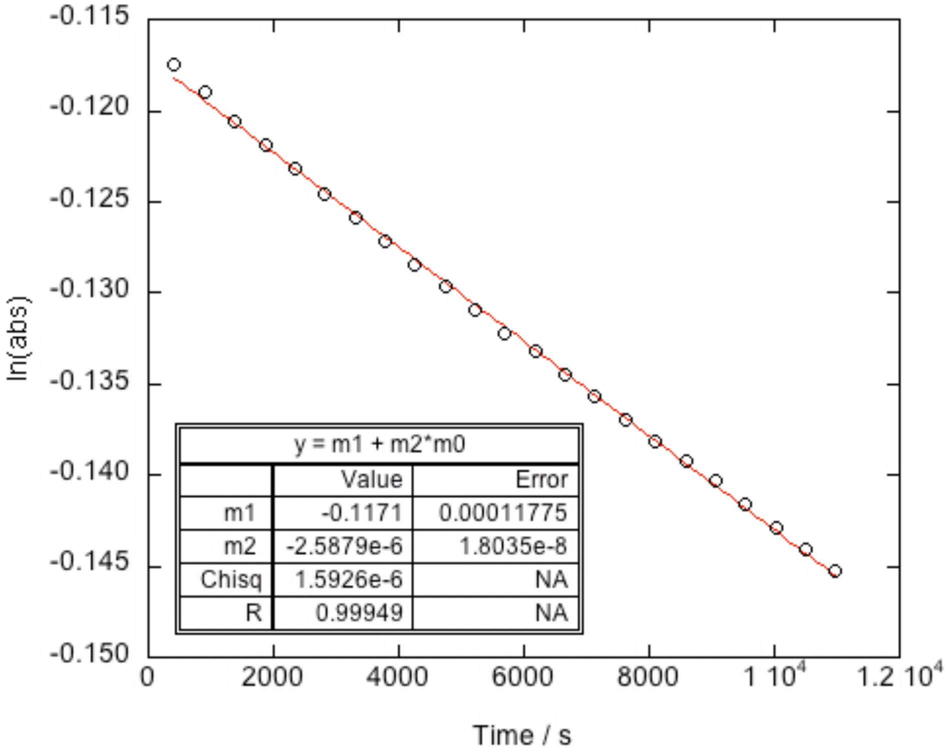

y = m1 + m2*m0

	Value	Error
m1	-0.1171	0.00011775
m2	-2.5879e-6	1.8035e-8
Chisq	1.5926e-6	NA
R	0.99949	NA

Figure 2.1. First-order plot for the isomerization of complex **2** to orthometallated isomer **6** at 25°C in toluene. (abs at 590 nm)

The determined value of k_{OM} was so small, 10^{-6} s^{-1}, that it could not be monitored over the ideal five lifetimes (278 h). Thus, only the order of magnitude of the rate constant is reported to account for the inaccuracy associated with only measuring over 0.06 lifetimes (18 h), approximately. Furthermore, the small rate constant indicates a very slow rate of isomerization at room temperature and is again most useful in a comparative sense, to describe the relative competitiveness of orthometallation against reaction rate constants that are orders of magnitude greater (*vide infra*, section 3.3.3 discusses rate constants of [2+2] cycloaddition).

To ensure that the conversion of **2** to **6** was not limited by the isomerization of **3** to **2**, a solution of **2** was also monitored by ^{31}P NMR over time. The interconversion of **2** with structural isomer **3** was determined to be fast with respect to the rate of orthometallation, since the ratio of **2** : **3** determined by integrations of respective ^{31}P shifts remained constant at 1 : 0.1 throughout the concurrent conversion of **2** to **6**. This constant value indicates a steady-state equilibrium between **2** and **3** and reflects the value of K_{eq} determined previously.

2.3 One-Pot Syntheses of Metallacycles From [RuCl(η^5-indenyl) (PPh_3)($PHCy_2$)] Precursor, 1a

Previous syntheses of metallacycle complexes of the form [Ru(η^5-indenyl)(κ^2-R$\underline{C}$HCH$_2$$\underline{P}Cy_2$)(PPh$_3$)] (**4**) had been conducted by Derrah[3] through the [2+2] cycloaddition of alkenes with *isolated* **2** in solution. The formation of [2+2] cycloadduct products from *in-situ* synthesis of **2** from **1a** (Scheme 2.2) was explored to test the viability of complex **2** as an intermediate in a possible catalytic cycle. In a functioning catalytic cycle all reagents, products and intermediates must be present simultaneously in solution without detriment to the individual component steps. Furthermore, one-pot synthesis has the potential to increase metallacycle product yield, not only by reducing the number of synthetic steps and bypassing the isolation of the very reactive **2**, but by minimizing the time complex **2** is in solution and preventing loss of starting material due to the irreversible orthometallation described in section 2.2.2. These one-pot syntheses allowed for the formation and isolation of metallacycle products on a larger scale (300 mg) than the previous step-wise syntheses conducted by Derrah[6] for characterization purposes.

2.3.1 One-Pot Syntheses of Alkene Cycloaddition Products (4c-e)

Metallacycles [(η^5-indenyl)Ru(κ^2-Bu^n-$\underline{C}$HCH$_2$PCy$_2$)(PPh$_3$)] (**4c**), [(η^5-indenyl)Ru(κ^2-(CH$_3$CH$_2$O)-$\underline{C}$HCH$_2$PCy$_2$)(PPh$_3$)] (**4d**), and [(η^5-indenyl)Ru(κ^2-Ph-$\underline{C}$HCH$_2$PCy$_2$)(PPh$_3$)] (**4e**) were prepared by adding excess neat alkene (1-hexene, ethyl vinyl ether, or styrene) to a stirring suspension of [(η^5-indenyl)RuCl(PPh$_3$)(PHCy$_2$)], **1**, and KOBu^t in toluene (Scheme 2.2).

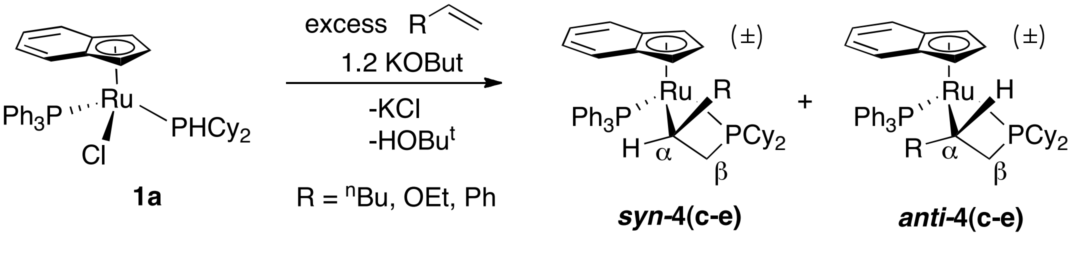

Scheme 2.2. In situ synthesis of alkene cycloadducts **4c-e** from ruthenium-chloride precursor **1a**

The formation of the five-coordinate intermediate **2** was observed in all cases by initial solution colour change from orange to blue. The blue colour increased in intensity, then became muddy as **2** slowly converted to the respective yellow or orange metallacycle product, **4c-e**, over the duration of the reaction. The slow colour change implied that the [2+2] cycloaddition proceeded at a slower rate than the preceding step of proton abstraction, thus controlling the rate of product formation.

Full NMR characterization of complex **4c** (R = ^{n}Bu) and partial $^{31}P\{^{1}H\}$ NMR characterization of **4d** (R = OEt) by Derrah *et al.*[6] allowed the identification of the one-pot synthetic products by comparison of diagnostic $^{31}P\{^{1}H\}$ NMR shifts to literature values (Table 2.1). The most diagnostic $^{31}P\{^{1}H\}$ NMR signals were those of the metallacyclic –PCy_2- ligands, which were observed as doublets far upfield (-7.5 to -15.6 ppm).

Table 2.1. $^{31}P\{^{1}H\}$ NMR shifts of metallacycles synthesized by the one-pot procedure

	$^{31}P\{^{1}H\}$ NMR Shifts (δ = ppm)	
Complex (R =)	*P*Ph$_3$ (multiplicity)	-*P*Cy$_2$- (m, J_{PP} = Hz)
***syn*-4c** (^{n}Bu)	63.8 (d)	-15.6 (d, 22)
***anti*-4c** (^{n}Bu)	60.3 (d)	-10.5 (d, 28)
***syn*-4d** (OEt)	64.0 (d)	-9.8 (d, 20)
***anti*-4d** (OEt)	61.5 (d)	-7.5 (d, 28)
***syn*-4e** (Ph)	63.0 (d)	-21.9 (d, 21)
***anti*-4e** (Ph)	59.0 (d)	-10.3 (d, 27)

Complex **4e**, however, had not been synthesized previously and was thus fully characterized by ESI-MS, NMR, elemental analysis, and x-ray crystallography (Figure

2.2). Regiochemistry for the styrene adduct **4e** was found to be the same as for previously-described alkene adducts **4b-d**, with the alkene substituent being found exclusively on the α-carbon of the metallacycle. Complex **4e** was also initially formed as the *syn* isomer of the metallacycle, though solution epimerization allowed for NMR characterization of the *anti* isomer as well. Regio- and stereochemistry of **4e** was determined by x-ray crystallography as well as 2D-NMR, which is described in greater detail in Chapter 3 (Section 3.2.1). Diagnostic $^{31}P\{^1H\}$ NMR shifts were similar to those of complexes **4c-d** (Table 2.1).

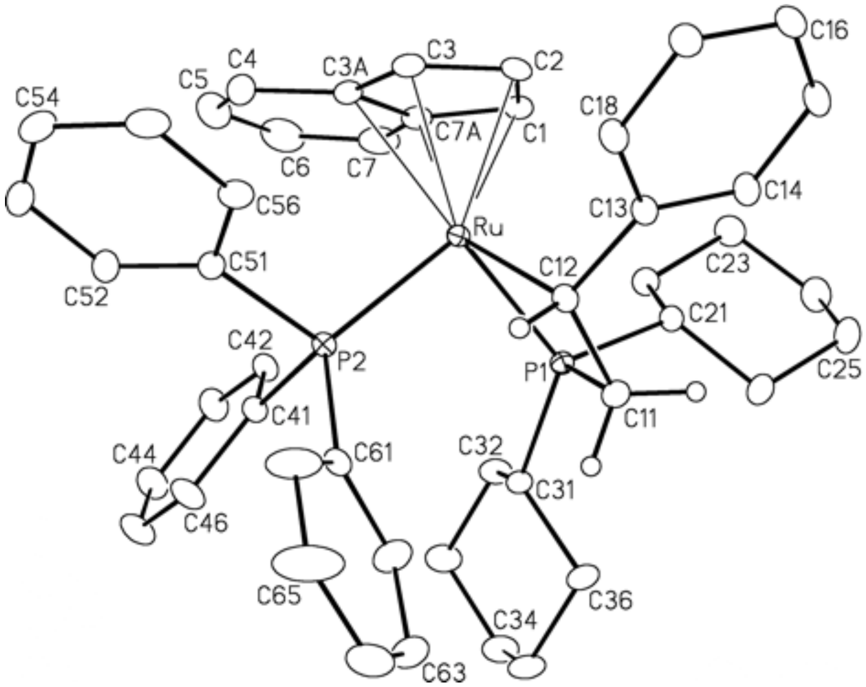

Figure 2.2. View of [Ru(η^5-indenyl)(κ^2-Ph-CHCH$_2$PCy$_2$)(PPh$_3$)] (**4e**). The hydrogen atoms attached to C11 and C12 are shown with arbitrarily small thermal parameters; all other hydrogens are not shown. Non-hydrogen atoms are represented by Gaussian ellipsoids at the 20% probability level.

Table 2.2. Selected interatomic distances and bond angles for [Ru(η^5-indenyl)(κ^2-Ph-CHCH$_2$PCy$_2$)(PPh$_3$)] (**4e**).

Bond(s)	*Interatomic Distance* (Å)	Bond(s)	*Bond Angles* (deg)
Ru – P1	2.2927(4)	P1 – Ru – P2	97.154(13)
Ru – P2	2.2830(4)	P1 – Ru – C12	69.90(4)
Ru – C12	2.1869(13)	P2 – Ru – C12	88.96(4)
Ru – C*	1.959	C* – Ru – P1	130.9
P1 – C11	1.8336(13)	C* – Ru – P2	125.4
C11 – C12	1.5407(18)	C* – Ru – C12	127.0
C12 – C13	1.4903(17)	Ru – P1 – C11	84.04(4)
Δ	0.151	P1 – C11 – C12	98.72(9)

[a]C* denotes the centroid of the plane defined by C7a-C1-C2-C3-C3a, and Δ (indenyl slip distortion) = *d*[Ru-C7a,C3a] - *d*[Ru-C1,C3].

2.3.2 One-Pot Synthesis of an Alkyne Cycloaddition Product (5)

One-pot synthesis of the metallacycle **5** was also carried out for the alkyne substrate, phenylacetylene. Complex **5**, [(η^5-indenyl)Ru(κ^2-Ph-C=CH$_2$PCy$_2$)(PPh$_3$)], is formed by the addition of KOBu^t and excess phenylacetylene to a suspension of the ruthenium-chloride complex **1a** in toluene (Scheme 2.3), whereas previously it had only been prepared directly from **2**. Importantly, the side product (**5'**) previously observed[3] by Derrah, formed from the deprotonation of phenylacetylene by the nucleophilic phosphido ligand of **2**, was not observed or isolated with the one-pot synthesis product.

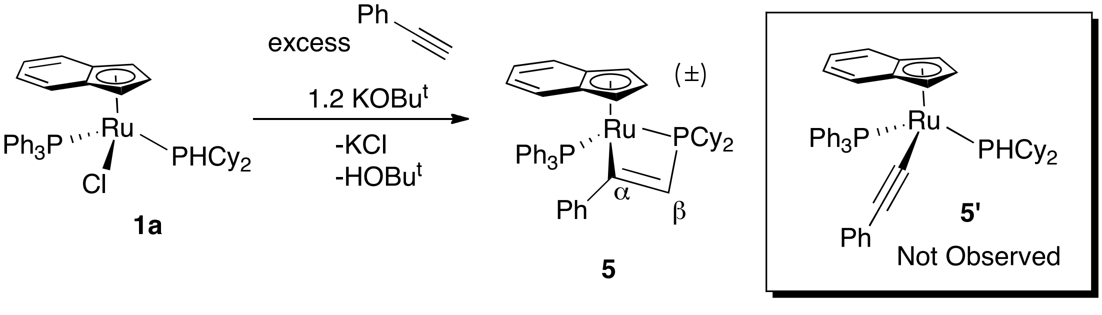

Scheme 2.3. In-situ synthesis of complex **5** from ruthenium-chloride precursor **1a**

As with complexes **4c** and **4d**, complex **5** had been previously characterized by Derrah *et al.*[5] and thus diagnostic $^{31}P\{^{1}H\}$ NMR shifts were compared with literature values to confirm the successful synthesis of **5**. $^{31}P\{^{1}H\}$ NMR shifts of coordinated metallacyclic –*P*Cy$_2$- and PPh$_3$ ligands were observed at -37.0 ppm and 58.0 ppm (d, $^{2}J_{PP}$ = 28 Hz), respectively.

2.4 Evidence for an Olefin η^2-Coordination Intermediate Prior to [2+2] Cycloaddition to Complex 2

2.4.1 Computational Models of [2+2] Cycloaddition

The reaction trajectory of the [2+2] cycloaddition of [(η^5-indenyl)Ru=PCy$_2$(PPh$_3$)] (**2**) with ethylene was modeled computationally by our collaborator at the Max Plank Institute for Bioinorganic Chemistry, Dr. D. Pantazis. The model (containing smaller CH$_3$ substituents on both the coordinated phosphine and the phosphido) predicts the formation of an intermediate complex, **C**, in which the alkene is coordinated η^2 to the ruthenium centre prior to cycloaddition (Figure 2.3). This complex has a predicted ground state energy of -109 kJ/mol relative to the reactants (**A**, Figure 2.3). An in-depth discussion of the concerted nature of the [2+2] cycloaddition mechanism, as determined experimentally, can be found in the work published by Derrah *et al.* [3].

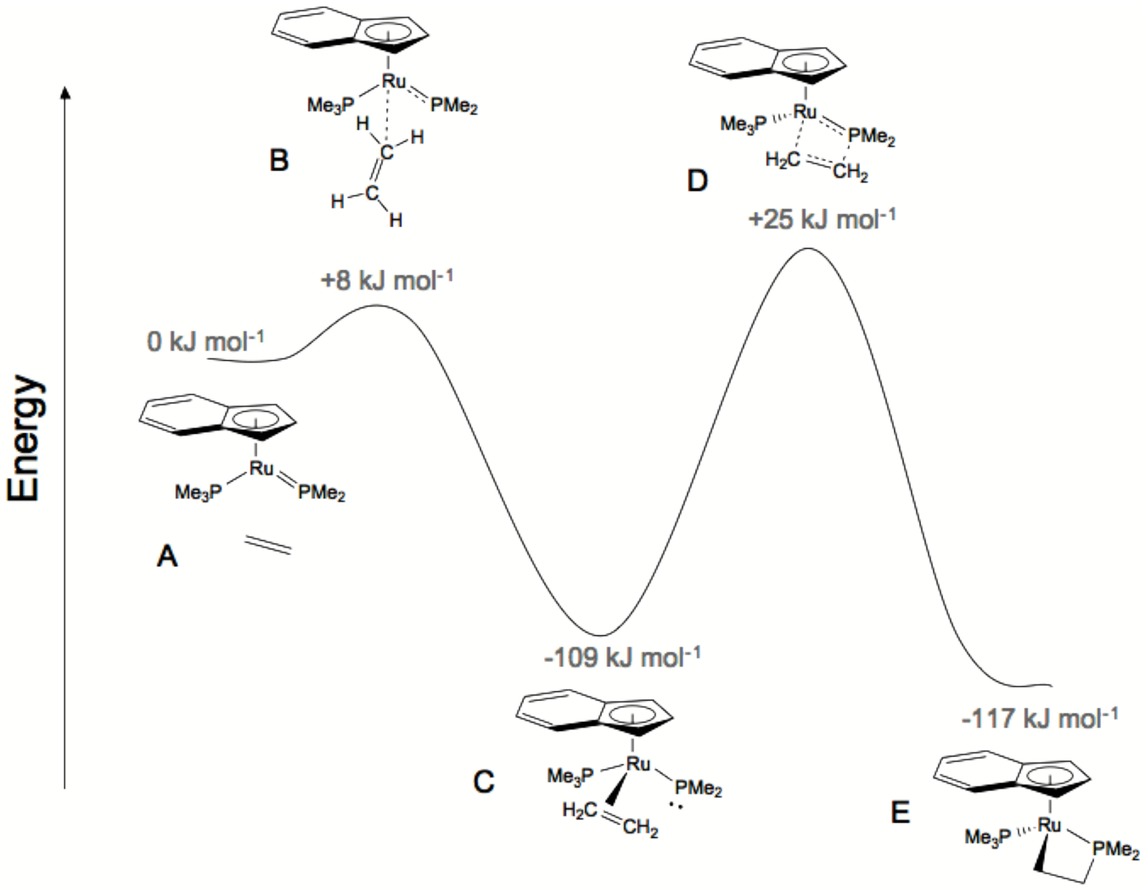

Figure 2.3. DFT-calculated [2+2] cycloaddition reaction trajectory as depicted by relative ground-state energies of complexes involved (PBE/DKH2-TZVP).

2.4.2 Direct Observation of an Ethylene η^2-Coordination Intermediate by Low Temperature NMR Studies

In confirmation of the computational trajectory, the ethylene coordination intermediate **7a** was observed experimentally at low temperature (-80°C) both visually and by $^{31}P\{^1H\}$ NMR spectroscopy (Scheme 2.4). When ethylene was mixed with a cooled dark blue solution of **2** in toluene-d_8, the solution turned a deep red. The sample remained deep red while at -80°C, but became a bright, clear yellow when warmed to room temperature (identical to the previously observed colour of the [2+2] cycloaddition product, **4a**). In the $^{31}P\{^1H\}$ NMR spectrum recorded for the sample at -80°C (Figure 2.4), two broad singlets were observed (δ 55.3 ppm, $J_{1/2}$ = 40 Hz, *P*Ph₃ ; δ 27.6 ppm, $J_{1/2}$ = 148 Hz, *P*Cy₂), along with signals indicating the presence of cycloaddition product **4a**, and a small amount of the phosphaalkene species, complex **3**. It seems reasonable that the low temperature slowed the isomerization of the phosphaalkene **3** to **2**, preventing its reaction with ethylene to form the intermediate **7a**. Upon warming to room temperature the sample converted completely and cleanly to the [2+2] cycloaddition product **4a**, with no traces of other species in solution (Figure 2.4).

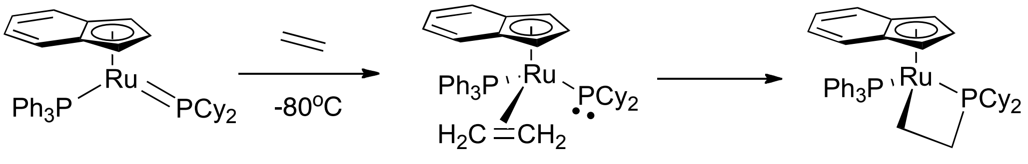

2 **7a** **4a**

Scheme 2.4. [2+2] cycloaddition of **2** with ethylene proceeds through an intermediate, **7a**, in which ethylene coordinates η^2 to the ruthenium centre.

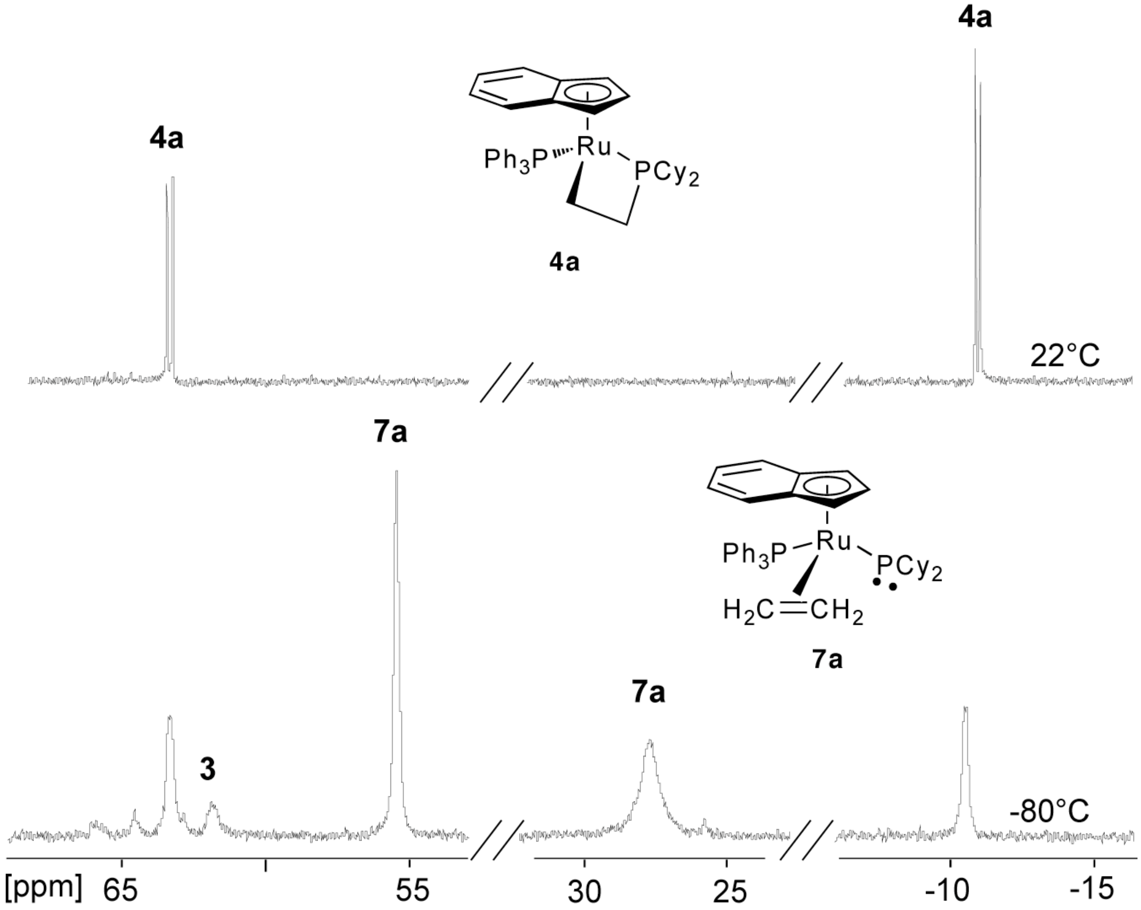

Figure 2.4. $^{31}P\{^1H\}$ NMR of the [2+2] cycloaddition of **2** with ethylene, showing formation of the intermediate **7a** at low temperature (-80°C) and subsequent conversion to the metallacycle product **4a** upon warming to room temperature. Unreacted phosphaalkene isomer **3** is present at -80°C due to the slowed isomerization to reactive species **2**. (202.46 MHz, d_8-toluene)

The $^{31}P\{^1H\}$ NMR signal of the terminal dicyclohexylphosphido ligand in complex **6** is comparable to those of other pyramidal, terminal phosphido ligands in complexes characterized by Hoyle et al[6] (Figure 2.5). Benzonitrile adducts of terminal diarylphosphido complexes of the form [Ru(η^5-indenyl)(PAr_2)(NCPh)(PPh_3)] exhibit $^{31}P\{^1H\}$ signals at 26.1 and 25.6 ppm for pyramidal phosphido ligands PPh$_2$ (**F**, Figure 2.5) and PTol$^p_2$ (**G**, Figure 2.5), respectively.

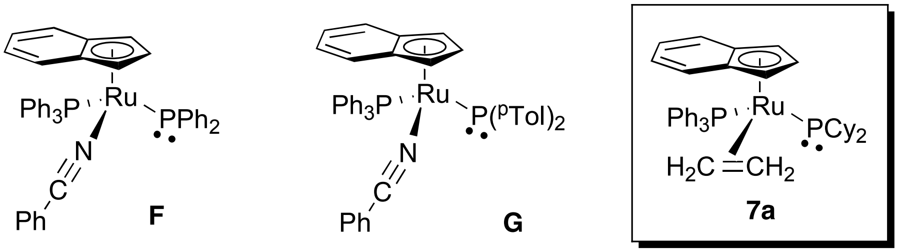

Figure 2.5. Coordination complexes of benzonitrile adducts analogous to the ethylene coordination intermediate **7a**.

2.4.3 Attempts to Observe an Ethyl Vinyl Ether η^2-Coordination Intermediate by Low Temperature NMR

Although the ethylene coordination complex, **7a**, was observed at low temperature, all attempts to observe the equivalent complex with ethyl vinyl ether, **7d**, were unsuccessful (Scheme 2.5). At -80°C the reaction between complex **2** and ethyl vinyl ether did not progress. When the sample was warmed in 10° increments to -50°C, slow conversion to metallacycle product **4d** was observed by $^{31}P\{^{1}H\}$ NMR, with no peaks observed due to other, intermediate complexes.

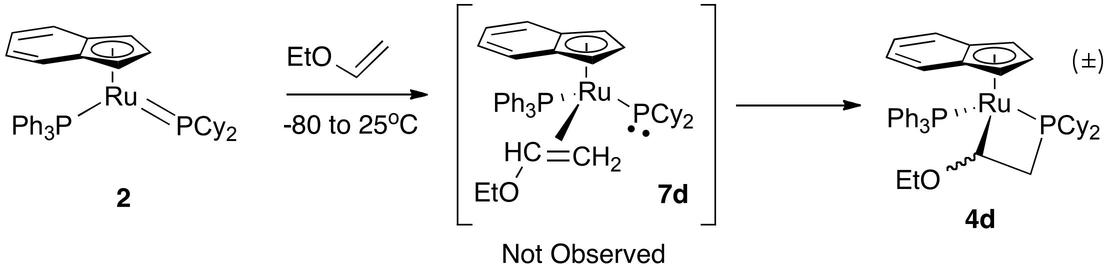

Scheme 2.5. [2+2] Cycloaddition of ethyl vinyl ether to complex **2**, proceeding through an η^2 coordination intermediate, **7d**.

This inability to observe the proposed intermediate **7d** under conditions similar to the ethylene coordination intermediate **7a** highlights a difference in relative stabilities of these intermediates. The model compounds used by Dr. Pantazis to calculate relative energies in the cycloaddition trajectory shown in Figure 2.3 are most applicable to the [2+2] cycloaddition of ethylene, since the model alkene posseses no substituents. The ethoxy substituent therefore likely plays a role in destabilizing the proposed ethyl vinyl ether coordination intermediate, **7d**, increasing its ground-state energy relative to the starting complex **2** so that it is not formed in any observable amount (Figure 2.6). However, other factors likely play a role as well. Since the relative rates of cycloaddition (*vide infra*) favour a lower activation energy for the [2+2] cycloaddition of ethylene than for ethyl vinyl ether, intermediate destabilization (resulting in the decrease of E_{CD}) by the ethoxy substituent must be offset by other factors to decrease the rate of cycloaddition relative to that of ethylene.

To further this idea, alkene substituents could influence the relative stabilities of reaction transition states **B** and **D** (Figure 2.6). These effects are less easy to predict, but the overall result would be the decrease in activation energy from **C** to **D** (E_{CD}, [2+2] cycloaddition) relative to **A** to **B** (E_{AB}, alkene coordination) so that alkene coordination (**A** to **B**) was the slower, rate-limiting step, causing any of the intermediate **C** produced to quickly undergo [2+2] cycloaddition to the metallacycle **E** through transition state **D**. The overall expected observation would be a lack of build-up of intermediate **C** in the reaction mixture, which is what is found in the reaction of ethyl vinyl ether and complex **2**.

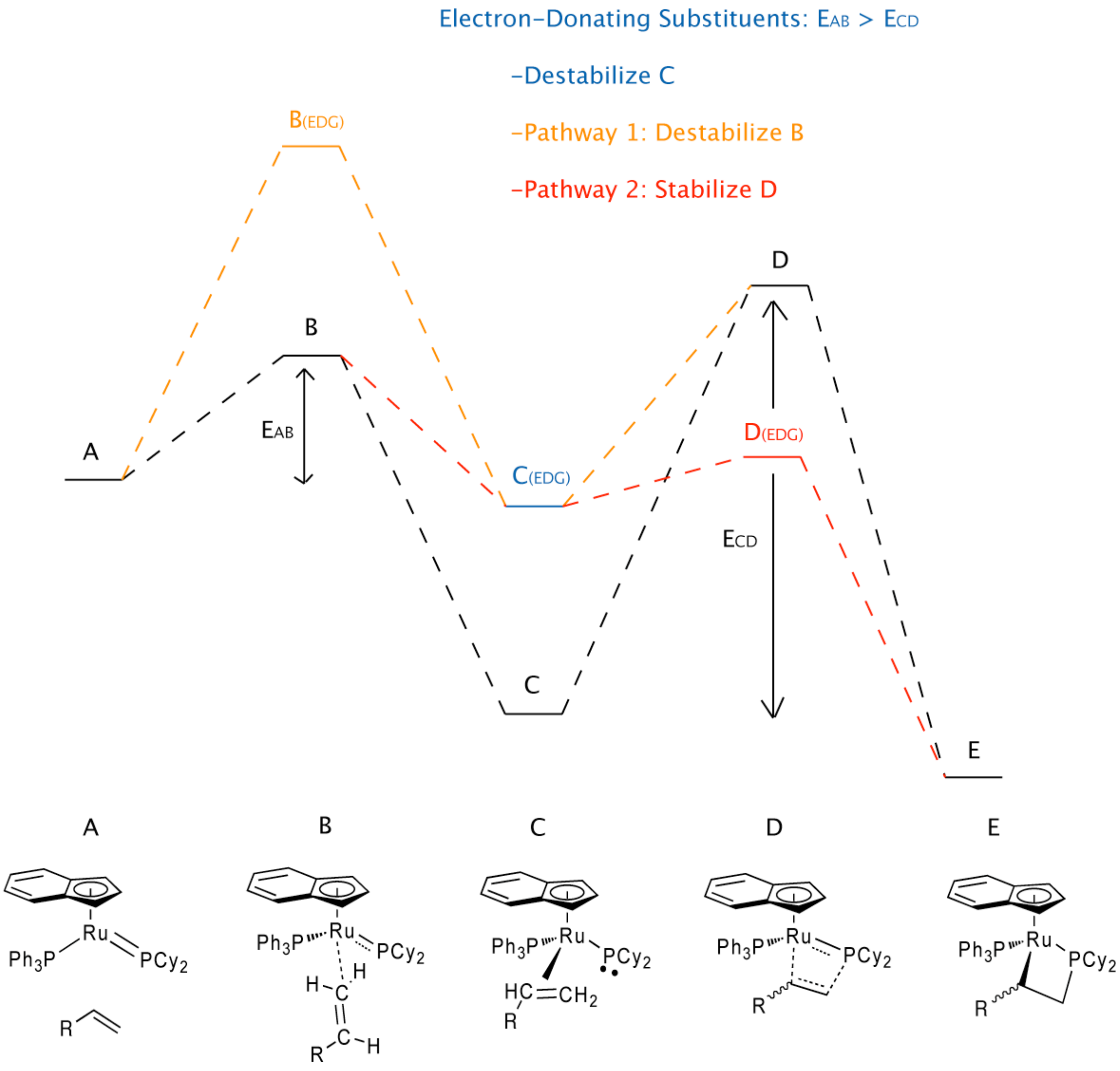

Figure 2.6. Possible effects of electron-donating alkene substituents on relative energies of [2+2] cycloaddition species.

2.5 Solution Stability of Metallacyclic Products

Thermal cycloreversion was observed, directly or indirectly, for all metallacycles, **4a-e**, {R = H (**a**), CN (**b**), ^{n}Bu (**c**), OEt (**d**) or Ph (**e**)} upon heating to 60°C in solution (d_8-toluene) for varying lengths of time. For metallacycles with either electron-donating or bulky substituents (^{n}Bu, OEt and Ph), formation of the five coordinate precursor **2** was observed visually (solution colour change from orange to dark blue) and confirmed by $^{31}P\{^{1}H\}$ NMR spectroscopy (Figures 2.7-2.9). Interestingly, visual observation of the formation of **2** was much more sensitive than $^{31}P\{^{1}H\}$ NMR, as the dark blue colour of **2** was noticeable in solution before the corresponding NMR shifts could be detected. This is highlighted by the low intensity of the $^{31}P\{^{1}H\}$ NMR shift of **2** in Figure 2.7.

Cycloreversion was observed visually by colour change from yellow to murky blue-yellow after 1 hour for the ethyl vinyl ether and styrene adducts, complexes **4d** and **4e**, and after 2 hours for the 1-hexene adduct, complex **4c**. In all cases, however, subsequent, irreversible orthometallation of **2** to complex **6** occurred, determined visually by colour reversion to golden-orange and confirmed by $^{31}P\{^{1}H\}$ NMR spectroscopy.

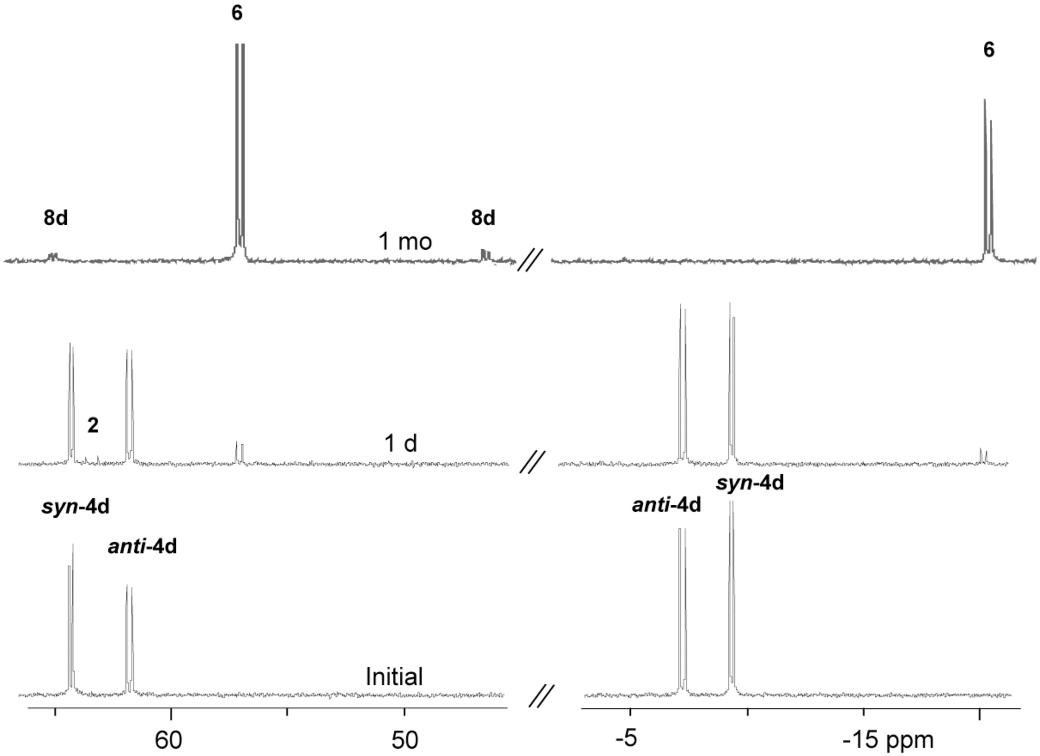

Figure 2.7. $^{31}P\{^{1}H\}$ NMR of ethyl vinyl ether adduct **4d** at 60°C. *Syn* and *anti* isomers are visible, as well as reversion product **2** (other doublet at 243.3 ppm), and orthometallated isomer **6**. Suspected vinyl phosphine **8d** is also observed (*vide infra*, Section 3.2.2.3). (121.49 MHz, d_8-toluene, 60°C)

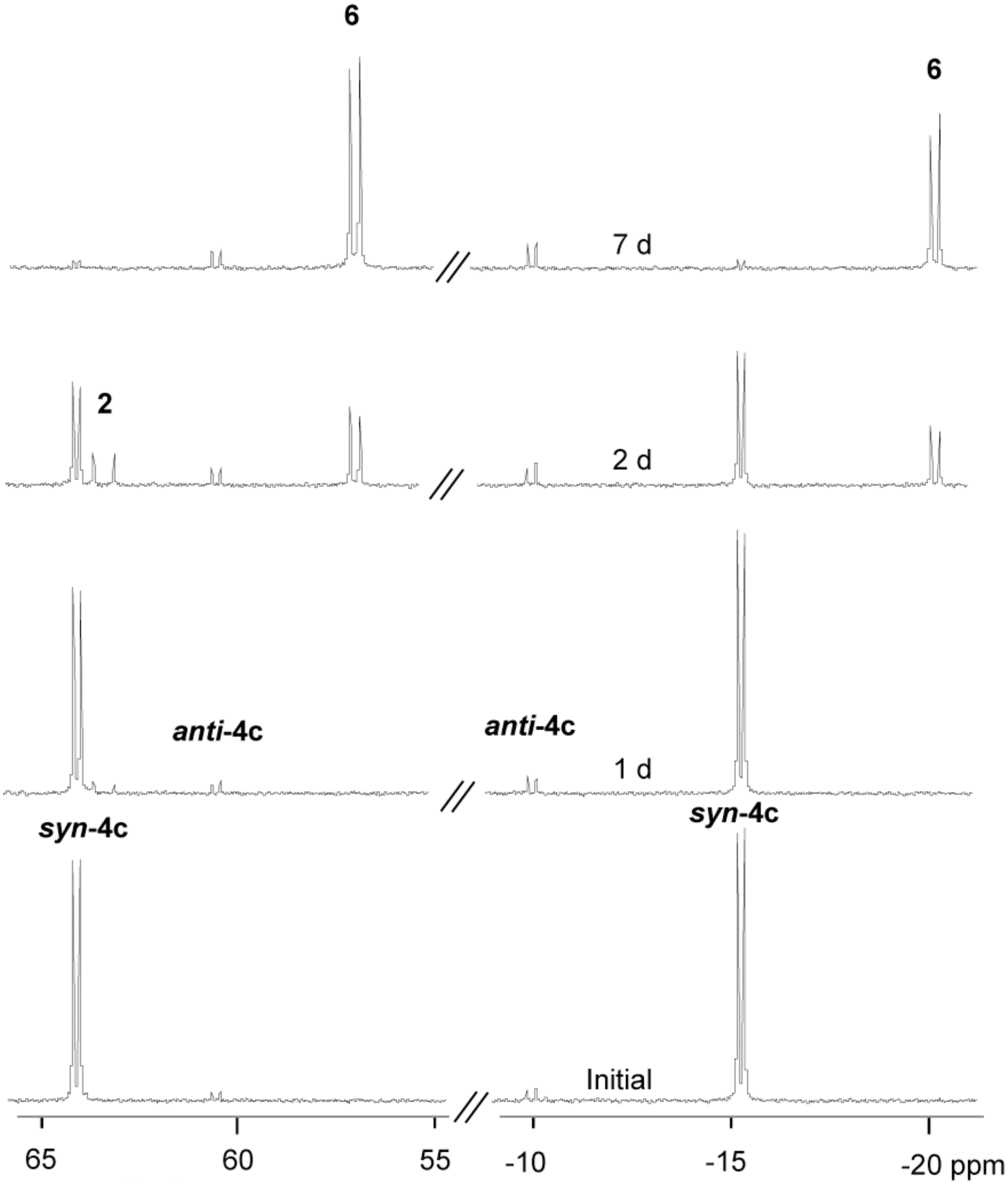

Figure 2.8. $^{31}P\{^1H\}$ NMR of 1-hexene adduct **4c** at 60°C over time, showing *syn* and *anti* isomers, as well as the reversion product **2** (other doublet at 243.3 ppm) and its orthometallated isomer **6**. (121.49 MHz, d_8-toluene, 60°C)

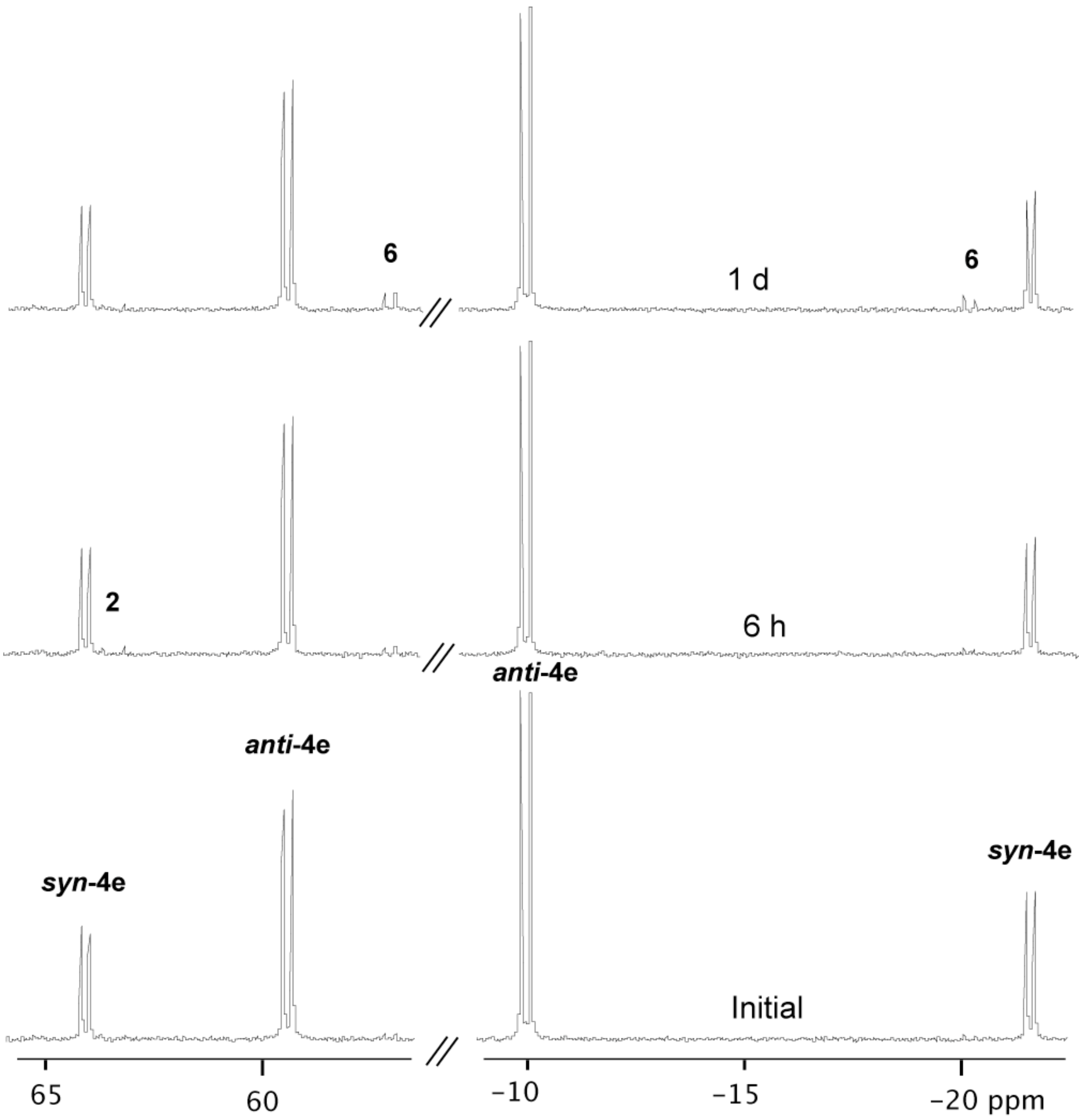

Figure 2.9. $^{31}P\{^1H\}$ NMR of styrene adduct **4e** at 60°C over time, showing *syn* and *anti* isomers, as well as the reversion product **2** (other doublet at 243.3 ppm) and its orthometallated isomer **6**. (121.49 MHz, d_8-toluene, 60°C)

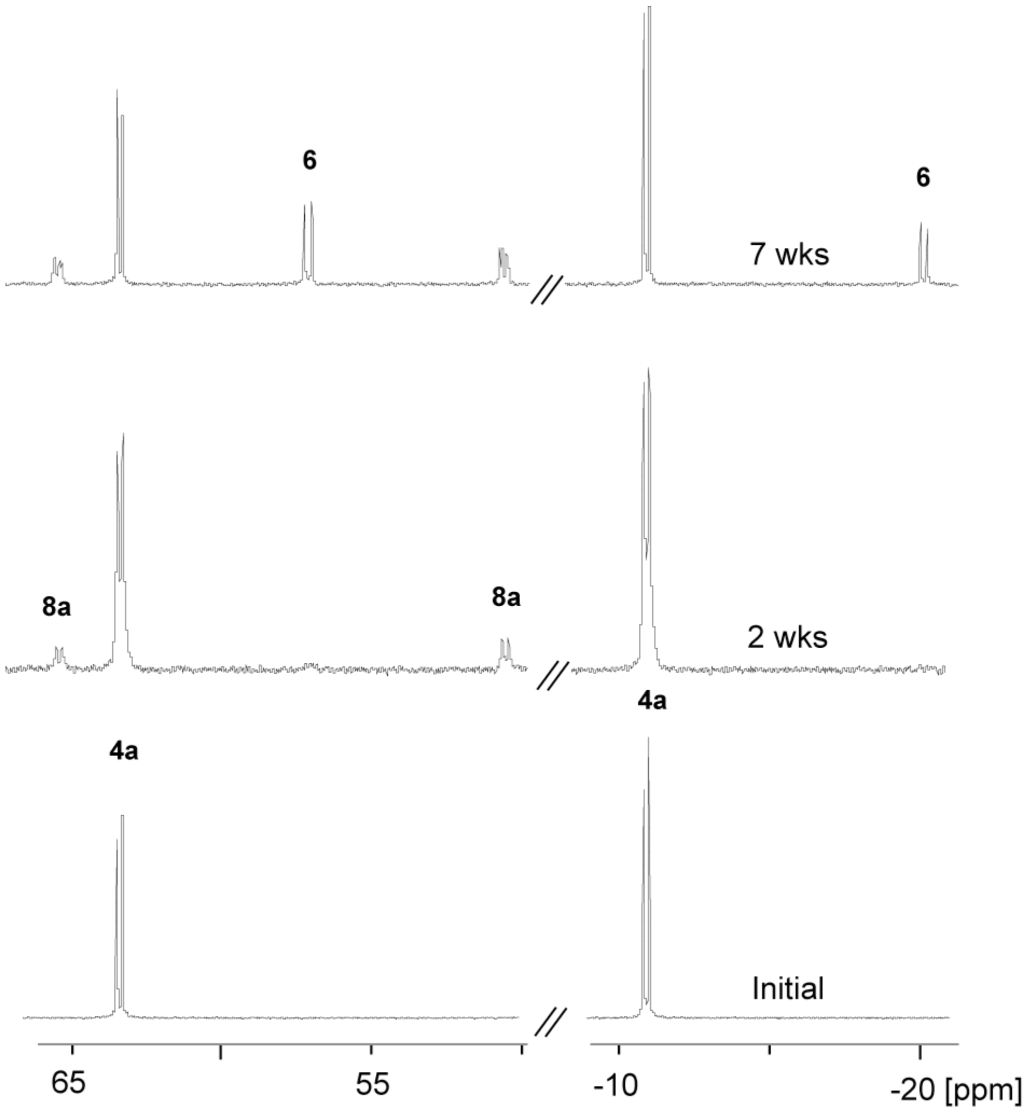

Figure 2.10. $^{31}P\{^{1}H\}$ NMR of ethylene adduct **4a** at 60°C over time, indirectly indicating cycloreversion through formation of the orthometallated product **6**. Formation of suspected vinyl phosphine **8a** is also observed (*vide infra*, Section 3.2.2.3). (121.49 MHz, d_8-toluene, 60°C)

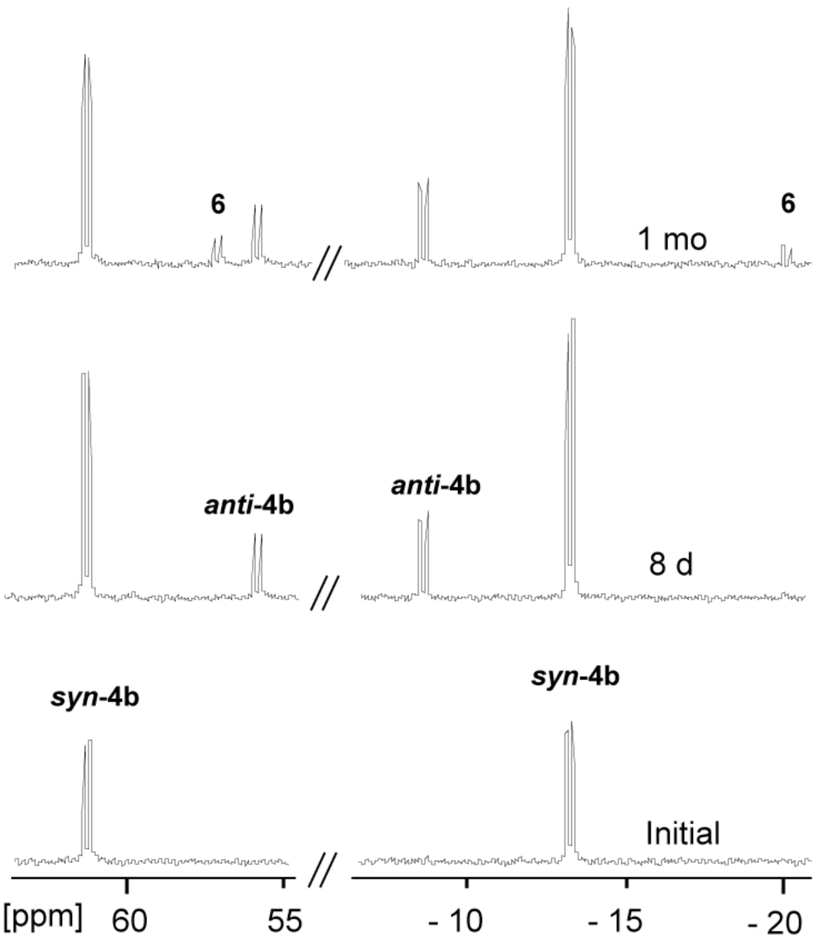

Figure 2.11. $^{31}P\{^{1}H\}$ NMR of acrylonitrile adduct **4b** at 60°C over time, showing *syn* and *anti* isomers, as well as indirectly indicating cycloreversion through formation of the orthometallated product **6**. (121.49 MHz, d_8-toluene, 60°C)

For metallacycle complexes with sterically small or electron-withdrawing substituents at the α-carbon {R = H (**4a**), CN (**4b**)}, cycloreversion was inferred from the formation of the orthometallated isomer **6**, again observed in the $^{31}P\{^{1}H\}$ NMR spectrum, after 10 and 9 days of heating, respectively (Figures 2.10 and 2.11).

The fact that complex **2** is not observed in the cycloreversion of metallacyles bearing electron-withdrawing (CN, **4b**) or sterically small (H, **4a**) substituents, suggests that the equilibrium between cycloaddition and cycloreversion must lie heavily toward the metallacyle products. Furthermore, the faster (occurring within hours, not days) rate of cycloreversion observed for metallacycles with electron-donating (^{n}Bu **4c**, OEt **4d**) and sterically bulky (Ph, **4e**) substituents indicates that the electronic and steric properties of these substituents have an effect on the cycloaddition/cycloreversion equilibria, likely by destabilizing the metallacycle products relative to the starting complex **2**. Unfortunately, the subsequent orthometallation of **2** to **6** prevents further investigation into these equilibria (Figure 2.11).

2.6 Conclusions

The species present in solution during the [2+2] cycloaddition of alkenes to **2** have been investigated in great detail. The relationships between solution isomerization of **2** and formation and cycloreversion of metallacycle products **4a-e** are complex (Figure 2.12). The findings of this chapter give a better understanding of these relationships and how they may affect overall outcomes of desired product formation.

The extent of isomerization of [Ru(η^5-indenyl)(PCy_2)(PPh_3)] (**2**) to the phosphaalkene isomer **3** and the orthometallated isomer **6** was quantified by room-temperature equilibrium- and rate-constants, respectively. The values of K_{eq} (0.1) and k_{OM} (10^{-6} s^{-1}) describe an equilibrium between **2** and **3** heavily weighted to the desired reactive species **2** and a very slow, irreversible solution isomerization of **2** to **6**. K_{eq} and k_{OM} will be used in kinetic (Chapter 3) and reactivity (Chapter 4) studies to quantitatively describe the effects of isomerization on the reactivity of **2**.

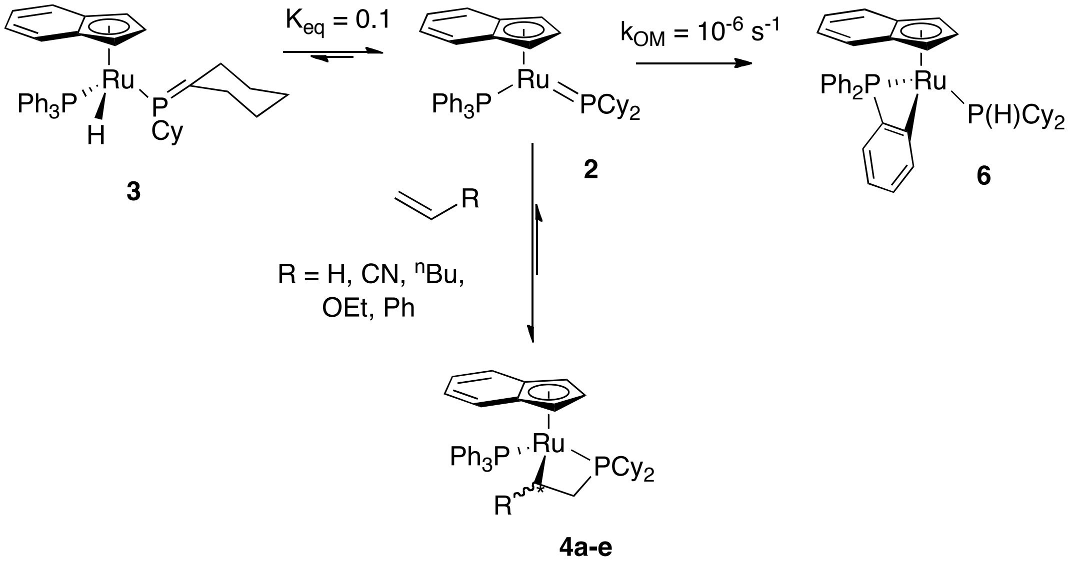

Figure 2.12. Reaction manifold of complex **2** isomerization and [2+2] cycloaddition.

Metallacycle complexes **4c-e** and **5** were synthesized by in-situ synthesis of **2** from the ruthenium-chloride precursor **1a**. This one-step process minimizes irreversible solution isomerization of **2** to **6** and decreases the number of synthetic steps to **4c-e** and **5**, thereby increasing overall product yield. The success of these syntheses is also relevant to the potential use of complex **1a** as a hydrophosphination catalyst. It is notable that **1a** does not react independently with the alkene and alkyne substrates present in these mixtures. This suggests that a potential catalytic cycle involving **1a** as the catalyst precursor will be free of catalyst poisoning by substrate alkenes and alkynes.

The mechanism of [2+2] cycloaddition of alkene substrates to **2** was also further elucidated by a combination of computational prediction by D. Pantazis and low-temperature NMR studies. The observation of the η^2-ethylene adduct **7a** supports the relevance of the model computational reaction trajectory (Figure 2.3) to the [2+2] cycloaddition of ethylene. On the other hand, the model is less applicable to the [2+2] cycloaddition of ethyl vinyl ether, mostly in terms of the relative stability of the η^2

coordination intermediate **7d**. The inability to observe **7d** by low-temperature NMR studies under conditions similar to those in which the ethylene adduct **7a** was observed suggests that **7d** is less stable relative to the starting complex **2** and is not formed in observable quantities prior to subsequent cycloaddition and formation of the metallacycle product **4d**. Alkene substituents are thus found to have an effect on the reaction trajectory of the [2+2] cycloaddition mechanism.

Alkene substituents also affect the observed facile cycloreversion of metallacyle complexes **4a-e**. The increased rate of cycloreversion of metallacycles bearing an electron-donating (^{n}Bu, OEt) or sterically bulky (Ph) substituent at the α-carbon relative to those bearing electron-withdrawing (CN) or sterically small (H) substituents indicates that these metallacyle complexes are destabilized relative to the starting complex **2** by bulky, electron-rich substituents. Thus subtituent effects play a role in the stability and potential reactivity of the metallacyle complexes of the form $[Ru(\eta^5\text{-indenyl})(\kappa^2\text{-R-}\underline{C}HCH_2\underline{P}Cy_2)(PPh_3)]$.

While this chapter explores the reactivities and stabilities of the various species involved in the [2+2] cycloaddition of **2** with unsaturated substrates, the next chapter, Chapter 3, examines the relationships between these species in greater detail through rate constants and activation parameters of [2+2] cycloaddition. Alkene steric and electronic substituent effects on metallacycle formation are also investigated, with specific emphasis on stereoselectivity through computational prediction versus experimental observation and transistion-state effects through Hammett plot analysis.

2.7 Experimental

2.7.1 General Experimental Details

Unless otherwise specified, all preparatory procedures were carried out under a nitrogen atmosphere in an MBraun Unilab 1200/780 glovebox or using conventional Schlenk techniques. All glassware was oven dried at 180 °C, except for quartz cuvettes, which were dried by passing a stream of nitrogen through the interiors. Solvents were dried using an MBraun solvent purification system (SPS) after being sparged with nitrogen for 25 min. Deuterated solvents d_8-toluene and d_6-benzene were purchased from Cambridge Isotope Labs (CIL), dried over sodium/benzophenone, degassed with a minimum of three freeze-pump-thaw cycles and vacuum transferred before use. NMR samples were prepared in either J.Young or flame-sealable tubes. Flame-sealing was conducted with a static vacuum within the NMR tube after degassing by a freeze-pump-thaw cycle. NMR spectra were recorded at ambient temperature, unless otherwise noted, on a Bruker AVANCE 500 operating at 500.13 MHz for ^{1}H, 125.77 MHz for ^{13}C, and 202.46 MHz for ^{31}P, or on a Bruker AVANCE 300 operating at 300.13 MHz for ^{1}H, and 121.49 MHz for ^{31}P. Chemical shifts are reported in ppm and referenced to residual protonated solvent peaks: 7.16 ppm (C_6D_5H), 7.09 ppm (C_7D_7H) for ^{1}H; 128.39 ppm (C_6D_6), 137.86 ppm (C_7D_8) for ^{13}C. All ^{1}H and ^{13}C chemical shifts are reported relative to tetramethylsilane (TMS) and ^{31}P shifts are relative to 85% H_3PO_4(aq). UV-Vis spectra and kinetic data were acquired using a Varian Cary-5 or Varian Cary-100 UV-Vis-NIR spectrophotometer that had been zeroed with toluene. Unless otherwise noted, all kinetics runs were monitored at 590 nm after cuvettes had equilibrated at a stated temperature for 10 minutes.

2.7.2 UV-Vis Monitoring of Conversion of [Ru(η^5-indenyl) (PCy_2)(PPh_3)] (2) to 6 (Orthometallated Isomer)

A solution of [(η^5-indenyl)Ru(PCy_2)(PPh_3)] (**2**) in toluene (0.44 mM) was prepared analytically by adding **2** (3 mg, 0.004 mmol) to a volumetric flask (10 mL) and diluting with toluene. The blue-green solution (3.0 mL) was transferred to a cuvette via syringe and capped with a Teflon cap. Disappearance of **2** (λ = 590 nm) was monitored at 25 °C on a Cary-5 spectrophotometer over 18 hours, with readings taken every 20 min and averaged over 60 s. The average first-order rate constant for the loss of **2** was determined from triplicate runs.

2.7.3 One-Pot Syntheses of Metallacyclic Complexes 4c-e and 5 from [RuCl(η^5-indenyl)($PHCy_2$)(PPh_3)] (1a)

2.7.3.1 One-Pot Synthesis of Metallacycle [(η^5-indenyl)Ru(κ^2-Bu^n-$\underline{C}HCH_2\underline{P}Cy_2$)($PPh_3$)] (4c)

In a Schlenk flask containing [(η^5-indenyl)RuCl($HPCy_2$)(PPh_3)] (100 mg, 0.14 mmol) and $KOBu^t$ (19 mg, 0.17 mmol, 1.2 equiv) an orange suspension/solution was formed by addition of toluene (10 mL). With stirring the solution turned quickly to brown with a blue meniscus, and 1-hexene (52 μL, 0.42 mmol, 3 equiv) was added. The blue solution was stirred over 18 hours to give a clear, yellow solution. The solvent was removed under vacuum and the yellow product was extracted with a 5:1 hexanes:toluene mixture (25 mL) and filtered through Celite. The solvent was removed by vacuum again and the orange-brown oil was triturated with hexanes (10 mL) and pentanes (2 x 10 mL) to give an orange powder of complex **4c**, [(η^5-indenyl)Ru(κ^2-Bu^n-$\underline{C}$HCH$_2$PCy$_2$)(PPh$_3$)] (54 mg, 0.07 mmol, 50%). ^{1}H and ^{31}P NMR shifts were in accordance with those previously reported by Derrah *et al.* for the same complex[3] (Table 2.1).

2.7.3.2 One-Pot Synthesis of Metallacycle [(η^5-indenyl)Ru(κ^2-EtO-$\underline{C}$HCH$_2\underline{P}$Cy$_2$)(PPh$_3$)] (4d)

In a Schlenk flask containing [(η^5-indenyl)RuCl(HPCy$_2$)(PPh$_3$)] (349 mg, 0.49 mmol) and KOBu^t (69 mg, 0.62 mmol, 1.3 equiv) an orange suspension/solution was formed by addition of toluene (10 mL). With stirring the solution turned quickly to brown with a blue meniscus and ethyl vinyl ether (0.14 mL, 1.5 mmol, 3 equiv) was added. The blue solution was stirred over 18 hours to give a clear orange solution. The solvent was removed under vacuum to give an orange residue. This was extracted with hexanes (5 mL), filtered through Celite to remove solid impurities, and the filtrate placed in the freezer (-23^{o}C) for a day. Further filtering with a Hirsch funnel was required to remove oily black precipitate. Orange crystals of **4d**, [(η^5-indenyl)Ru(κ^2-EtO$\underline{C}$HCH$_2\underline{P}$Cy$_2$)(PPh$_3$)] (260 mg, 0.35 mmol, 71%) formed from the filtrate by slow evaporation but were unsuitable for X-ray analysis (too disordered). EI-MS *m/z* (relative intensity): 748 (21%) [M$^+$], 674 (27%) [M$^+$ - CH$_2$CHOCH$_2$CH$_3$], 548 (31%) [M$^+$ - PCy$_2$], 479 (62%) [M$^+$ - Cy$_2$PCH$_2$CHOCH$_2$CH$_3$]. Anal. calcd for $C_{43}H_{52}P_2ORu$: C, 69.06; H, 7.01. Found: C, 69.05; H, 7.23. mp: 128-131°C (dec). See Tables 2.3 to 2.5 for full NMR characterization.

2.7.3.3 One-Pot Synthesis of Metallacycle [(η^5-indenyl)Ru(κ^2-Ph-$\underline{C}HCH_2\underline{P}Cy_2$)($PPh_3$)] (4e)

In a Schlenk flask containing [(η^5-indenyl)RuCl($HPCy_2$)(PPh_3)] (307 mg, 0.43 mmol) and $KOBu^t$ (60 mg, 0.50 mmol, 1.2 equiv) an orange suspension/solution was formed by addition of toluene (10 mL). With stirring the solution turned quickly to brown with a blue meniscus and styrene (0.16 mL, 1.39 mmol, 3 equiv) was added via gas-tight syringe. The blue solution was stirred over 18 hours to give a clear, orange solution. The solution was filtered through Celite and the solvent was removed from the filtrate to give a red-orange powder of complex **4e**, [(η^5-indenyl)Ru(κ^2-Ph-$\underline{C}HCH_2PCy_2$)(PPh_3) (273 mg, 0.35 mmol, 81% crude yield). A crude sample (120 mg, 0.15 mmol) was recrystallized from dichloromethane (5 mL) by slow layer diffusion of acetonitrile (~50 mL) to give pure **4e**, [(η^5-indenyl)Ru(κ^2-Ph-$\underline{C}HCH_2\underline{P}Cy_2$)($PPh_3$)] (94 mg, 0.12 mmol, 80% yield). EI-MS *m/z* (relative intensity): 675 (24%) [M^+ - Ph-$CHCH_2$], 583 (14%) [M^+ - PCy_2], 238 (23%) [M^{2+} - PCy_2 – Ph-$CHCH_2$]. Anal. calcd: C, 72.38; H, 6.72 Anal. found: C, 71.85; H, 6.81. mp 164°C. Full x-ray crystallographic analysis is included in Appendix A. See Tables 2.3 to 2.5 and Appendix C for full NMR characterization.

2.7.3.4 One-Pot Synthesis of Metallacycle [(η^5-indenyl)Ru(κ^2-Ph-$\underline{C}=CH_2\underline{P}Cy_2$)($PPh_3$)] (5)

In a Schlenk flask containing [(η^5-indenyl)RuCl($HPCy_2$)(PPh_3)] (781 mg, 1.1 mmol) and $KOBu^t$ (148 mg, 1.3 mmol, 1.2 equiv) an orange suspension/solution was formed by addition of toluene (20 mL). With stirring the solution turned quickly to brown with a blue meniscus and neat phenylacetylene (0.36 mL, 3.3 mmol, 3 equiv) was added via gas-tight syringe. The blue solution was stirred overnight to give a clear, orange solution. The solvent was removed under vacuum and the yellow product was extracted with a 5:1 hexanes:toluene mixture (2 x 25 mL) and filtered through Celite. The solvent was removed by vacuum again and the orange oil was triturated with hexanes (3 x 30 mL) to give a bright orange-yellow powder of complex **5** (735 mg, 0.94 mmol, 86%). ^{1}H and ^{31}P NMR shifts were in accordance with those previously reported by Derrah *et al.* for the same complex[5].

2.7.4 Low Temperature NMR Studies of [2+2] Cycloaddition Reactions

2.7.4.1 Low Temperature [2+2] Cycloaddition of Ethylene to 2

A dark blue NMR sample of **2** (12 mg, 0.02 mmol) in d_8-toluene (0.6 mL) was prepared in a J.Young tube and FPT degassed (x 1). The headspace of the tube was evacuated and backfilled with ethylene (1 atm) and the tube was sealed. The blue sample with a thin yellow top layer was quickly cooled to -80°C in a dry ice/acetone bath. The sample rapidly turned dark red upon inversion (x 1) and was quickly placed in a pre-cooled (193 K) 500 MHz NMR instrument. Three ruthenium-phosphorus species were observed in solution by ^{31}P{^{1}H} NMR: the phosphaalkene isomer **3** of the starting complex {61.8 ppm (*P*Ph$_3$, br s, $\omega_{1/2}$ = 61 Hz)}, the metallacyle product **4a** {-10.5 (*P*Cy$_2$, br s) and 63.2 ppm (*P*Ph$_3$, br s, $\omega_{1/2}$ = 51 Hz)}, and the intermediate **7a** {55.4 (*P*Ph$_3$, br s, $\omega_{1/2}$ = 45 Hz) and 27.6 ppm (*P*Cy$_2$, br s, $\omega_{1/2}$ = 152 Hz)}. The presence of all three species in solution complicated the ^{1}H NMR spectrum and prevented the full characterization of the intermediate **7a** by ^{1}H NMR. Upon removing from the cooled instrument and warming to room temperature, the sample turned from dark red to a clear, bright yellow, indicative of full conversion to the metallacyclic product **4a**, which was confirmed by $^{31}P\{^{1}H\}$ NMR.

2.7.4.2 Low Temperature [2+2] Cycloaddition of Ethyl Vinyl Ether to 2

A dark blue NMR sample of **2** (15 mg, 0.02 mmol) in *d$_8$*-toluene (0.6 mL) was prepared and capped with a septum cap. A reference $^{31}P\{^{1}H\}$ NMR spectrum was obtained on a 500 MHz instrument, whereupon both instrument and sample were cooled to 193 K and the instrument re-tuned and shimmed at the lower temperature. The sample was removed from the instrument and cooled (4°C) ethyl vinyl ether (105 μL) was injected via gas-tight syringe. The sample was inverted x3 to mix and quickly returned to the cooled instrument. $^{31}P\{^{1}H\}$ NMR spectra (256 scans) were obtained every 15 minutes for 1 hour each at the initial temperature of 193 K, 200 K, 210 K, 220 K and at 230 K. At 230 K, slow conversion of **2** to metallacyle product **4d** began to be observed.

2.7.5 Monitoring of Cycloreversion of Metallacycles 4a-e by NMR

Solutions of each metallacyclic complex **4a-e** (5 to 9 mg) in *d$_8$*-toluene (0.7 mL) were placed in NMR tubes. The tubes were flame-sealed and NMR spectra (^{1}H and ^{31}P $\{^{1}H\}$, 300 MHz) of the yellow-orange solutions were acquired. The samples were placed in a 60°C (±5°C) oil bath and further spectra (^{1}H and ^{31}P $\{^{1}H\}$, 300 MHz) were obtained after varying amounts of time (Figures 2.7 - 2.11). Relative amounts of all phosphorus-containing species in solution were determined using ^{31}P $\{^{1}H\}$ NMR shifts.

2.7.6 ^{1}H, ^{13}C{^{1}H} and ^{31}P{^{1}H} NMR Data Tables for Compounds 4d-e

Table 2.3. ^{31}P{^{1}H} NMR data for metallacycles **4d-e** at 300K: shift in ppm (multiplicity, J_{PP} in Hz)

Compound	Number	Ru-PCy$_2$-	Ru-PPh$_3$
[Ru(η^5-indenyl)(κ^2-EtO-$\underline{C}$HCH$_2\underline{P}$Cy$_2$)(PPh$_3$)] *syn*	***syn*-4d**	-9.8 (d, 20)	64.0 (d)
[Ru(η^5-indenyl)(κ^2-EtO-$\underline{C}$HCH$_2\underline{P}$Cy$_2$)(PPh$_3$)] *anti*	***anti*-4d**	-7.5 (d, 28)	61.5 (d)
[Ru(η^5-indenyl)(κ^2-Ph-$\underline{C}$HCH$_2\underline{P}$Cy$_2$)(PPh$_3$)] *syn*	***syn*-4e**	-21.9 (d, 21)	63.6 (d)
[Ru(η^5-indenyl)(κ^2-Ph-$\underline{C}$HCH$_2\underline{P}$Cy$_2$)(PPh$_3$)] *anti*	***anti*-4e**	-10.3 (d, 27)	59.0 (d)

Table 2.4. 500.13 MHz ^{1}H NMR data for metallacycles **4d-e** at 300K: δ in ppm (multiplicity, J_{avg} or $\omega_{1/2}$ in Hz, RI,)

	η^5 - C_9H_7					
Compound	H_7, H_4	H_6, H_5	H_2	H_3, H_1	PPh_3	Others
***syn*-4d** *d*$_6$-benzene	7.71 (dd, 1H, 1 8) 6.20 (dd, 1H, 1 8)	6.94 (t, 2H, 7, overlaps with H_6 anti) 6.70 (t, 1H, 7)	5.91 (t, 1H, 3)	4.25 (s, 1H) 5.75 (s, 1H)	H_o 7.44 (br, 6H, 34) H_m, H_p 7.15-6.97 (br om, ~16H, overlaps with anti H_m, H_p)	$CH_3CH_2O\underline{C}HCH_2$: 4.76 (ddd, 1H, 6 11 19, H_A), 3.49 (dq, 1H, 2 7, CH_2), 3.40 (dq, 1H, 2 7, overlaps with H_C and CH_2 *anti*, CH_2) ~3.42 (om, overlaps with CH_2, H_C), 1.66 (om, overlaps with Cy, H_B), 1.26 (t, 7, overlaps with Cy) Cy (PCy_2): 2.81 (d, 1H, 13, PCH), 2.35 (t, 1H, 11), 2.15 (d, 1H, 13, PCH), 1.99 (d, 1H, 13), 0.31 (q, 1H, 12), other peaks indistinguishable from other isomer
***anti*-4d** *d*$_6$-benzene	7.60 (dd, 1H, 1 8) 6.43 (dd, 1H, 1 8)	6.94 (t, 2H, 7, overlaps with H_6 syn) 6.66 (t, 1H, 8)	5.52 (t, 1H, 3)	4.19 (s, 1H) 5.48 (s, 1H)	H_o 8.24 (br, 2H, 43) 7.89 (br, 2H, 43) 6.75 (br, 2H, 43, overlaps with H_5) H_m 7.21 (br, ~2H, ~40) H_m, H_p 7.15-6.97 (br om, ~16H, overlaps with syn H_m, H_p)	$CH_3CH_2O\underline{C}HCH_2$: 5.10 (dd, 1H, 7 10, H_D), 3.71 (ddd, 1H, 3 6 13, H_C), 3.42 (dq, 1H, 2 7, overlaps with *syn* CH_2 and H_C, CH_2), 3.29 (dq, 1H, 2 7, CH_2), 1.82 (om, overlaps with Cy), 1.41 (t, 7, overlaps with Cy) Cy (PCy_2): 2.28 (d, 1H, 13, PCH), 2.05 (d, 1H, 13, PCH), 0.42 (q, 1H, 12), other peaks indistinguishable from other isomer
***syn*-4e** *d*$_8$-toluene	7.40 (d, 8, 1H) 5.80 (d, 8, 1H)	6.81 (om, 5H, overlaps with H_o, H_m of styrene) 6.62 (t, 7, 1H)	4.22-4.19 (m, 1H)	4.94 (s, 1H) 4.04 (s, 1H)	H_o 7.84-7.54 (br, 5H) H_m, H_p 6.99-6.88 (om, 9H, overlaps with H_6 anti)	$CHCH_2$: 3.58 (ddd, 3 9 12, 1H H_C), 3.26 (ddd, 3 11 15, 1H, H_A), 2.30 (om, 1H, H_B, overlaps with H_B anti) Ph: 7.39-7.21 (om, 2H, H_p, overlaps with H_p anti), 6.81-6.78 (om, 5H, H_o, H_m, overlaps with H_6) Cy (PCy_2): 2.93 (br, 28), 2.64-2.56 (m), other peaks overlapping with other isomer
***anti*-4e** *d*$_8$-toluene	7.60 (d, 8, 1H) 5.99 (d, 8, 1H)	6.91 (t, 8, 1H) 6.59 (t, 7, 1H)	5.73-5.70 (m, 1H)	5.58 (s, 1H) 3.94 (s, 1H)	H_o, H_m, H_p 7.17-7.00 (om, 15H)	$CHCH_2$: 4.12 (ddd, 3 5 12, 1H, H_D), 3.42 (ddd, 6 7 13, 1H, H_C), 2.35 (dt, 13 8, 1H, H_B) Ph: 7.34 (t, 8, 1H, H_p), 7.30-7.20 (br m, 2H, H_o), 6.43-6.28 (br, 2H, H_m) Cy (PCy_2): 2.73-2.65 (m), 2.25-2.17 (m), other peaks overlapping with other isomer

Table 2.5. 125.77 MHz $^{13}C\{^1H\}$ NMR data for metallacycles **4d-e** at 300K: δ in ppm (multiplicity, J_{avg} or $\omega_{1/2}$ in Hz, RI,)

	η^5 - C_9H_7							
Compound	C_6, C_5	C_7, C_4	C_{3a}, C_{7a}	$\Delta\delta(C_{3a,7a})^b$	C_2	C_3, C_1	PPh_3	Others
***syn*-4d** d_6-benzene	121.2 (s) 124.1 (s)	124.4 (s) 120.6 (s)	108.0 (s) 110.5 (s)	-21.5 (av)	101.1 (s)	74.0 (d, 11) 66.5 (d, 10)	C_i 138.6 (br, 73) C_o 135.2 (br, 30) C_m 127.7 (d, 9) C_p 129.2 (s)	$CH_3CH_2O\underline{C}HCH_2$: 64.4 (s, CH_2), 59.8 (dd, 11 35, C_A), 43.7 (d, 5, C_B), 16.5 (s) PCy_2: PCH 44.4 (d, 14), 31.2 (d, 3) Others 42.8 (d, 8), 39.4 (d, 17), other peaks are indistinguishable from *anti* isomer
***anti*-4d** d_6-benzene	121.6 (s) 124.0 (s)	123.1 (s) 119.9 (s)	108.8 (s) 112.4 (s)	-20.1 (av)	97.8 (s)	75.9 (d, 10) 63.4 (d, 10)	C_i 135.6 (br, 69) C_o 127.3 (br, 26) C_m 128.9 (d, 12) C_p 128.7 (s)	$CH_3CH_2O\underline{C}HCH_2$: 65.1 (s, CH_2), 55.6 (dd, 8 24, C_A), 43.5 (d, 6, C_B), 16.3 (s) PCy_2: PCH 31.6 (s), 31.0 (s) Others 29.6 (s), other peaks are indistinguishable from *syn* isomer
***syn*-4e** d_8-toluene	121.6 (s) 124.0 (s)	126.1 (s) 121.4 (s)	109.2 (s) 104.6 (s)	-23.8 (av)	103.0 (s)	68.5 (d, 9) 70.6 (d, 9)	C_i 135.5 (br, 29) C_o 134.2 (d, 11) C_m 125.4 (s) C_p 129.0 (s)	$CHCH_2$: 39.8 (d, 29, C_B), 0.7 (dd, 8 28, C_A) Ph: 162.0 (s, C_i), 127.7 (br om, C_o), 124.6 (s, C_p), 121.9 (s, C_m) PCy_2: PCH 48.3 (dd, 3 12), 43.3 (d, 4) Others 31.2 (s), 30.3 (d, 8), 30.2 (s), 30.1 (s), 28.9 (d, 7), 28.7 (d, 11), 27.7 (d, 7), 26.8 (s)
***anti*-4e** d_8-toluene	121.5 (s) 123.9 (s)	124.3 (s) 120.4 (s)	110.7 (s) 104.3 (s)	-23.2 (av)	96.8 (s)	64.6 (d, 11) 74.2 (d, 11)	C_i 138.8 (br, 24) C_o 133.6 (d, 10) C_m 128.3 (s) C_p 129.2 (s)	$CHCH_2$: 38.4 (d, 30, C_B), -1.4 (dd, 8 27, C_A) Ph: 156.6 (dd, 4 20, C_i), 128.5 (s, C_p), 127.3 (br om, C_o), 126.5 (s, C_m) PCy_2: PCH 43.4 (d, 6), 41.4 (d, 15) Others 31.0 (d, 3), 30.0 (s), 29.8 (s), 29.3 (d, 8), 28.4 (d, 11), 27.9 (d, 11), 27.4 (d, 8), 26.6 (s)

b: $\Delta\delta(C_{3a,7a}) = \delta(C_{3a,7a}(\eta\text{-indenyl complex}))-\delta(C_{3a,7a}(\eta\text{-sodium indenyl}))$. $\delta(C_{3a,7a})$ for sodium indenyl = 130.7 ppm (EJD p 188)

2.8 References

(1) Derrah, E. J.; Pantazis, D. A.; McDonald, R.; Rosenberg, L. *Organometallics* **2007**, *26*, 1473.

(2) Anslyn, E. V.; Dougherty, D. A. *Modern Physical Organic Chemistry*; University Science Books, 2006.

(3) Derrah, E. J.; Pantazis, D. A.; McDonald, R.; Rosenberg, L. *Angew. Chem., Int. Ed.* **2010**, *49*, 3367.

(4) Faller, J. W.; Crabtree, R. H.; Habib, A. *Organometallics* **1985**, *4*, 929.

(5) Derrah, E. J.; McDonald, R.; Rosenberg, L. *Chem. Commun.* **2010**, *46*, 4592.

(6) Hoyle, M.-A. M.; Pantazis, D. A.; Burton, H. M.; McDonald, R.; Rosenberg, L. *Organometallics* **2011**, *30*, 6458.

Chapter 3 Metallacycle Selectivity: Steric and Electronic Effects

3.1 Introduction

The previous chapter focused on identifying and characterizing the various species involved in the [2+2] cycloaddition of terminal alkenes to the Ru-P π-bond of complex **2**. This chapter examines the [2+2] cycloaddition mechanism in greater detail, elaborating on the formation of *syn* and *anti* diastereomers of the metallacycle products as well as investigating the steric and electronic effects of alkene substituents on stereo- and regioselectivity of metallacycle formation.

Variable stereoselectivity has been previously reported by Derrah *et al.* [1] in the formation of these metallacycle complexes. Further investigation through computational DFT analysis of metallacycle diastereomers, experimental [2+2] cycloaddition rate constant and activation parameter determination, as well as investigation by Hammett plot, described in detail in the following sections, has led to a greater understanding of the sources of this selectivity. As a good catalyst is both predictable in its product outcome and applicable to a wide variety of substrates, these studies are beneficial to the overall goal of the development of a stereoselective hydrophosphination catalyst.

3.2 Kinetic and Thermodynamic Isomer Distributions

3.2.1 Isomer Distributions: Experimental

As reported previously by Derrah *et al*[1], concerted [2+2] cycloadditions of substituted alkenes (acrylonitrile, 1-hexene) at the ruthenium-phosphorus π-bond of complex **2** result in varying mixtures of diastereomers exhibiting chirality at both the ruthenium centre and at the α-carbon of the metallacycle (**4b-c**) (Table 3.1): this was described in section 1.3.1. In this work, these syntheses were repeated with the above-mentioned alkenes and extended to include both ethyl vinyl ether and styrene to observe the diastereomer distribution of metallacycles resulting from the [2+2] cycloaddition of alkenes with electron-donating (OEt, **4d**) and aromatic (Ph, **4e**) substituents.

Table 3.1. Isomer Distributions of Substituted Metallacycles **4b-e**

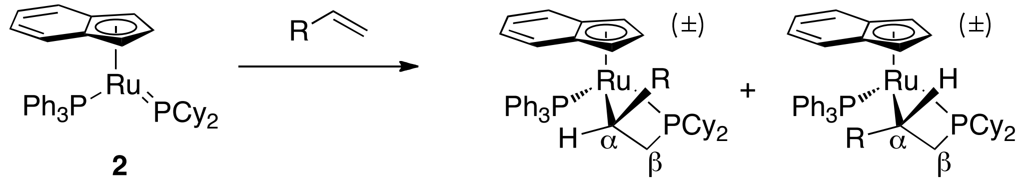

2

***syn*-4(b-e)**

***anti*-4(b-e)**

<table>
<tr><td rowspan="2">Metallacycle
(R =)</td><td rowspan="2">Kinetic
<i>syn:anti</i>
distribution
observed</td><td colspan="4">Thermodynamic <i>syn:anti</i> distribution predicted by ground-state energies using computational models[a]</td></tr>
<tr><td colspan="2">Model A[b]</td><td colspan="2">Model B[c] (simplified)</td></tr>
<tr><td>4b (CN)</td><td>1 : 0</td><td rowspan="4">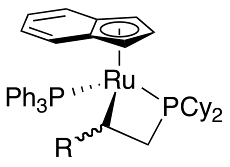</td><td>1 : 1</td><td rowspan="4">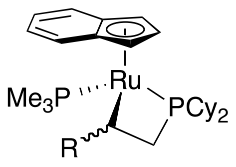</td><td>1 : 37</td></tr>
<tr><td>4c (^{n}Bu)</td><td>1 : 0</td><td>-</td><td>1 : 32</td></tr>
<tr><td>4d (OEt)</td><td>1 : 1</td><td>1 : 1</td><td>1 : 7</td></tr>
<tr><td>4e (Ph)</td><td>1 : 0</td><td>-</td><td>1 : 51</td></tr>
</table>

(a) Based on relative energies obtained by DFT calculations performed by D. Pantazis.

(b) 2010 values reported by Derrah *et al.* [1] (level: PBE-DFT (TZVP)).

(c) From relative energies determined by D. Pantazis[2] (unpublished results) from a simplified (using PMe_3 in place of PPh_3) computational model (level: PBE-D3, DKH2).

Regiochemistries of [2+2] cycloaddition of all metallacycles synthesized in this work (**4b-e**), including both *syn* and *anti* diastereomers, were determined using the relative long-range ^{31}P-^{1}H NMR correlations of the two coordinated phosphines to the metallacycle β-protons, identified by a combination of 2D ^{1}H-^{13}C HSQC NMR and ^{31}C DEPT NMR. $^{31}P\{^{1}H\}$-^{1}H HMBC NMR cross peaks between the metallacycle β-protons and metallacyclic -*P*Cy$_2$- centres had consistently stronger correlations with one another than that between the β-protons and *P*Ph$_3$ phosphorus centres, indicating that the non-substituted β-carbon were in closer proximity to the metallacyclic *–PCy*$_2$- centre than to *P*Ph$_3$. In this way regiochemistry was confirmed for both *syn* and *anti* isomers of all metallacycles **4b-e**.

Syn and *anti* configurations of substituents at the α-carbon in the product metallacycles **4b-e** showed distinct $^{31}P\{^{1}H\}$ NMR signals, which correlated cleanly with distinct ^{1}H signals in ^{1}H-$^{31}P\{^{1}H\}$ HSQC and HMBC experiments (Tables 2.3-2.5). Stereochemistry at each α-carbon was confirmed by 2D NMR NOESY correlation (Appendix C) between the metallacycle α-proton (H_a) and coordinated triphenylphosphine *ortho*-protons (H_O) (example: R = Ph, Figure 3.1). As noted above in Table 3.1, exclusive formation of the *syn* isomer was observed for the previously uncharacterized metallacycle **4e** (R = Ph). Full NMR characterization (^{1}H, ^{13}C, $^{31}P\{^{1}H\}$), including stereochemical assignment by 2D NMR, was conducted for ***syn*-4e** with NMR samples of pure *syn* in solution. To fully characterize the *anti* isomer of **4e**, NMR spectra (Appendix C) were obtained of a mixture of ***syn*-4e** and ***anti*-4e**, which was formed by solution equilibration of the pure *syn* NMR sample before sample degradation occurred (*vide infra*). NMR signals due to the *syn* isomer were subtracted from the spectra of the mixture and the remaining signals were assigned to the *anti* isomer. Figure 3.1 shows a partial view of the ^{1}H NOESY spectrum of the *syn*-*anti* mixture, used to assign stereochemistry at the α-carbon of the metallacycle. Full NMR characterization of ***syn*-** and ***anti*-4d** (R = OEt) isomers (Tables 2.3 - 2.5, Appendix C) was conducted with mixtures of the isomers only, as they were formed in a 1 : 1 ratio (Table 3.1) and could not be isolated from one another. Metallacycles **4b** (R = CN) and **4c** (R = ^{n}Bu) had been fully characterized by Derrah[1] previously.

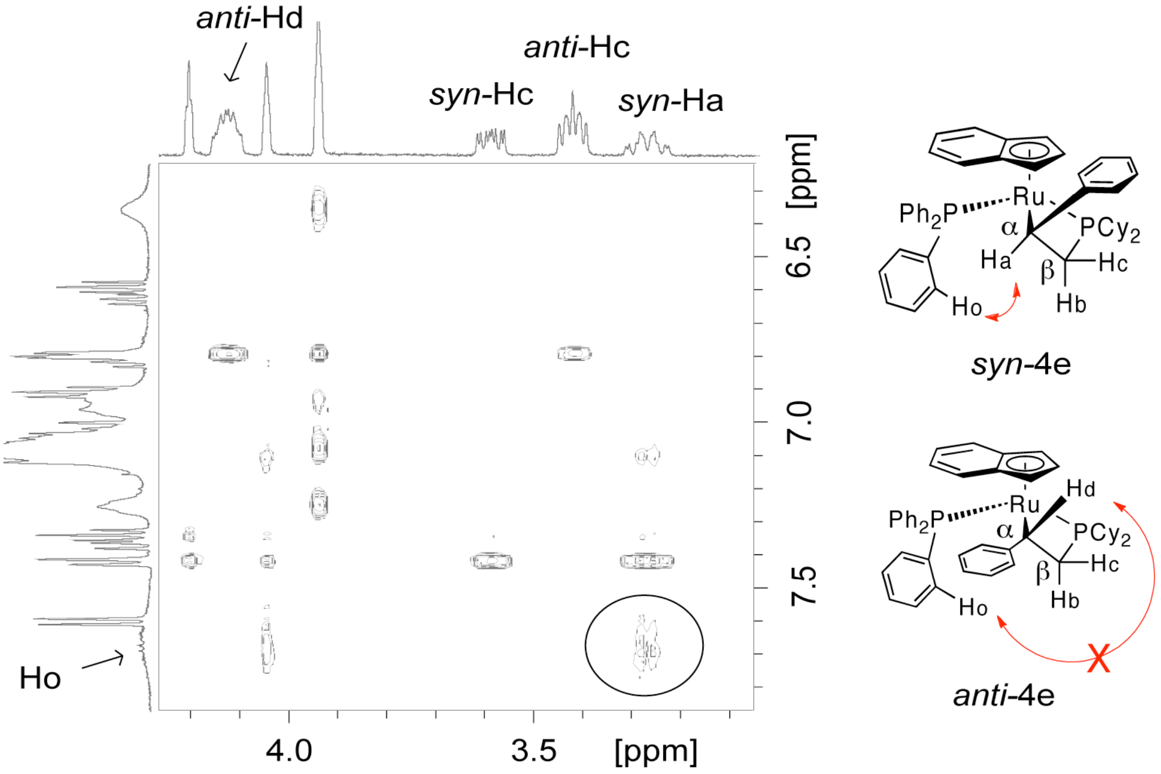

Figure 3.1. Partial ^{1}H NOESY NMR spectrum of a mixture of *syn* and *anti* **4e** shows stereochemical determination of ***syn*-4e** from $H_a \rightarrow H_O$ correlation. (500.13 MHz, d_6-benzene)

[2+2] cycloadditions of acrylonitrile, 1-hexene and styrene with **2** resulted in the exclusive formation of the *syn* isomer of all three metallacycles **4b**, **4c**, and **4e**, respectively (Table 3.1). Cycloadditions of **2** with ethyl vinyl ether, however, resulted in a *syn*:*anti* isomer distribution of 1:1.

Electronic effects of the strongly electron-donating ethoxy substituent could be responsible for this discrepancy in observed isomer distribution. However, isomer distributions of 1:0 *syn*:*anti* are observed for metallacycles with both the strongly electron-withdrawing cyano susbtituent (**4b**) and the mildly electron-donating *n*-butyl substituent (**4c**) (Hammett sigma parameter: used to quantify strength of electron donation, σ_p = -0.16 for –^{n}Bu and -0.24 for –OEt)[3], which argues against electronic control of selectivity. The selectivity observed for the 1-hexene cycloaddition, which is notably absent for the cycloaddition of ethyl vinyl ether, could be due to differences between steric bulk at the primary atom of ethoxy and *n*-butyl substituents (Taft size parameter, E_s: used to quantify steric bulk at the primary atom of a substituent. E_s = +0.99 for –OEt and -0.39 for –^{n}Bu)[4]. In summary, as a preliminary hypothesis, *syn* isomer formation appears to be favoured by both bulky (^{n}Bu, Ph) and electron-deficient (CN) alkene substrates. A lack of stereoselectivity (i.e. a 1:1 *syn*:*anti* isomer ratio) is observed when these driving factors are not present, as with ethyl vinyl ether. Further examination was required to better understand both steric and electronic effects of alkene substitution on stereoselectivity in these cycloaddition reactions.

3.2.1.1 Monitoring of $[\mathrm{Ru}(\eta^5\text{-indenyl})(\kappa^2\text{-EtO}\underline{\mathrm{C}}\mathrm{HCH_2}\underline{\mathrm{P}}\mathrm{Cy_2})(\mathrm{PPh_3})]$ (4d) Isomer Formation

To confirm that **4d** was formed in a 1:1 *syn*:*anti* ratio, as opposed to a 1:0 ratio followed by rapid solution epimerization of *syn* to *anti*, the [2+2] cycloaddition between ethyl vinyl ether and **2** was monitored by $^{31}P\{^1H\}$ NMR. The simultaneous formation of both *syn* and *anti* isomers was observed along with concurrent loss of starting complex **2** (Figure 3.2). Although this observation supports an initial isomer distribution of 1:1, rapid equilibration of isomers from an alternate initial distribution remains a possibility if the rate of epimerization is greater than that of cycloaddition (*vide infra*). Rates and mechanism of metallacycle epimerization should be subject to further investigation to definitively determine the process of isomer ratio formation.

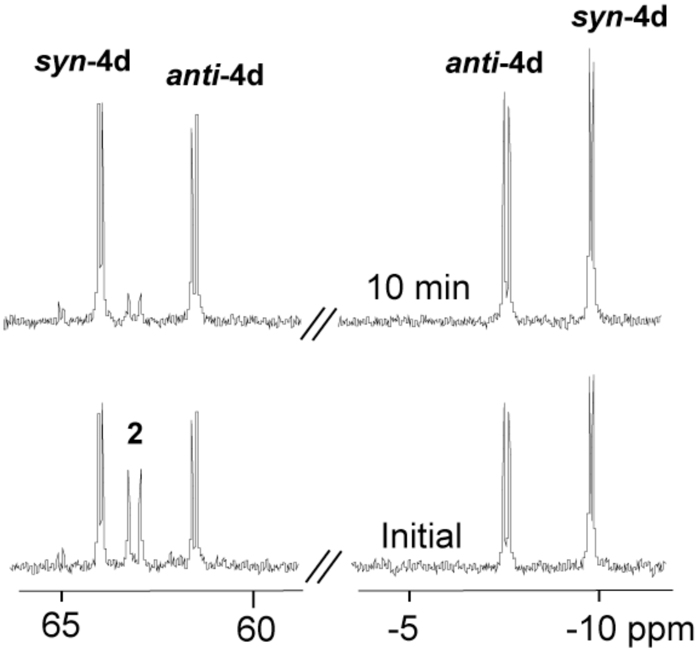

Figure 3.2. Formation of ethyl vinyl ether adduct **4d** from **2** in a 1:1 *syn*:*anti* ratio monitored by $^{31}P\{^1H\}$ NMR (d_6-benzene).

3.2.2 Isomer Distributions: Computational

DFT calculations performed by D. Pantazis[1] using a non-simplified model system (**A**, Table 3.1), predict the *syn* and *anti* isomers of the ethyl vinyl ether adduct, **4d**, to be isoenergetic, correlating with experimental observations of a 1:1 *syn*:*anti* ratio of product formation (Table 3.1). However, *syn* and *anti* isomers of the acrylonitrile adduct **4b** were also found to be isoenergetic by the same calculations[1], though they were observed to form in a 1:0 *syn*:*anti* ratio. These DFT findings suggest that isomer product distributions are kinetically controlled, at least for the acrylonitrile adduct **4b**.

More recent (December 2011), unpublished DFT analyses[2] of the stereoisomers of metallacycles **4b-e** by D. Pantazis using a simplified model system (**B**, Table 3.1) show the *anti* isomer to be thermodynamically favoured over *syn* in all cases. Using a computational model containing PMe_3 in place of PPh_3 to reduce computing time, *anti* isomers were found to be 8.9 (**4b**, R = CN), 8.5 (**4c**, R = ^{n}Bu), 4.7 (**4d**, R = OEt), and 9.7 $kJ \cdot mol^{-1}$ (**4e**, R = Ph) lower in energy than their *syn* counterparts. Using equation 3.1, the Boltzmann distribution[5] for the ratio of the populations of molecules,

$$N_i/N_j = \exp[-(E_i-E_j)/RT] \qquad \ldots\ldots (3.1)$$

where N = number of molecules in a given energy state, E = electronic energy of a given state, R is the ideal gas constant, and T is the absolute temperature, thermodynamic *syn*:*anti* isomer distributions were calculated for metallacycles **4b-e** (Table 3.1). Strongly *anti*-favouring product distributions of 1:37, 1:32 and 1:51 *syn*:*anti* for acrylonitrile (**4b**), 1-hexene (**4c**) and styrene (**4e**) adducts also show a marked difference from the experimentally observed *syn* selectivity for these three metallacycles. On the other hand, the calculated 1:7 *syn*:*anti* thermodynamic isomer distribution for the ethyl vinyl ether adduct **4d** still favours the *anti* isomer, but is much closer to the experimentally observed 1:1 ratio. Again, the discrepancy between experimentally observed and computationally predicted isomer distributions (though different from previous predictions by use of a simplified model system) suggest that metallacycle stereoselectivity is kinetically-controlled for [2+2] cycloadditions with these alkenes, though less pronounced for ethyl vinyl ether.

These recent predicted thermodynamic isomer distributions echo the experimental observations in that stereoselectivity is apparent for the electron-withdrawing and sterically bulky alkene substituents CN, Ph, and ^{n}Bu, but not as pronounced for the sterically small and electron-donating ethoxy substituent. The major difference is that stereoselectivity favours the *syn* isomer kinetically (by experimental observation), and the *anti* isomer thermodynamically (by computational prediction) for metallacycles **4b**, **4c** and **4e**.

3.2.3 Attempts to Experimentally Determine Metallacycle Thermodynamic Isomer Distributions

In an attempt to clarify the uncertainty surrounding the experimentally-determined initial product distributions (assumed to be kinetic) versus the two sets of computationally-predicted thermodynamic isomer distributions, studies were done to experimentally determine the thermodynamic isomer distributions of metallacycles **4b-e**.

Initial experiments were conducted by heating NMR samples of each metallacycle in d_8-toluene to 60°C. Unfortunately, slow conversion to the orthometallated complex **6** occurred through facile cycloreversion to **2** and prohibited the eventual equilibration of metallacycle isomers (see Chapter 2, Section 2.5). Subsequent studies were conducted by heating NMR samples of the metallacycles **4b-e** in the presence of excess alkene (50 equivalents), successfully preventing cycloreversion to **2** and demonstrating that metallacycle isomer epimerization could occur in the absence of cycloreversion. The following subsections describe the results of these studies.

3.2.2.1 [Ru(η^5-indenyl)(κ^2-NC$\underline{C}$HCH$_2\underline{P}$Cy$_2$)(PPh$_3$)] (4b)

A sample of **4b** and excess acrylonitrile in *d$_8$*-toluene was heated at 60°C and *syn* and *anti* isomer ratios were monitored by $^{31}P\{^1H\}$ NMR. Over a period of 4 months ***syn*-4b** slowly converted to ***anti*-4b** to give a steady ratio of 4:1 *syn*:*anti* that persisted over the next two months of monitoring (Figure 3.3).

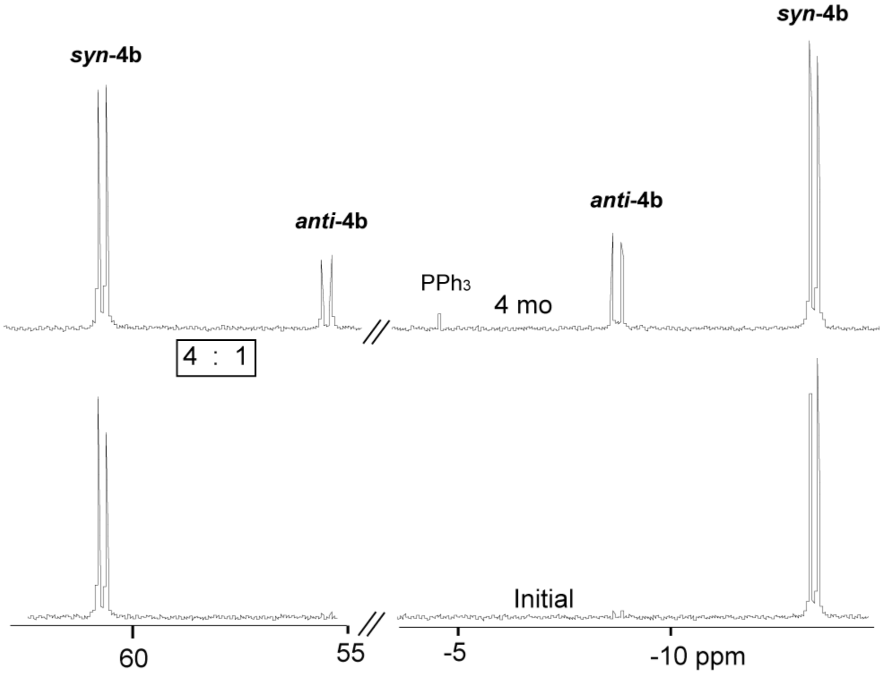

Figure 3.3. Thermal equilibration of ***syn-*** and ***anti*-4b** at 60°C in the presence of 50 equivalents acrylonitrile. A small amount of free triphenylphosphine is visible after 4 months. $^{31}P\{^1H\}$ NMR, 121.46 MHz, *d$_8$*-toluene.

The 4:1 *syn*:*anti* ratio of **4b** represents the experimentally-determined thermodynamic distribution of metallacycle isomers in solution and in the presence of excess acrylonitrile. This experimental observation is in closer agreement with DFT predictions of a 1:1 isomer ratio than those predicting the favouring of the *anti* isomer in a 1:37 ratio (Table 3.1). Since the steric bulk of the PPh_3 ligand was not accounted for by PMe_3 in the model used for this second DFT prediction, this suggests that steric interactions with the coordinated triphenylphosphine must play a role in the destabilization of the anti isomer in complex **4b**, resulting in the observed 4:1 *syn*:*anti* distribution.

3.2.2.2 [Ru(η^5-indenyl)(κ^2-^{n}Bu$\underline{C}$HCH$_2\underline{P}$Cy$_2$)(PPh$_3$)] (4c)

Unfortunately, attempts to achieve a thermodynamic distribution of isomers for the 1-hexene adduct **4c** by a similar method to that described above were complicated by competing catalytic isomerization of the alkene. After 24 h at 60°C in the presence of 50 equiv of 1-hexene, metallacycle **4c** had converted to a number of unidentified ruthenium-bisphosphine species, identified as pairs of doublets in the $^{31}P\{^1H\}$ NMR spectrum. The doublets arise from the interaction of each inequivalent phosphine on the other, resulting in the splitting of the NMR signal. Further heating increased the relative amounts of these species, along with other $^{31}P\{^1H\}$ singlets, including free triphenylphosphine (δ = -4.6 ppm). Other singlets in the $^{31}P\{^1H\}$ NMR spectrum are indicative of either free phosphine species or ruthenium-monophosphine complexes.

The ^1H NMR spectrum of the sample solution confirmed the presence of at least 5 ruthenium-hydride species (Figure 3.4). A number of ruthenium hydride species are known to catalyze internal olefin isomerization[6]. Signals corresponding to a mixture of 2-

and 3-hexene were also observed in the ^{1}H NMR spectrum (Figure 3.4). The number and variety of compounds in solution after one day prohibited the determination of hexene isomer distribution by ^{1}H NMR, or structural characterization of the new ruthenium-phosphorus complexes. Due to time constraints, the mechanism of ruthenium-hydride formation from the ^{n}Bu-substituted metallacycle **4c** was not determined, but would be an interesting direction for future investigation.

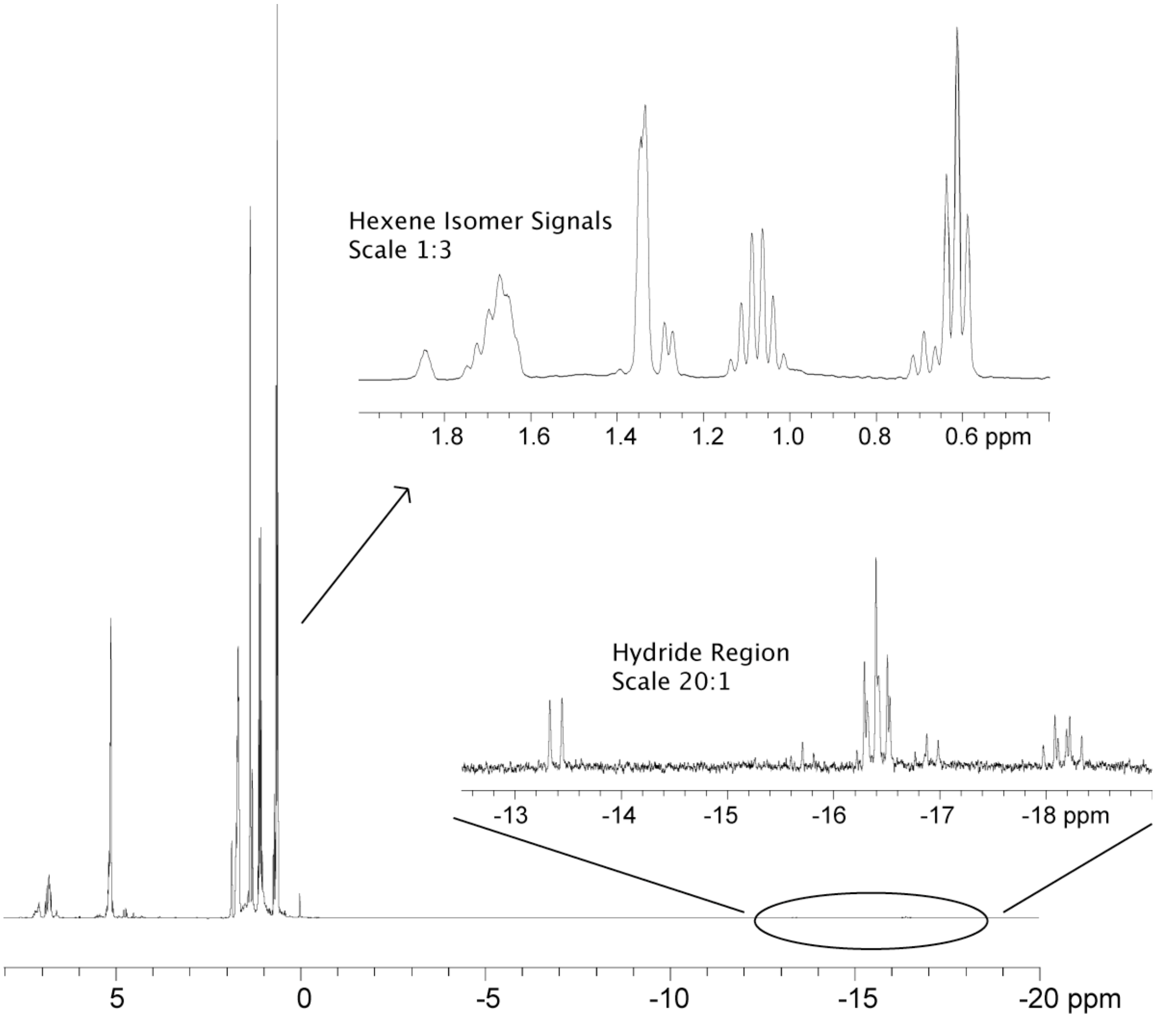

Figure 3.4. Isomerization of 1-hexene in the presence of unknown ruthenium-hydride species, formed from complex **4c** in the presence of 50 equivalents 1-hexene. ^{1}H NMR, 300.13 MHz, d_8-toluene, 60°C.

3.2.2.3 [Ru(η^5-indenyl)(κ^2-EtO$\underline{C}$HCH$_2\underline{P}$Cy$_2$)(PPh$_3$)] (4d)

The thermodynamic distribution of isomers of the ethyl vinyl ether adduct **4d** also could not be confirmed, due to the formation of a new ruthenium-phosphorus product in solution over 6 days of heating to 60°C in the presence of 50 equivalents of the vinyl ether. The initial 1:1 *syn*:*anti* distribution of isomers gradually decreased, favouring the *anti* isomer as the unknown complex was formed. The complex was identified in the $^{31}P\{^1H\}$ NMR spectrum as two sets of doublets (or doublets of doublets) at 65.2 and 46.4 ppm (J_{PP} = 27 Hz, 10Hz) (Figure 3.5).

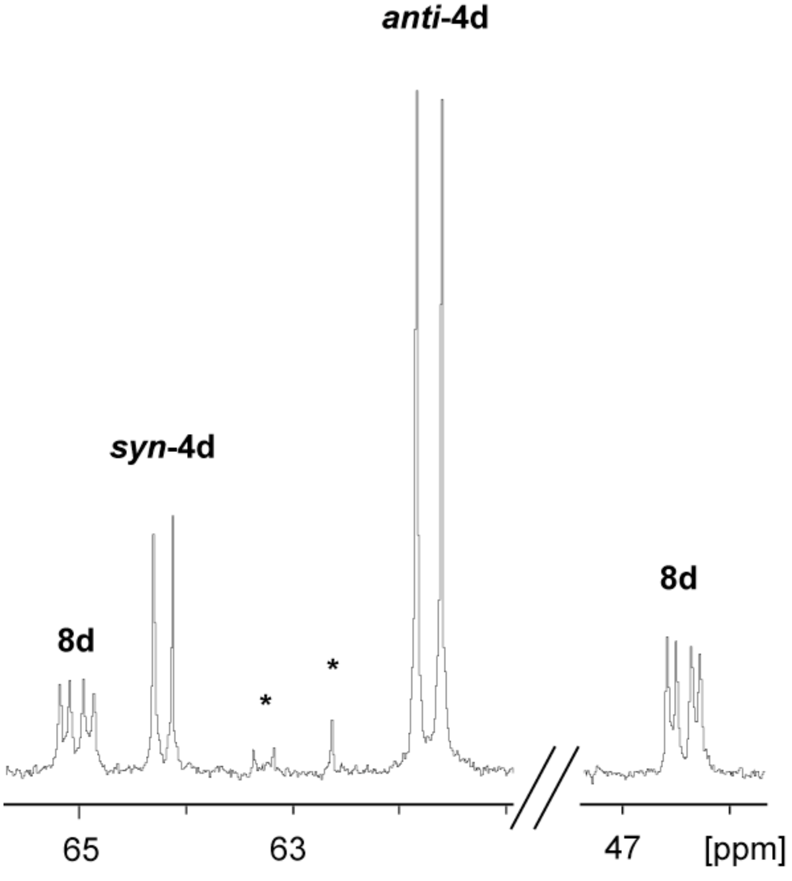

Figure 3.5. Formation of a new product, **8d**, and other unknown phosphorus compounds (*), in the attempted equilibration of *syn* and *anti* isomers of **4d**. ($^{31}P\{^1H\}$ 121.49 MHz, d_8-toluene)

The absence of a P-H bond (such as that which forms in the orthometallation reaction) and the presence of a Ru-hydride, confirmed by ^{31}P and ^{1}H NMR respectively, suggest that this new product may be a vinyl phosphine complex, **8d** (Scheme 3.1). The two sets of doublets observed may be due to *E* and *Z* configurations of the ethoxy group on the vinyl phosphine. Agostic interactions between ruthenium and the C_α-C_β bond in ruthenacyclobutanes have previously been noted[7,8], reducing the expected Ru-C_β distance in these compounds. The inclusion of phosphorus within the metallacycle **4d** results in a more electron-rich ruthenium centre relative to the exclusively carbon-containing ruthenacyclobutanes, which may allow for β-hydride elimination at C_β to form the vinyl phosphine complex **8d**. A decrease in steric strain in the metallacycle, caused by the larger atomic radius of phosphorus relative to that of carbon, may also facilitate the proposed hydride elimination. Complete characterization of the unknown compound is underway.

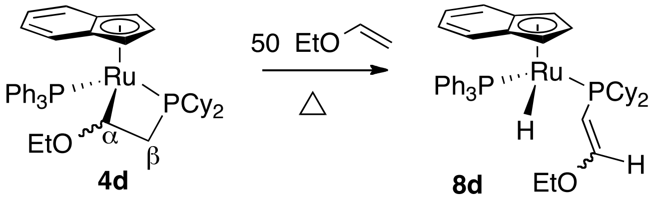

Scheme 3.1. Suspected conversion of metallacycle **4d** to coordinated vinyl phosphine complex **8d**.

3.2.2.4 [Ru(η^5-indenyl)(κ^2-Ph<u>C</u>HCH$_2$<u>P</u>Cy$_2$)(PPh$_3$)] (4e)

The styrene metallacycle **4e** epimerized much more readily in solution than the acrylonitrile adduct **4b**. A initial sample of ***syn*-4e** in the presence of excess styrene in solution achieved a thermodynamic isomer distribution of 1:1 *syn*:*anti* within 24 hours at

60°C (Figure 3.6). No evidence for formation of a putative vinyl phosphine product such as **8d** was observed over the next 24 hours that the solution was monitored.

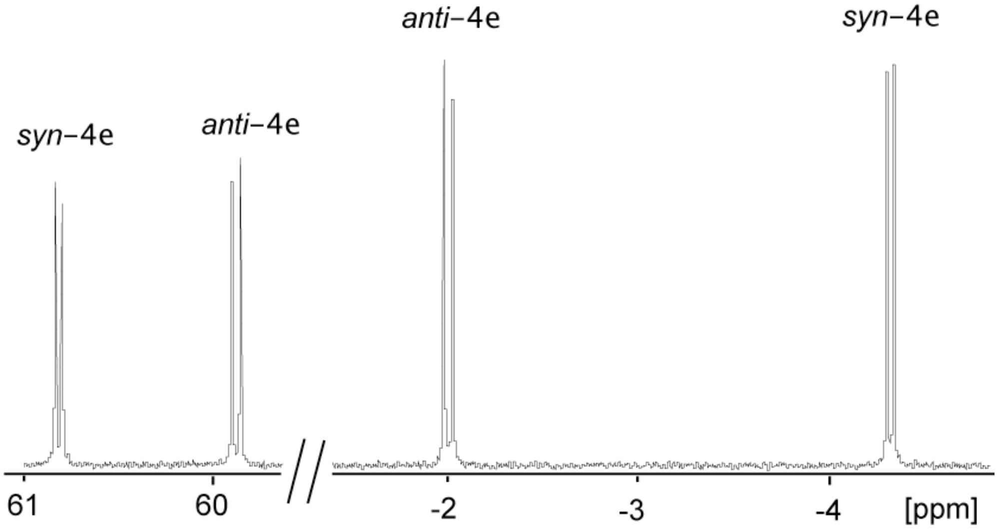

Figure 3.6. Equilibration of **4e** isomers to a 1:1 *syn*:*anti* ratio. ($^{31}P\{^1H\}$ 121.49 MHz, d_8-toluene)

3.3 Steric and Electronic Effects of Alkene Substituents on the [2+2] Cycloaddition of Terminal Olefins with Complex 2

3.3.1 Regiochemistry of Addition is Controlled Sterically

The formation of the metallacyclic complexes **4b**-**e** demonstrate a conservation of regioselectivity in cycloaddition that is independent of alkene electronics. We have found no evidence for the formation of β-substituted metallacycles in any of these reactions. Previous studies conducted by Derrah *et al.* [9] established the bond polarity of the π-bond of the terminal phosphido complex **2** to be nucleophilic at the phosphido and electrophilic at the ruthenium centre. Although the bond polarization for the activated alkene, acrylonitrile, is consistent with the observed regioselectivity of its cycloaddition (Figure 3.7), the inverse regioselectivity for electron rich alkenes, such as ethyl vinyl ether, does not occur. It is likely that the steric bulk of the coordinated –*P*Cy$_2$- prevents the opposing approach of the substituted alkene, precluding the electronic preference of the [2+2] cycloaddition.

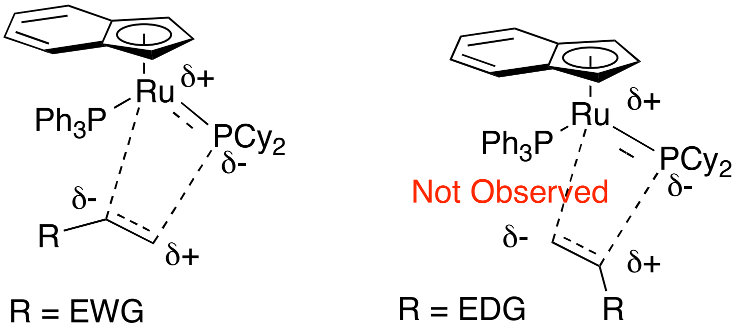

Figure 3.7. Regioselectivity of [2+2] cycloaddition as predicted by alkene bond polarization resulting from electronic effects of alkene substituents.

3.3.2 Electronic Effects of Alkene Substituents Determine Kinetic Control of Stereoselectivity

3.3.2.1 Rate Constants of [2+2] Cycloaddition

Table 3.2. Rate Constants for [2+2] Cycloaddition of Terminal Alkenes to Complex **2**

Alkene Substituent	k / M^{-1} s^{-1}
-CN	5×10^{-1} [(a)]
-^{n}Bu	$(2.5 \pm 0.1) \times 10^{-3}$
-OEt	$(6.1 \pm 0.2) \times 10^{-3}$
-Ph	$(5.7 \pm 0.2) \times 10^{-3}$

(a) maximum rate constant measurable by method used[10]

Second-order rate constants for the [2+2] cycloaddition reaction were obtained for both activated and simple alkenes by monitoring the disappearance of **2** by UV-Vis spectroscopy under pseudo first order conditions (Table 3.2, Figure 3.8, Appendix E). The strongly activated alkene, acrylonitrile, reacted too rapidly with **2** to obtain kinetic data, and so the maximum rate constant measurable by the method used was determined to describe this reaction for comparison purposes (5×10^{-1} M^{-1} s^{-1})[10].

The [2+2] cycloaddition rate constant for the electron-deficient styrene [k_{Ph} = (5.7 ± 0.2) x 10^{-3} M^{-1} s^{-1}] was found to be greater than that of the relatively electron-rich 1-hexene [k_{nBu} = (2.5 ± 0.1) x 10^{-3} M^{-1} s^{-1}], which is consistent with the theory that activated (electron-deficient) alkenes react rapidly with complex **2** due to favourable bond polarization in the regioselectivity of the [2+2] cycloaddition (Figure 3.7). However, it is surprising that the second-order rate constant for ethyl vinyl ether [k_{OEt} = (6.1 ± 0.2) x 10^{-3} M^{-1} s^{-1}] is greater than that of 1-hexene, as the ethoxy substituent has a greater strength of electron-donation (σ_p = -0.16 for $-{}^{n}$Bu and -0.24 for –OEt)[5] and should thus be less favoured by bond polarization (Table 3.2).

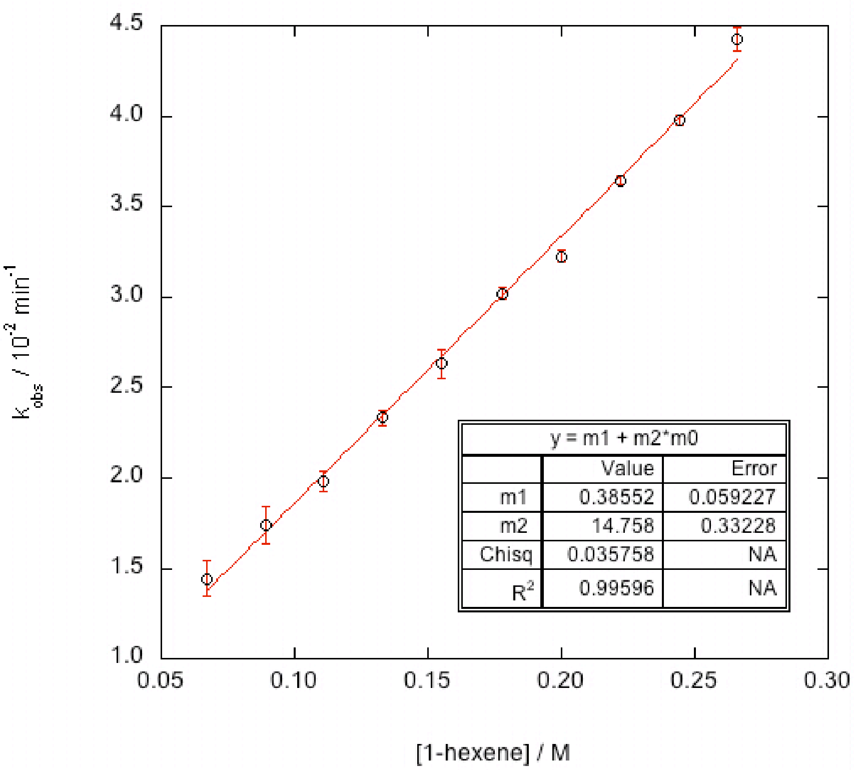

y = m1 + m2*m0		
	Value	Error
m1	0.38552	0.059227
m2	14.758	0.33228
Chisq	0.035758	NA
R^2	0.99596	NA

Figure 3.8. Example of the determination of second order rate constant for the cycloaddition of 1-hexene to **2** at 25°C in toluene. Determined from UV-Vis monitoring at λ = 590 nm where $k_{obs} = k$[1-hexene] - $k_{reverse}$ and m1 = -$k_{reverse}$ and m2 = k.

3.3.2.2 Activation Parameters for [2+2] Cycloaddition

Table 3.3. Activation Parameters for [2+2] Cycloaddition of Terminal Alkenes to Complex **2**

Alkene Substituent	$\Delta H^{\ddagger}$ / kJ mol^{-1}	$\Delta S^{\ddagger}$ / J mol^{-1} K^{-1}	$\Delta G^{\ddagger}$ (295K) / kJ mol^{-1}	E_a / kJ mol^{-1}
-^{n}Bu	30 ± 1	-210 ± 70	90 ± 20	32 ± 1
-OEt	24 ± 2	-220 ± 70	90 ± 20	26 ± 3
-Ph	28 ± 1	-210 ± 80	90 ± 20	31 ± 1

Activation parameters $\Delta H^{\ddagger}$ and $\Delta S^{\ddagger}$ were extracted from Eyring plots obtained from pseudo-first order rate constants at various temperatures and used to calculate $\Delta G^{\ddagger}$ and E^{a} (Table 3.3, Figure 3.9, Appendix C). Activation parameters are very similar for the [2+2] cycloaddition of 1-hexene, styrene and ethyl vinyl ether. The reactions of each of these terminal alkenes with **2** has a large, negative entropy of activation (ΔS = -210, -220 and -210 J mol^{-1} K^{-1} for R = ^{n}Bu, OEt, and Ph respectively) that is consistent with our concerted [2+2] cycloaddition model[1]. The enthalpy of activation is slightly greater for 1-hexene ($\Delta H^{\ddagger}$ = 30 ± 1 kJ mol^{-1}) and styrene ($\Delta H^{\ddagger}$ = 28 ± 1 kJ mol^{-1}) than for ethyl vinyl ether ($\Delta H^{\ddagger}$ = 24 ± 2 kJ mol^{-1}), but the free energies of activation for the alkenes appear identical ($\Delta G^{\ddagger}$ at 295K = 90 ± 20 kJ mol^{-1} for 1-hexene, ethyl vinyl ether and styrene) due to the large error associated with the entropy of activation, $\Delta S^{\ddagger}$, inherent in the method used due to the comparatively narrow range of temperatures examined.

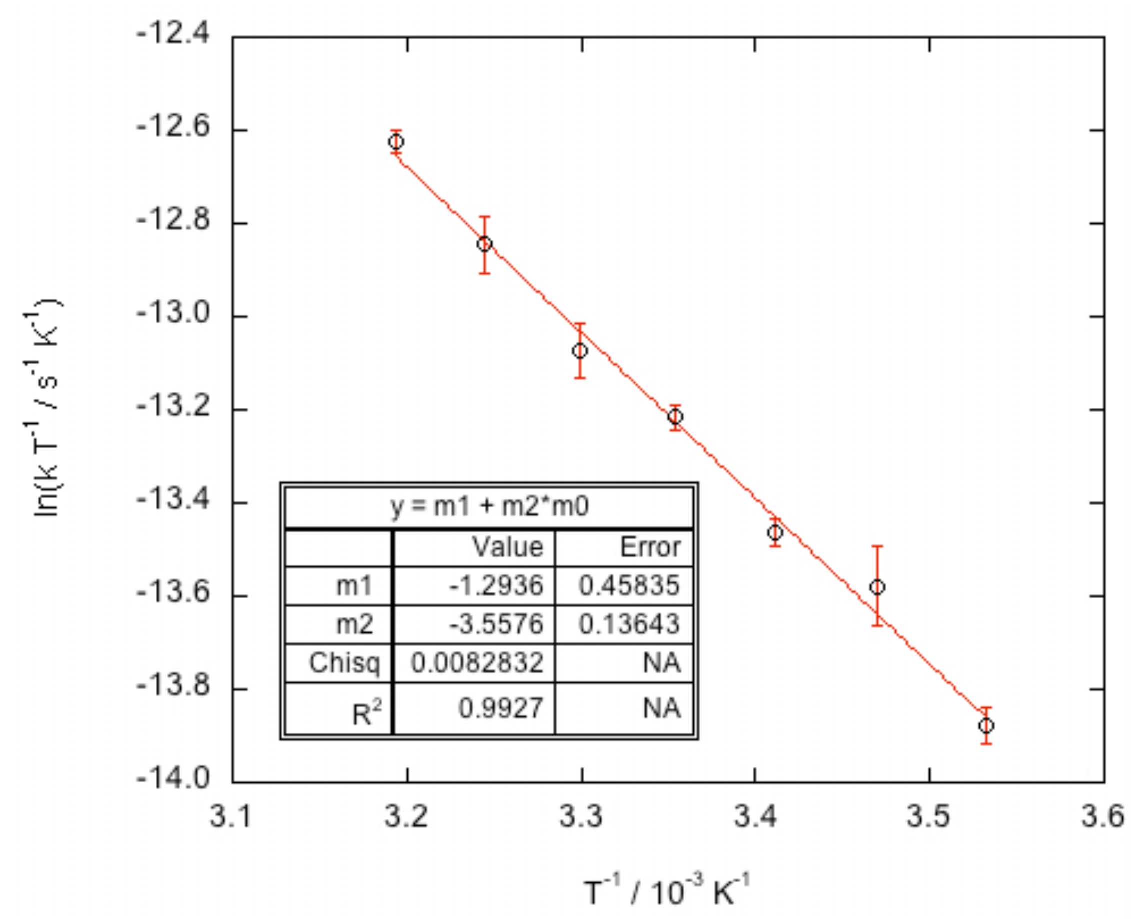

Figure 3.9. Example of the Eyring relationship for the [2+2] cycloaddition of 1-hexene to **2**. Pseudo first order rate constants obtained for 500 equiv 1-hexene.

3.3.3 Variable Sensitivity of [2+2] Cycloaddition Transition State to Alkene Substituent Electronics Observed by Hammett Plot

The effect of substituent electronics on regio- and diastereoselectivity was probed by monitoring [2+2] cycloadditions of various substituted styrenes to **2** by ^{31}P{^{1}H} NMR to obtain initial isomer distributions before solution epimerization could occur (Table 3.4).

Table 3.4. Rate constants for the [2+2] cycloaddition of *p*-substituted styrenes and their resulting isomer distributions

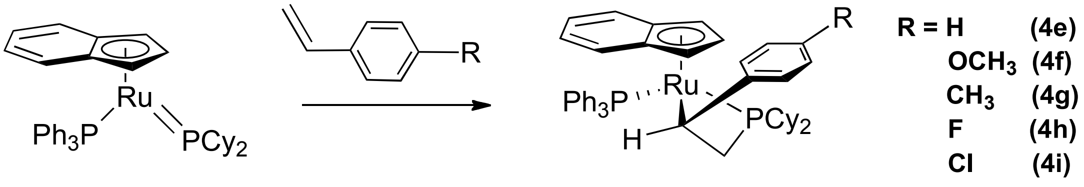

2

4e-j

		Ratio of Complexes[(b)] **4**-*syn*:**4**-*anti*:**6**	
Styrene substituent	k_{obs}[(a)] / s^{-1}	Initial	After 16 h at RT
-OMe	[(c)]	1 : 0 : 0	10 : 2 : 1
-Me	0.9×10^{-3}	1 : 0 : 0	40 : 2 : 1
-H	1.2×10^{-3}	1 : 0 : 0	5 : 2 : 0
-F	1.1×10^{-3}	1 : 0 : 0	20 : 3 : 1
-Cl	2.2×10^{-3}	1 : 0 : 0	20 : 1 : 0
-Br	3.1×10^{-3}	1 : 0 : 0	5 : 1 : 0

(a) Pseudo-first order, obtained for 500 equivalents functionalized styrene.

(b) Obtained from $^{31}P\{^1H\}$ NMR integrations at 50 equivalents functionalized styrene.

(c) Not obtained for 500 equivalents due to the formation of an unidentified, non-[2+2] cycloaddition product.

All styrenes gave both 100 % regio- and diastereoselectivity, resulting in the P-C bond formation at the least substituted end of the alkene and 100% *syn* isomer formation, regardless of the para-substituent (Figure 3.10, Table 3.4). Stereochemistry for each cycloadduct was again confirmed by 2D NOESY, ^{13}C DEPT and J_{PC} values (Figure 3.10). The functionalized styrene metallacycles also showed evidence of cycloreversion (for R = OCH_3 and F) and solution epimerization (for R = H, CH_3, OCH_3, F, Cl and Br), as orthometallated complex **5** and *anti* isomers of the metallacyles were present, as determined by $^{31}P\{^1H\}$ NMR, after 16 hours in solution.

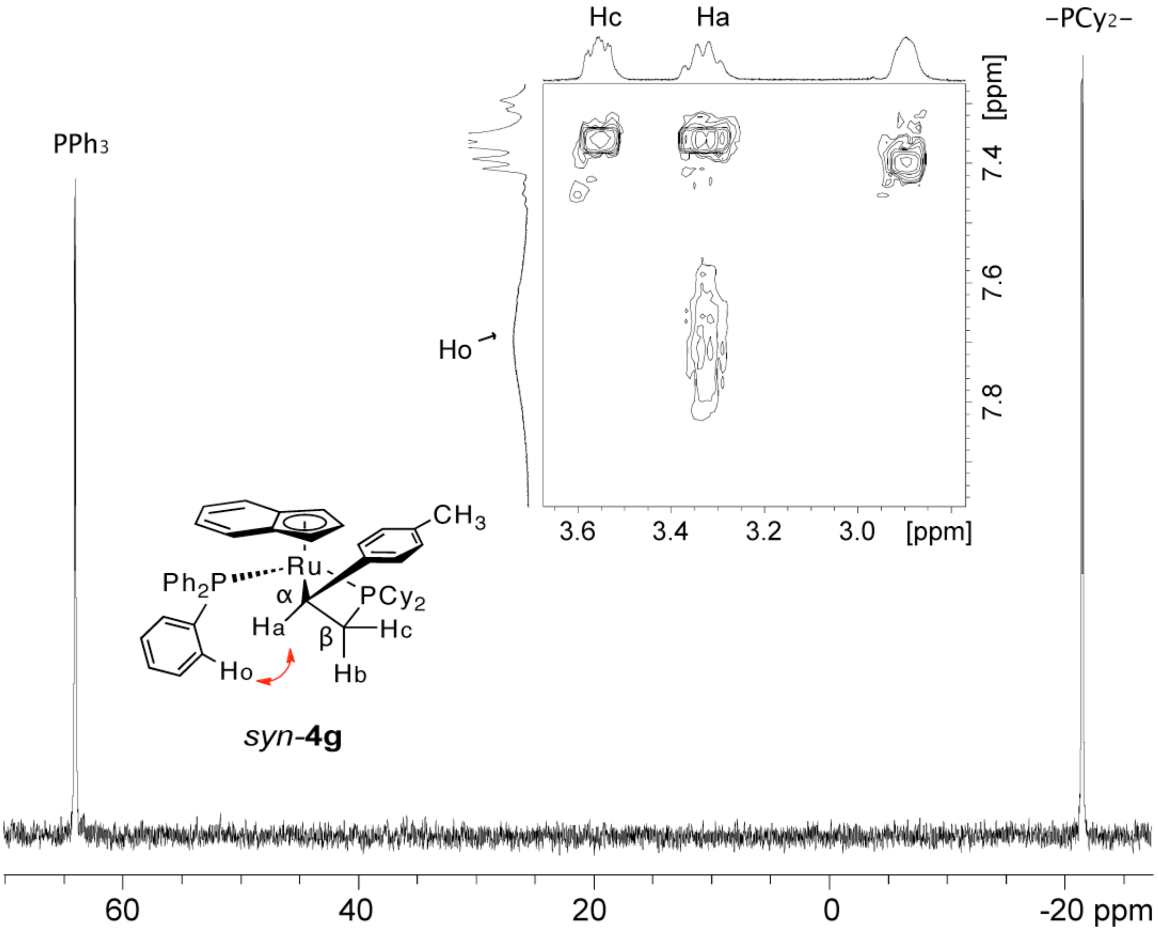

Figure 3.10. $^{31}P\{^1H\}$ NMR demonstrating the exclusive formation of ***syn*-4g** from the [2+2] cycloaddition of 4-methylstyrene to **2**. Inset of partial ^{1}H-NOESY spectrum shows stereochemical determination from H_a → H_o correlation. (202.46 MHz, *d*$_6$-benzene)

A Hammett plot demonstrating the sensitivity of the [2+2] cycloaddition to substituent effects was obtained using pseudo-first-order rate constants for the cycloaddition of various functionalized styrenes to **2** (4-methylstyrene, 4-fluorostyrene, 4-chlorostyrene and 4-bromostyrene) (Figure 3.11). Rate constants were again obtained by monitoring reaction progress by UV-Vis spectroscopy (exponential decay of solution absorbance at 590 nm due to **2**). Pseudo-first order conditions were maintained at 250 equiv of functionalized styrene and confirmed by repeating the cycloadditions at 500 equiv. A general, non-linear increase in rate constant with electron-withdrawing capacity of substituent was observed (Figure 3.11).

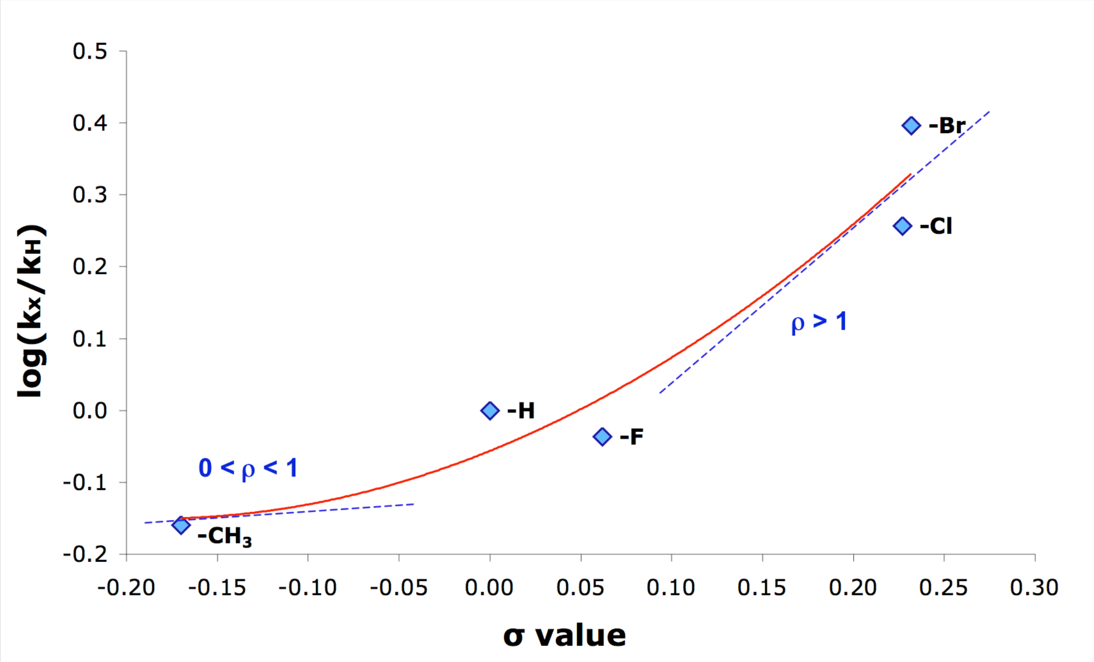

Figure 3.11. Hammett relationship for the [2+2] cycloaddition of functionalized styrenes and **2**. (σ_p parameters[3]; k_X, k_H obtained as pseudo-first order rate constants at 500 equiv. functionalized styrene; error bars are included within the symbol size)

The slope of a Hammett plot is described as the reaction parameter ρ. An increase in ρ equates to an increase in the reaction's sensitivity to substituent effects[3,5]. The gradual increase in slope in the Hammett plot observed indicates that there is a gradual increase in the sensitivity of the [2+2] cycloaddition to substituent electronics with increasing alkene electron-deficiency (Figure 3.11). The curve in the Hammett relationship indicates a gradual change in reaction mechanism, commonly associated with a change in the amount of partial charge developed at the reaction transition state[5]. The increase in ρ describes an increase in partial charge development in the transition state with more electron-withdrawing alkene substituents, indicating that the reaction may be proceeding through a transition state other than that described by the [2+2] cycloaddition (Figure 3.12).

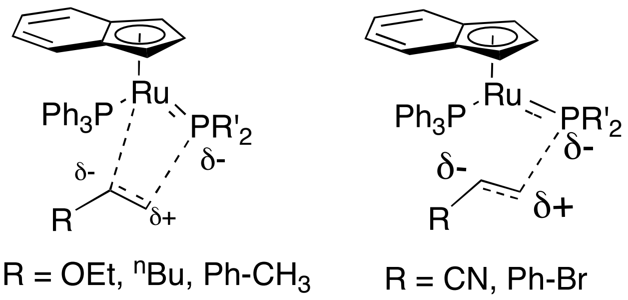

Figure 3.12. Possible change in transition state structure from a mildly charge-separated [2+2] cycloaddition mechanism to a greater charge-separated transition state for electron-deficient alkenes indicated by the Hammett Plot.

Options for examining the cycloaddition rates for electron-rich styrenes were limited, due to the strong basicity of the phosphido ligand in complex **2**. Styrenes containing acidic protons (4-hydroxy- and 4-aminostyrene) were expected to undergo nucleophilic proton abstraction before the desired [2+2] cycloadditions and so were not examined[11]. The [2+2] cycloddition of the ether compound, 4-methoxystyrene, was monitored, but was found by ^{31}P {^{1}H} NMR to form at least three ruthenium-phosphorus complexes in addition to the metallacycle **4f** when used in concentrations greater than 50 equiv (Figure 3.13). The extremely electron-poor styrene 4-nitrostyrene was also used to examine cycloaddition kinetics, but resulted in a non-[2+2] cycloaddition ruthenium-phosphorus product (Figure 3.14).

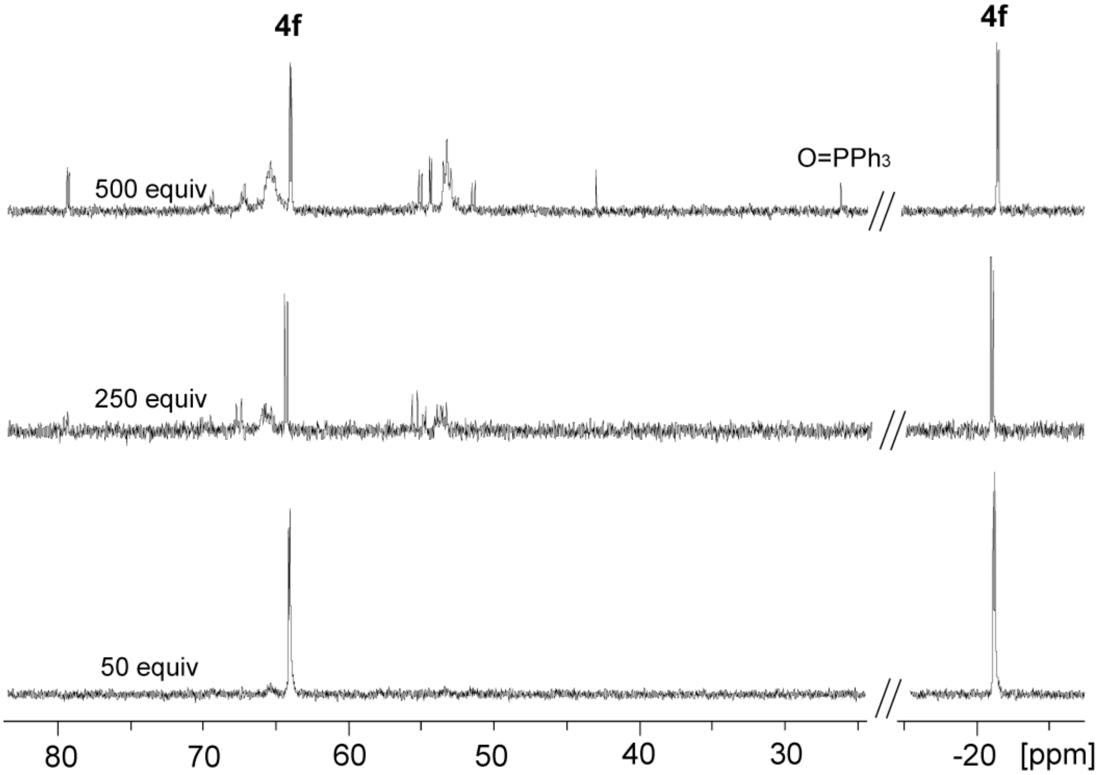

Figure 3.13. The reaction of **2** with 4-methoxystyrene results in the formation of unidentified products in addition to the [2+2] cycloaddition product (**4f**) at high equivalencies of the styrene (> 50 equiv). (^{31}P{^{1}H} NMR, 202.46 MHz, d_6-benzene)

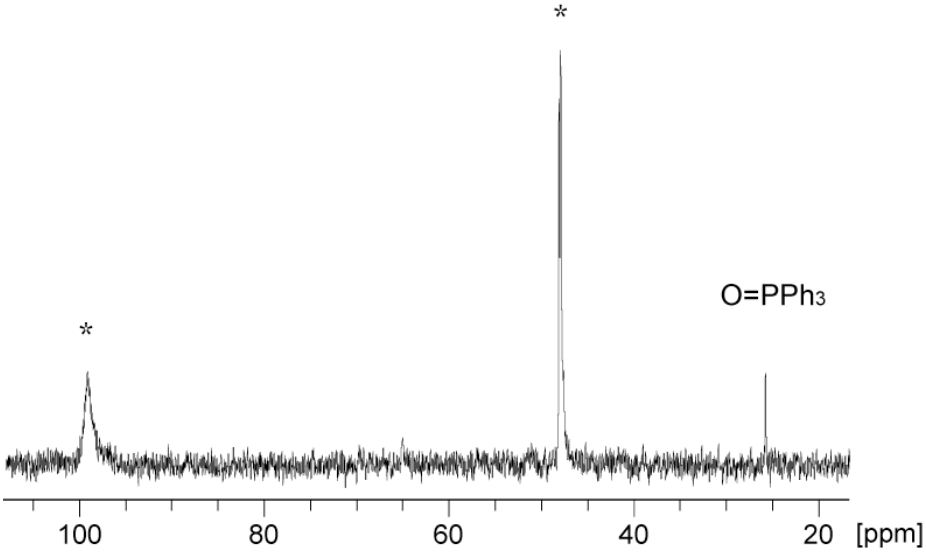

Figure 3.14. ^{31}P{^{1}H} NMR of the unidentified ruthenium-phosphorus product (*) formed by reaction of 4-nitrostyrene with **2**. (121.49 MHz, d_6-benzene)

3.4 Conclusions

The results described in this chapter demonstrate that [2+2]-cycloadditions of terminal alkenes at the ruthenium-phosphorus π-bond of complex **2** are stereoselective for alkenes that have either sterically bulky (^{n}Bu) or electron-withdrawing (CN) substituents. DFT and experimental observations suggest that this stereoselectivity is controlled kinetically, with metallacycles equilibrating to different thermodynamic distributions over time. While experimental attempts to determine the thermodynamic isomer distributions of **4c** and **4d** were unsuccessful, the surprising results of these studies (namely, 1-hexene isomerization and possible vinyl phosphine **8d** formation) give further insight into the solution reactivities of these types of metallacycle complexes.

Variable sensitivity of the rates of [2+2] cycloaddition to electronic effects of alkene substituents was established through construction of a Hammett plot (Figure 3.9). As alkene susbtituents become more electron-withdrawing, the [2+2] cycloaddition becomes increasingly sensitive to electronic effects. This observation suggests that the [2+2] cycloaddition mechanism experiences an increase in charge separation in the transition state with increasing alkene electron-deficiency, with the possibility of a different transisiton state structure. Our collaborator, D. Pantazis, is investigating the possibility of alkene-dependent transition-state charge separation by computational analysis.

Second order rate-constants and isomer distributions for the [2+2] cycloaddition of alkenes to **2** suggest that steric effects of alkene substituents become more prevalent when sensitivity to electronic effects are diminished, specifically for electron rich alkenes. The second order rate constant of the strongly electron-donating ethyl vinyl ether [$k = (6.1 \pm 0.2) \times 10^{-3}\ M^{-1}\ s^{-1}$] was found to be greater than that of the comparatively less-strongly electron-donating 1-hexene [$k = (2.5 \pm 0.1) \times 10^{-3}\ M^{-1}\ s^{-1}$), due to the relatively smaller size of the alkene substituent (steric parameter E_s values relative to –CH_3, 0.00, are +0.99 and -0.39 for –OEt and –^{n}Bu, respectively[4]). Although occurring at a slower rate, cycloaddition of 1-hexene with the relatively bulkier ^{n}Bu substituent is stereoselective, resulting in the exclusive formation of the *syn* isomer or **4c**, as opposed to the 1:1 *syn*:*anti* distribution of ethyl vinyl ether adduct, **4d**.

These findings in combination suggest that diastereoselectivity of metallacyle formation results from a shift from electronic to steric control of the [2+2] cycloaddition as alkenes become increasingly electron-rich. Alkene substituents –OEt and –CN have opposing electronics, but are similar in terms of steric bulk at the primary atom. Conversely, -OEt and –^{n}Bu have similar electronics, but a greater discrepancy in steric bulk than between –OEt and –CN. While the electron-withdrawing ability of –CN leads to transition-state effects that favour the formation of ***syn*-4b** over ***anti*-4b**, the same cannot be said for the selectivity observed for 1-hexene cycloaddition. In this instance, the relatively greater steric bulk of 1-hexene drives the *syn*-selectivity of cycloaddition. This theory is supported by the findings of the Hammett plot, which suggests that the [2+2] cycloaddition is less sensitive to alkene substituent electronic effects for electron-rich alkenes such as ethyl vinyl ether and 1-hexene than for electron-deficient alkenes (acrylonitrile).

The next chapter focuses on what comes after the [2+2] cycloaddition in a possible catalytic hydrophosphination cycle (Chapter 1). To effect hydrophosphination of alkenes, the metallacycle intermediate must be protonolyzed at the Ru-C bond to give the new, coordinated tertiary phosphine. Studies towards this goal are described in Chapter 4.

3.5 Experimental

See Chapter 2, Section 2.7.1 for general experimental details. Chapter 2, Section 2.7.3 describes the syntheses of **4c-e** from which initial isomer distributions were obtained. Metallacycle complex **4b** was prepared as per the literature method established by a former graduate student, Eric J. Derrah[1].

3.5.1 Monitoring of Diastereomer Ratios During Formation of [Ru(η^5-indenyl)(κ^2-EtO$\underline{\mathrm{C}}$HCH$_2\underline{\mathrm{P}}$Cy$_2$)(PPh$_3$)] (4d)

An NMR sample of **1** (10 mg, 0.014 mmol) in d_6-benzene (0.6 mL) was prepared and capped with a small septum. Degassed ethyl vinyl ether (71 μL, 0.74 mmol, 50 equiv) was injected via gas-tight syringe, the sample was inverted to mix (x 5) and the collection of ^{31}P{^{1}H} NMR spectra at 5 minute intervals was immediately initiated.

3.5.2 Attempts to Monitor Thermal Equilibration of the *Syn* and *Anti* Isomers of Metallacycles 4b-e

A solution of each metallacycle complex **4b-e** (10-15 mg) and its corresponding alkene substrate (acrylonitrile **4b**, 1-hexene **4c**, ethyl vinyl ether **4d**, styrene **4e**; 40-50 μL, 50 equiv) in d_8-toluene (0.7 mL) was made in an NMR tube. The tubes were flame-sealed and NMR spectra (^{1}H and ^{31}P {^{1}H}, 300 MHz) of each yellow-orange solution were acquired. The samples were placed in a 60°C (±5°C) oil bath and further spectra (^{1}H and ^{31}P {^{1}H}, 300 MHz) were obtained after varying amounts of time. Relative amounts of all phosphorus-containing species in solution were determined by integration of ^{31}P {^{1}H} NMR peaks. Since *syn* and *anti* isomers are very similar structurally, it was assumed that their T$_1$ values in the ^{31}P{^{1}H} NMR would be very similar. This assumption is important because the T_1 values, which determine peak size and hence accurate integration and relative amounts of species in solution, are much more dependent on molecular structure in $^{31}P\{^1H\}$ NMR than in ^1H NMR. Thus non-quantitative $^{31}P\{^1H\}$ NMR spectra, which were obtained in these experiments, may give non-accurate representations of relative species distributions if T_1 values are very different for the species in solution.

3.5.3 Determination of the Second Order Rate Constants, *k*, for the [2+2] Cycloaddition of Terminal Alkenes at 2

A 0.44 mM solution of [Ru(η^5-indenyl)(PCy_2)(PPh_3)] (**2**) was made in the glovebox by adding 15 mg (0.022 mmol) of the blue powder to a 50 mL volumetric flask and diluting with toluene. This blue-green solution was transferred (3.0 mL) via syringe to each of three cuvettes, which were then capped with Teflon septa caps. The UV-Vis-NIR spectrophotometer had been previously zeroed with toluene and set at a block temperature of 25°C and the cuvettes were placed in the sample block and allowed to equilibrate for 15 minutes. A kinetics program set to monitor absorbance at 590 nm was created with the following parameters: 2s signal averaging time, 30s cycle time. Neat alkene (ethyl vinyl ether, acrylonitrile, 1-hexene, styrene, as well as *p*-substituted styrenes for the Hammett plot; 150 to 600 equiv.) was injected into each of the three cuvettes via gas tight syringe (oven-dried), which were then inverted ten times, and data collection was initiated. Data was collected over five lifetimes for each reaction. The pseudo-first order rate constant, k_{obs}, for the decrease in absorbance at 590 nm (corresponding to the consumption of **2**) was calculated using the Cary-5 or Cary-100 data manipulation software. Three trials of the cycloaddition were acquired at each alkene concentration, giving an average k_{obs} value. For the *p*-substituted styrenes, these

k_{obs} values were used directly in the Hammett Plot. In determining the second-order rate constants, the relationship between k_{obs} and alkene concentration was plotted and the slope was taken as the second order rate constant, k. Data and associated error were analyzed by Kaleidagraph. (See Figure 3.8, Appendix E for all plots and line-fitting parameters.)

3.5.4 Determination of Activation Parameters for the [2+2] Cycloaddition of Terminal Alkenes at 2

A 0.44 mM solution of **2** (15 mg, 0.022 mmol) in toluene (50 mL) was prepared analytically, as described above. The blue-green solution (3.0 mL) was transferred via syringe to a cuvette, which was then capped with a Teflon septum cap. The UV-Vis-NIR spectrophotometer was set to temperature (10 - 40°C) and programmed with the following parameters: 30 s signal averaging time, 2 min cycle time and 30 min total time. After temperature equilibration, an aliquot of alkene (500 equiv) was injected into the cuvette via gas-tight syringe, which was then inverted ten times. Data collection was initiated immediately.

The observed first order decay was analyzed by Varian data manipulation software to give the rate constant, k_{obs}, which was taken to be the pseudo first-order rate constant of the [2+2] cycloaddition. Three trials of the cycloaddition were conducted at each temperature.

The relationship between k_{obs} and temperature was examined with an Eyring plot (see Figure 3.9, Appendix C for all plots and line-fitting parameters) ($\ln(k_{obs}/T)$ vs. $1/T$), and the enthalpy and entropy of activation were obtained from the resulting slope and y-intercept, respectively, according to the relationship:

$$\ln(k_{obs}/T) = (-\Delta H^{\ddagger}/R)(1/T) + (\Delta S^{\ddagger}/R) + \ln(k_B/h) \qquad \ldots (3.2)$$

where R is the molar gas constant (8.3145101 J K^{-1} mol^{-1}), k_B is the Boltzmann constant (1.380658x10^{-23} J K^{-1}), and h is the Planck constant (6.6260755x10^{-34} J s).

The Gibb's free energy of activation, $\Delta G^{\ddagger}$, was obtained at 295 K using the values of $\Delta S^{\ddagger}$ and $\Delta H^{\ddagger}$ and the equation[12]

$$\Delta G^{\ddagger} = \Delta H^{\ddagger} - T\Delta S^{\ddagger} \qquad \ldots (3.3)$$

The activation energy at 295 K was obtained from the enthalpy of activation using the standard relationship[12]

$$E_a = \Delta H^{\ddagger} + RT \qquad \ldots (3.4)$$

3.5.5 NMR-Scale Syntheses of *p*-Substituted Styrene Adduct Metallacycles 4f-j

NMR samples of **2** (10 mg, 0.014 mmol) were prepared in C_6D_6 (0.6 mL) and capped with a small septa. Degassed (FPT x 3) *p*-substituted styrene reagent (4-methoxy-, 4-methyl-, 4-chloro-, 4-bromo-, 4-fluoro-, and 4-nitrostyrene; 50 equiv) was injected to each tube via gas-tight syringe, the samples were inverted to mix (x 5), and the collection of $^{31}P\{^1H\}$ NMR spectra at 5 minute intervals was immediately initiated.

3.6 References

(1) Derrah, E. J.; Pantazis, D. A.; McDonald, R.; Rosenberg, L. *Angew. Chem., Int. Ed.* **2010**, *49*, 3367.

(2) Pantazis, D. **2010** Unpublished results.

(3) Hammett, L. P. *Chem. Rev.* **1935**, *17*, 125.

(4) Relative to -CH_3 (0.00). Positive values indicate lesser steric bulk than methyl and negative values indicate greater steric bulk. Newman, M. S. *Steric Effects in Organic Chemistry*; J. Wiley & Sons Inc., Chapman & Hall Ltd: New York, London, 1956.

(5) Anslyn, E. V.; Dougherty, D. A. *Modern Physical Organic Chemistry*; University Science Books, 2006.

(6) Donohoe, T. J.; O'Riordan, T. J. C.; Rosa, C. P. *Angew. Chem., Int. Ed.* **2009**, *48*, 1014.

(7) Grubbs, R. H.; Wenzel, A. G. *J. Am. Chem. Soc.* **2006**, *128*, 16048.

(8) Grubbs, R. H.; Wenzel, A. G.; Blake, G.; VanderVelde, D. G. *J. Am. Chem. Soc.* **2011**, *133*, 6429.

(9) Derrah, E. J.; Pantazis, D. A.; McDonald, R.; Rosenberg, L. *Organometallics* **2007**, *26*, 1473.

(10) Maximum k_{obs} determined from rate = k_{obs}[alkene], where rate = 1/30s (average injection time of the alkene being 30 s) and [alkene] = 0.06 M.

(11) Derrah, E. J.; Giesbrecht, K. E.; McDonald, R.; Rosenberg, L. *Organometallics* **2008**, *27*, 5025.

(12) Engel, T.; Reid, P. *Thermodynamics, Statistical Thermodynamics, and Kinetics*; Pearson, Prentice Hall, 2006.

Chapter 4 Release of Phosphinated Product: Preliminary Investigation

4.1 Introduction

After P-C bond formation, the next step in a potential catalytic hydrophosphination cycle is the release of the phosphinated product from the metal centre and regeneration of the catalytically active species (Figure 4.1). To achieve this goal, the metallacycles formed from the [2+2] cycloaddition of unsaturated substrates to the π-bond of **2** must be cleaved at both the Ru-C and Ru-PCy_2- bond, followed by coordination of a substrate secondary phosphine. Proton abstraction from this coordinated secondary phosphine would regenerate the active, terminal phosphido species.

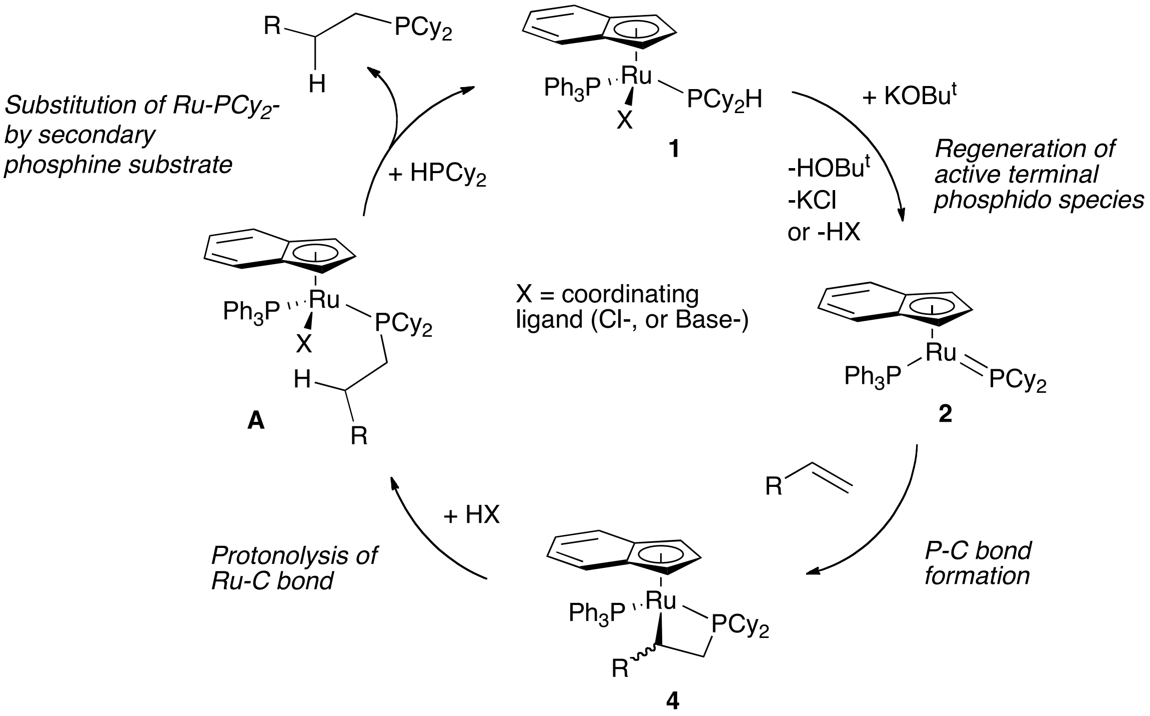

Figure 4.1. Processes involved in a possible catalytic hydrophosphination cycle.

In a number of mechanisms proposed for catalytic hydrophosphination, these processes, protonolysis and catalyst regeneration by phosphido coordination, are accomplished by the addition of a phosphine substrate containing a P-H bond[1-3]. In the calcium-catalyzed hydrophosphination of alkenes reported by Procopiou *et al.*[1], previously described in Chapter 1, the Ca-C bond in a proposed 1,2-insertion intermediate is protonolyzed by the incoming secondary phosphine, releasing the hydrophosphinated product. The secondary phosphine, stripped of its proton, coordinates to the calcium centre as a phosphido ligand, thereby regenerating the active catalyst (Figure 4.2).

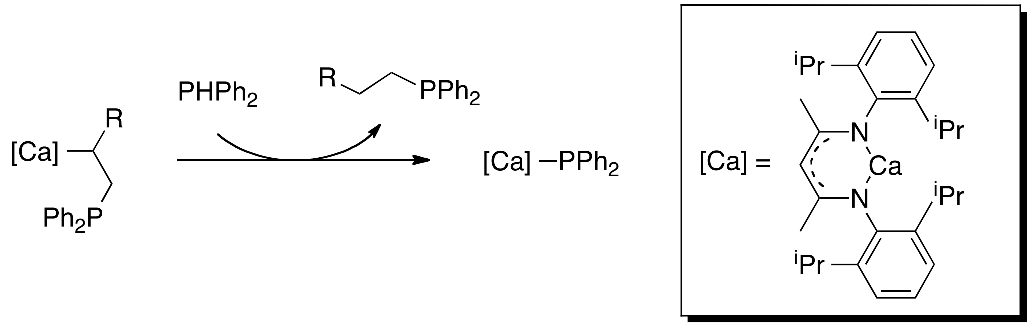

Figure 4.2. Protonolysis and catalyst regeneration by a diphenylphosphine in the calcium-catalyzed hydrophosphination of alkenes.

As is highlighted in the previous Ca-catalyzed example, the major challenge in hydrophosphination is not the substitution of the coordinated product phosphine, which is likely to be readily displaced by an incoming, smaller substrate phosphine, but the cleavage of the M-C bond. The major difference between the early and late metal systems is the decreased polarity of the M-C late metal bonds. In these late-metal systems, a proton “shuttle” is required to remove a proton from the secondary phosphine substrate and deliver it to the M-C bond for protonolysis[4,5]. In the mechanism proposed for the palladium (II) or nickel (II)-catalyzed hydrophosphination of alkyl vinyl ethers by Beletskaya[4], the M-C bond is protonolyzed by HCl or HBr, after Cl^- or Br^- has abstracted a proton from the secondary phosphine substrate (Figure 4.3).

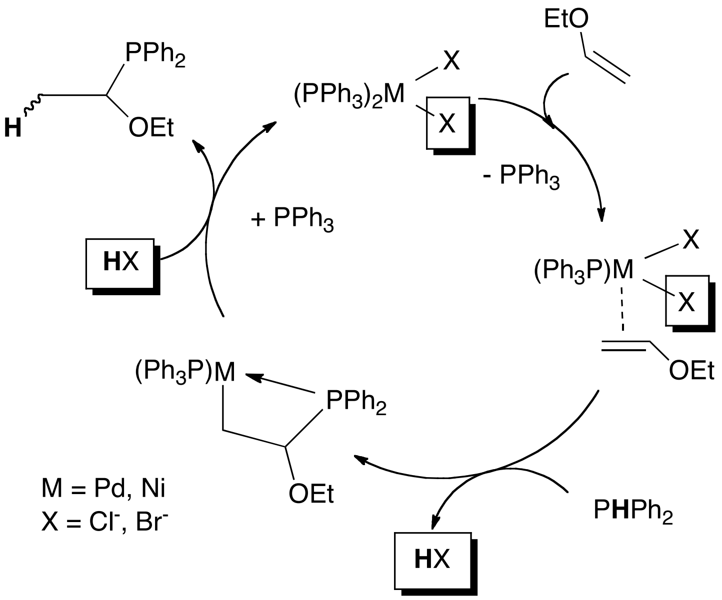

Figure 4.3. Pd- or Ni-catalyzed hydrophosphination of ethyl vinyl ether using catalytic proton “shuttle” (Cl^- or Br^-).

The following sections describe preliminary experimental work aimed at releasing a phosphinated product from the metallacycles formed from the [2+2] cycloaddition of unsaturated substrates at the π-bond of **2**. Based on the previously-described literature precedents, secondary phosphines and various acids were explored as proton sources.

4.2 Addition of Excess Secondary Phosphine to Metallacycles [Ru(η^5-indenyl)(κ^2-R$\underline{C}$HCH$_2\underline{P}$Cy$_2$)(PPh$_3$)] (4a,b,d,e) and [Ru(η^5-indenyl)(κ^2-Ph$\underline{C}$CH$\underline{P}$Cy$_2$)(PPh$_3$)] (5) in Solution

In an attempt to effect both metallacycle protonolysis and substitution of coordinated product tertiary phosphines, excess secondary phosphine was added to metallacycles **4a,b,d,e** and **5** in solution. Dicyclohexylphosphine, chosen to potentially promote catalytic turnover to complex **2**, did not react with any of the metallacycles to form either the protonolyzed product or even possible phosphine-substituted products (Figure 4.4). Diphenylphosphine was used next, with the hope that its smaller cone angle would allow it to at least successfully substitute the tertiary phosphine –PCy_2- of the metallacycle. It was also assumed that the greater acidity of the P-H bond of diphenylphosphine (pK_a = 22.9 for $HPPh_2$ and 34.6 for $HPCy_2$)[6] would make it a more accessible proton source. However, neither metallacycle **4e** nor **5** were observed to react with the excess diphenylphosphine in solution (Figure 4.4).

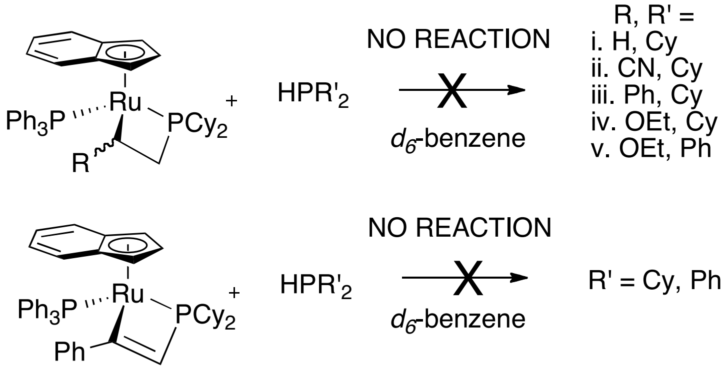

Figure 4.4. No reaction occurs between secondary phosphines and metallacycles **4a,b,d,e** and **5** in solution.

The phenylacetylene adduct, **5**, was chosen for initial tests with both dicyclohexyl- and diphenylphosphine, as the ring strain within the metallacycle was predicted to be the greatest of all the metallacycles due to the inclusion of the double bond[7]. Theoretically, protonolysis would remove this ring strain and would thus be highly favoured. Subsequent tests focused on the ethyl vinyl ether adduct **4d**. The fact that **4d** showed evidence for cycloreversion after a shorter duration of heating than any other metallacycle (**4a-e**) (see Chapter 2, Section 2.5), suggested that **4d** contains the weakest Ru-C bond of the metallacycles.

4.3 Reaction of [Ru(η^5-indenyl)(κ^2-Ph$\underline{C}$CH$\underline{P}$Cy$_2$)(PPh$_3$)] (5) with HCl

To test the feasibility of metallacycle protonolysis by stronger proton sources than secondary phosphines, the phenylacetylene adduct **5** was combined with hydrochloric acid in a solution of toluene. Dropwise addition of one equivalent of anhydrous 1.0M HCl in diethyl ether to **5** in toluene resulted in the incomplete conversion of **5** to three products, as determined by $^{31}P\{^1H\}$ NMR spectroscopy (Figures 4.5-4.7).

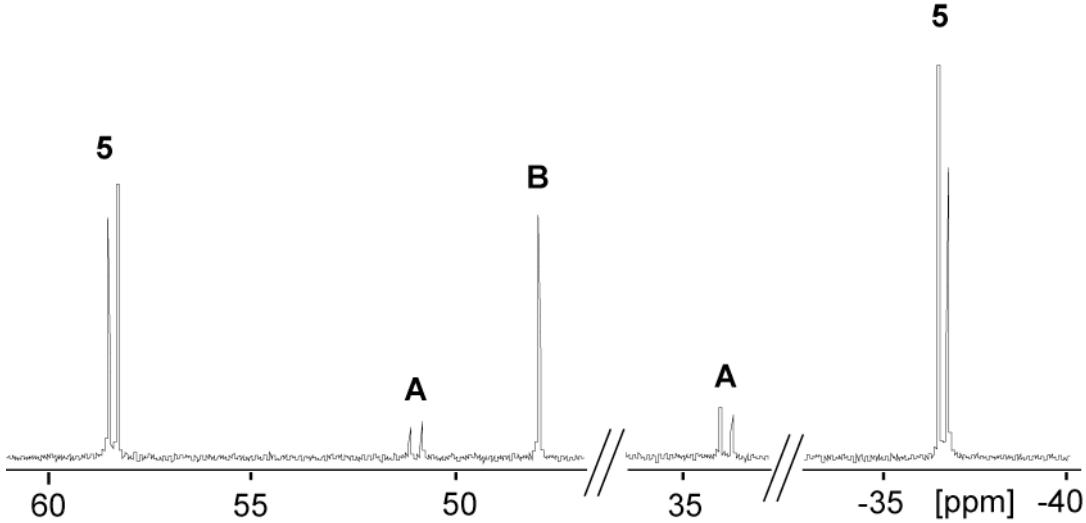

Figure 4.5. Formation of new toluene-soluble products (**A**, **B**) from the reaction of **5** with HCl. ($^{31}P\{^1H\}$ NMR 121.49 MHz, *d*$_6$-benzene)

Two of these products, **A** and **B**, were soluble in the original toluene solution. After decanting from the black precipitate that contained the third product (**C**), **A** and **B** were isolated a brown-orange powder mixture with **5** (Figure 4.5). Compound **A** is observed as two doublets at 51.3 and 33.1 ppm (J_{PP} = 37 Hz) in the $^{31}P\{^1H\}$ NMR spectrum and is therefore likely a ruthenium complex containing two coordinated phosphorus atoms. The chemical shifts suggest that neither of these coordinated phosphorus atoms is incorporated into a metallacycle: in the starting complex **5** a doublet at -36.5 ppm indicates the presence of the metallacyclic phosphine –PCy_2-. A ^1H NMR spectrum of the **A**, **B**, **5** mixture showed no evidence of a Ru-hydride. These observations suggest that **A** could potentially be the vinyl phosphine complex **9** (Figure 4.6), indicating that protonolysis of **5** may have been successful to some extent. However, the presence of other complexes in solution with **A**, namely the unknown compound **B** and starting material **5**, prevented full characterization of unknown **A**. Isolation of **A** in order to improve characterization was also made difficult by the similar solubilities of **B** and **5**.

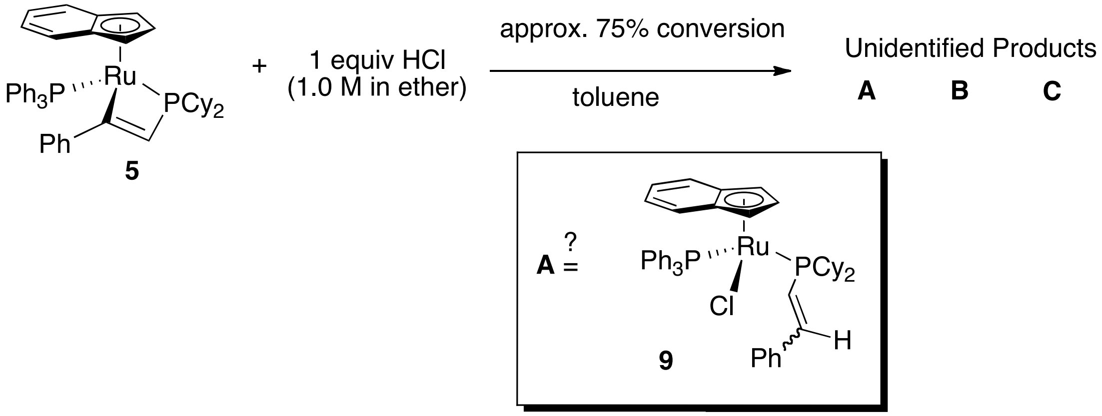

Figure 4.6. Formation of unknown products **A**, **B**, **C** from the reaction of **5** with HCl. **A** is tentatively identified as complex **9**.

The unknown compound **B** was observed in the $^{31}P\{^1H\}$ NMR spectrum as a singlet at 47.9 ppm (Figure 4.5). Based on this, **B** could be either a free phosphine species, or a ruthenium-phosphorus complex containing only one type of coordinated phosphorus atom. Again, difficulties in isolating **B** from the **A**, **B**, **5** mixture prohibited further characterization.

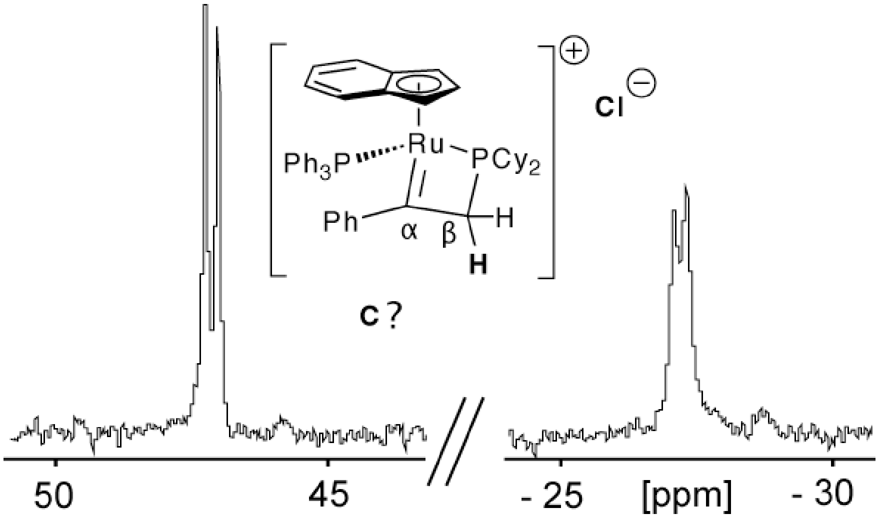

Figure 4.7. $^{1}P\{^{1}H\}$ NMR spectrum of the black precipitate product **C** from the reaction of **5** with HCl. Possible structure for **C** shown. (acetonitrile, d_6-benzene, 121.46 MHz)

The unknown compound **C** was a green-black precipitate that formed immediately upon the addition of HCl to **5** in toluene. It was insoluble in toluene, benzene, hexanes and pentanes, but was successfully dissolved in the more polar acetonitrile to make a murky brown solution, suggesting that **C** is highly polar and potentially charged. The acetonitrile required to get **C** into solution overwhelmed the ^{1}H NMR spectrum obtained and thus prevented identification of **C** by this method. Compound **C** was also formed in much smaller amounts than the isolated **A**, **B**, **5** mixture as a sticky green-black substance, making it difficult to purify and characterize. A $^{31}P\{^{1}H\}$ NMR spectrum of **C** in acetonitrile provided the clearest spectroscopic information on the compound and was obtained using a drop of d_6-benzene for a deuterium lock. Two doublets at 47.0 and -27.2 ppm (J_{PP} = 27 Hz) in the $^{31}P\{^{1}H\}$ NMR spectrum (Figure 4.7) suggest that **C** may also be a ruthenium complex containing two distinct coordinating phosphorus atoms. The upfield doublet at -27.2 ppm is in a similar region to the metallacyclic phosphine –PCy_2- in **5**, which indicates that **C** may also contain a metallacyclic phosphorus atom. The ^{31}P

coupling constant of **C**, $^2J_{PP}$ (27 Hz), is also comparable to that of the metallacycle complexes **4a-e** ($^2J_{PP}$ = 20 - 27 Hz).

In summary, the variety of products produced by the reaction between **5** and HCl made them difficult to fully characterize and identify. The reactivity of HCl, even when added slowly in a solution of ether, may have led to by-products resulting from the reaction of **5** with more than one equivalent of HCl. This theory is supported by the fact that the starting complex **5** was still present in solution after reaction with one total equivalent of HCl. With extra equivalents reacting to form by-products, there was a deficit of HCl to react with the remaining complex **5** in solution. Since compound **A** was tentatively identified as the desired protonolysis product I decided to attempt this protonolysis with a less reactive proton source to avoid the formation of undesirable side products.

4.4 Reactions with Triethylamine Hydrochloride

4.4.1 $NEt_3 \cdot HCl$ with $[Ru(\eta^5\text{-indenyl})(\kappa^2\text{-Ph}\underline{C}CH\underline{P}Cy_2)(PPh_3)]$ (5) in Solution

Triethylamine hydrochloride was used as a less reactive proton source than HCl to attempt protonolysis of the Ru-C bond in metallacycle **5**. When $NEt_3 \cdot HCl$ was combined with **5** in solution, however, no reaction was observed. $^{31}P\{^1H\}$ and ^1H NMR spectroscopy confirmed that both **5** and $NEt_3 \cdot HCl$ remained unreacted in solution. A stronger proton source than triethylamine hydrochloride (pK_a = 11), and weaker than hydrochloric acid (pK_a = -7)[8], is therefore required if protonolysis of **5** is to occur successfully and cleanly.

4.4.2 $NEt_3{\cdot}HCl$ with $[Ru(\eta^5\text{-indenyl})(\kappa^2\text{-EtO}\underline{C}HCH_2\underline{P}Cy_2)(PPh_3)]$ (4d)

While $NEt_3{\cdot}HCl$ was not a strong enough proton source to react with **5**, solution studies with the ethyl vinyl ether adduct **4d** were undertaken to assess the relative strengths of the Ru-C bonds in the two metallacycles. As mentioned previously, cycloreversion of **4d** occurred after less time at 60°C than other metallacycles examined, suggesting **4d** contained the weakest Ru-C bond in metallacycles **4a-e** (Chapter 2, Section 2.5), which would be beneficial in a desired protonolysis reaction.

Surprisingly, **4d** reacted with $NEt_3{\cdot}HCl$ in solution to form the unsaturated metallacycle $[Ru(\eta^5\text{-indenyl})(\kappa^2\text{-}\underline{C}HCH\underline{P}Cy_2)(PPh_3)]$ (**10**) with complete and clean conversion, as determined by $^{31}P\{^1H\}$ NMR (Scheme 4.1), which was isolated as bright red crystals. Complex **10**, resulting from the overall loss of a proton and an ethoxy group from **4d**, was identified and characterized by X-ray crystallography (Figure 4.8, Table 4.1, Appendix B), EI-MS, NMR spectroscopy (Tables 4.2 – 4.4, Appendix D) and microanalysis. Distinctive $^{31}P\{^1H\}$ NMR peaks appear as doublets at 59.4 and -27.0 ppm (J_{PP} = 26 Hz). A diagnostic ^1H NMR peak for the α-proton of the metallacycle appears as a doublet of doublet of doublets at 9.55 ppm (J = 4, 6, 34 Hz).

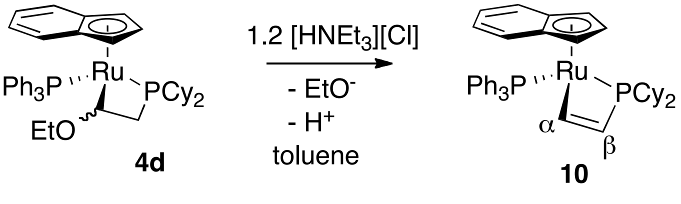

Scheme 4.1. Formation of **10** from **4d** and $NEt_3{\cdot}HCl$ in toluene.

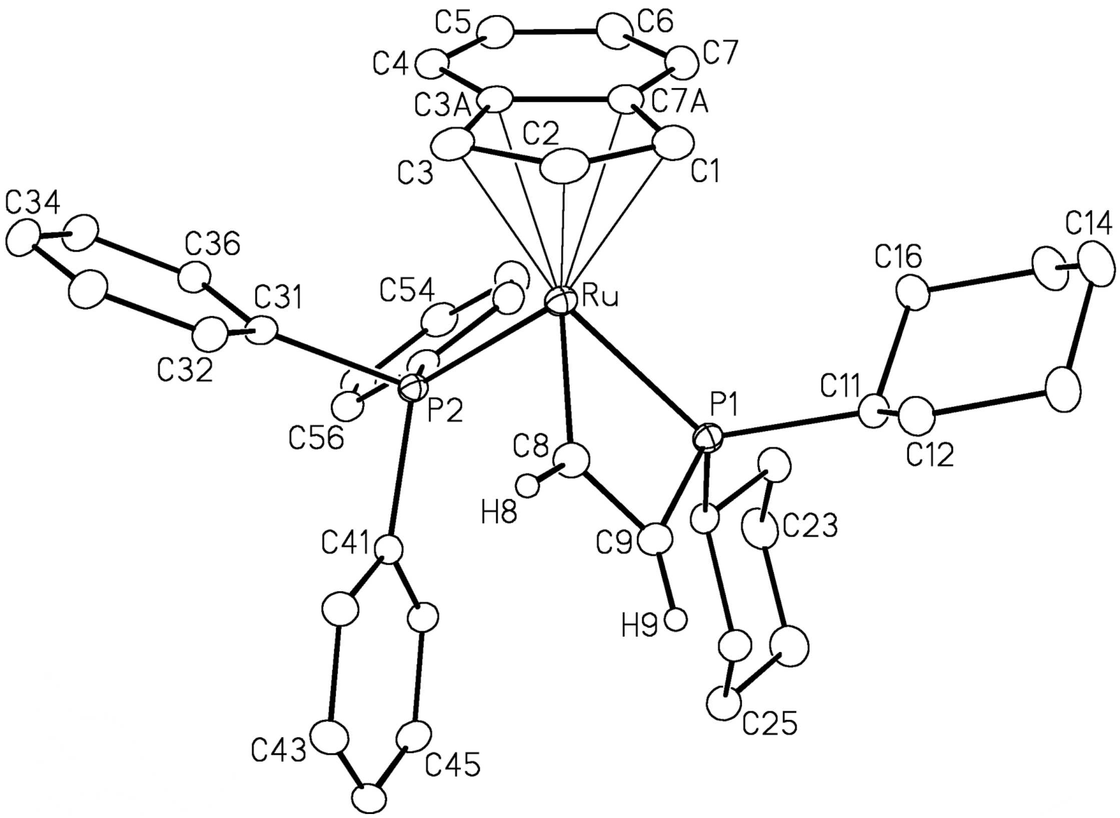

Figure 4.8. View of $[\mathrm{Ru}(\eta^5\text{-indenyl})(\kappa^2\text{-}\underline{\mathrm{C}}\mathrm{HCH}\underline{\mathrm{P}}\mathrm{Cy}_2)(\mathrm{PPh}_3)]$ (**10**). The hydrogen atoms attached to C11 and C12 are shown with arbitrarily small thermal parameters; all other hydrogens are not shown. Non-hydrogen atoms are represented by Gaussian ellipsoids at the 20% probability level. Full characterization tables found in Appendix B.

Table 4.1. Selected interatomic distances and bond angles for $[\mathrm{Ru}(\eta^5\text{-indenyl})(\kappa^2\text{-}\underline{\mathrm{C}}\mathrm{HCH}\underline{\mathrm{P}}\mathrm{Cy}_2)(\mathrm{PPh}_3)]$ (**10**).

Bond(s)	*Interatomic Distance* (Å)	Bond(s)	*Bond Angles* (deg)
Ru – P1	2.3242(8)	P1 – Ru – P2	95.27(3)
Ru – P2	2.2753(8)	P1 – Ru – C8	65.48(9)
Ru – C8	2.053(3)	P2 – Ru – C8	89.37(10)
Ru – C*	1.922	C* – Ru – P1	134.8
P1 – C9	1.793(3)	C* – Ru – P2	125.4
C8 – C9	1.339(5)	C* – Ru – C8	126.3
C8 – H8	0.98(4)	Ru – P1 – C9	85.55(11)
Δ	0.112	P1 – C9 – C8	97.7(2)

[a] C* denotes the centroid of the plane defined by C7a-C1-C2-C3-C3a and Δ (indenyl slip distortion) = *d*[Ru-C7a,C3a] - *d*[Ru-C1,C3].

The mechanism of formation of **10** from **4d** is not yet established. However, the fact that there is no net gain of a proton in the final product suggests that the triethylamine hydrochloride may be acting catalytically to effect the acid-catalyzed loss of ethanol from **4d** (Scheme 4.2). Additionally, significant Ru-C_β interactions have been noted in similar ruthenacyclobutane complexes[9,10], suggesting that β-hydride elimination may play a role in the loss of the proton from the β-carbon of the phosphorus-containing metallacycle. Further investigation is required to fully elucidate the mechanism of this transformation.

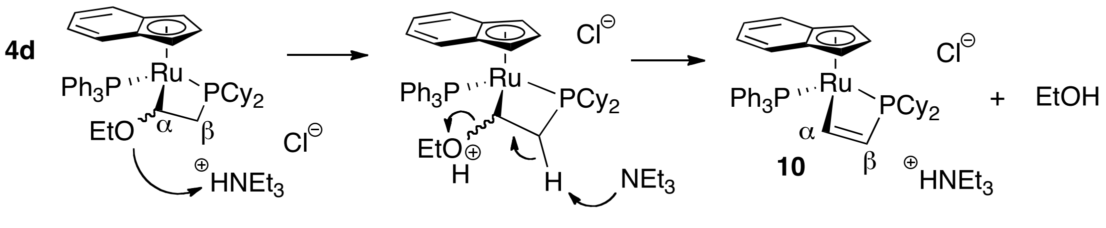

Scheme 4.2. Proposed mechanism for the formation of **10** from **4d**, through the acid-catalyzed loss of ethanol.

4.5 Conclusion

Preliminary phosphine substitution and Ru-C protonolysis studies were conducted with the overall goal of releasing a phosphinated product from metallacycles **4a-e** and **5**. Attempts to substitute the Ru-$PRCy_2$ bond of metallacycles **4a**, **b**, **d**, **e** and **5** and protonolyze the Ru-C bond with dicyclohexylphoshine were unsuccessful, yielding no reaction between the species in solution. Furthermore, no reaction was observed in subsequent attempts on metallacycles **4d** and **5** using the more acidic[6] and smaller cone angle diphenylphosphine. These results suggest that the release of the phosphinated product requires a stronger proton source to effect protonolysis before phosphine substitution can occur.

Protonolysis of the phenylacetylene adduct **5** was deemed feasible by experiments conducted with hydrochloric acid. The protonolyzed metallacycle **9** was tentatively identified by $^{31}P\{^{1}H\}$ NMR in the product mixture resulting from reaction of **5** with a solution of HCl in ether. However, undesirable by-products made concrete identification difficult, leading to experiments with the less reactive triethylamine hydrochloride. Unfortunately, $NEt_3 \cdot HCl$ was too weak a proton source to react with complex **5**.

When added to a solution of the ethoxy-substituted metallacycle **4d**, however, $NEt_3 \cdot HCl$ was found to promote the net loss of ethanol from **4d**, forming the new compound **10**. Since no net gain of a proton was noted in the final product, triethylamine hydrochloride may be acting catalytically to effect this transformation.

While no confirmed release of a phosphinated product was obtained by these studies, a better understanding of the reactivity of these metallacycles complexes towards various proton sources was gained. The next chapter discusses options for further investigation toward protonolysis and phosphine substitution, as well as other work that could expand upon topics explored in this thesis.

4.6 Experimental

See Chapter 2, Section 2.7.1 for general experimental details. Secondary phosphines were purchased from Strem as 0.3 M solutions in hexanes and used without further purification after checking phosphine concentration by $^{31}P\{^{1}H\}$ NMR. Hydrochloric acid in ether (1.0 M) was purchased from Sigma-Aldrich and used as received. Triethylamine hydrochloride was purchased from Sigma-Aldrich and dried under vacuum for 24 hours before use.

4.6.1 Experiments with Secondary Phosphines and Metallacycles **4a,b,d,e** and **5** in Solution

Solutions of metallacycles **4a,b,d,e** and **5** (10 mg) in *d*$_6$-benzene (0.3 mL) were prepared in small glass vials. Solutions of secondary phosphines ($HPCy_2$ and $HPPh_2$) in hexanes (0.45 mL, 0.3 M, 10 equiv.) were added by syringe. The yellow-orange solutions were transferred to J-Young NMR tubes and $^{31}P\{^1H\}$ NMR spectra were obtained.

4.6.2 Addition of HCl in Ether to Complex **5** in Solution

A solution of $[Ru(\eta^5\text{-indenyl})(\kappa^2\text{-Ph}\underline{C}CH\underline{P}Cy_2)(PPh_3)]$ (**5**) (86 mg, 0.11 mmol) in toluene (10 mL) was prepared in a Schlenk flask with a stir bar. HCl in ether (1.0 M, 0.11 mL, 1 equiv) was added dropwise via syringe to the stirring orange solution. Green-black precipitate formed immediately with each drop and full addition of the HCl yielded an orange-brown solution containing the black precipitate. The orange solution was decanted from the precipitate and a $^{31}P\{^1H\}$ NMR spectrum was obtained from a small aliquot of the sample using a drop of *d*$_6$-benzene for a deuterium lock. A $^{31}P\{^1H\}$ NMR spectrum of the black precipitate was obtained by dissolving it in acetonitrile and using a *d*$_6$-benzene lock. The solvent was removed from the supernatant to give a red oil, which was triturated with hexanes (4 x 30 mL) to give a brown-orange powder (42 mg). Attempts to recrystallize the powder were unsuccessful. Methods attempted included slow evaporation from both toluene and dichloromethane, and layering of acetonitrile on a toluene solution.

4.6.3 NMR-Scale Reactions of $NEt_3 \cdot HCl$ with Metallacycles **4d** and **5**

Triethylamine hydrochloride (3-5 mg, 1.5 equiv.) was added to solutions of **4d** and **5** (10 mg) in *d*$_6$-benzene (0.6 mL). The orange-yellow solutions were transferred to J.Young NMR tubes and $^{31}P\{^1H\}$ NMR spectra were obtained.

4.6.4 Synthesis of [Ru(η^5-indenyl)(κ^2-$\underline{C}HCH\underline{P}Cy_2$)($PPh_3$)] (**10**) from **4d** and $NEt_3 \cdot HCl$ in Solution

A clear orange solution of [Ru(η^5-indenyl)(κ^2-$EtO\underline{C}HCH_2\underline{P}Cy_2$)($PPh_3$)] (**4d**) (45 mg, 0.06 mmol) and $NEt_3 \cdot HCl$ (10 mg, 0.07 mmol, 1.2 equiv in toluene (5 mL) was prepared in a Schlenk flask and stirred for 1 hour. The solvent was reduced to 1 mL under vacuum and acetonitrile (20 mL) was layered on top. Bright yellow crystals formed after one day, were isolated by filtration, and washed with cold pentanes (3 x 1 mL) (29 mg, 0.04 mmol, 69% yield). X-ray crystallography, EI-MS, NMR spectroscopy and microanalysis of the product were used to identify it as [Ru(η^5-indenyl)(κ^2-$\underline{C}HCH\underline{P}Cy_2$)($PPh_3$)] (**10**). EI-MS *m/z* (relative intensity): 474 (27%) [M^+ - Cy_2PCHCH], 438 (24%) [M^+ - PPh_3], 411 (8%) [M^+ - PPh_3 - CHCH], 295 (34%) [M^+ - PPh_3 – CHCH – C_9H_7]. Anal. calcd for $C_{41}H_{46}P_2Ru$: C, 70.17; H, 6.61. Found: C, 69.66; H, 6.90. $^{31}P\{^1H\}$ NMR (121.49 MHz): 59.4 (d, 26 Hz, *P*Ph_3) and -27.0 ppm (d, 26 Hz, *P*Cy_2). See Tables 4.2 – 4.4 for full NMR characterization and Appendix D for ^1H, ^{13}C NMR spectra of **10**.

Table 4.2. 202.26 MHz $^{31}P\{^1H\}$ NMR data for protonolysis product **10** at 300K: shift in ppm (multiplicity, J_{PP} in Hz)

Complex	Number	Ru-PCy_2-	Ru-PPh_3
[Ru(η^5-indenyl)(κ^2-$\underline{C}H{=}CH\underline{P}Cy_2$)($PPh_3$)]	**10**	-27.1 (d, 26)	59.1 (d)

Table 4.3. 500.13 MHz ^{1}H NMR data for protonolysis product **10** at 300K: δ in ppm (multiplicity, RI, J_{avg} or $\omega_{1/2}$ in Hz)

η^5 - C_9H_7					
H_7, H_4	H_6, H_5	H_2	H_3, H_1	PPh_3	Others
7.60 (d, 1H, 8) 6.18 (d, 1H, 8)	6.93 (t, 1H, 7) 6.71 (t, 1H, 7)	4.36 (s, 1H)	5.37 (s, 2H)	H_O 7.36 (t, 6H, 7) H_m, H_p 7.10-7.04 (om, 9H)	$H\underline{C}$=CH: 9.55 (ddd, 1H, 4, 6, 34, H_α), 7.12 (m, ~1H, overlaps with $H_{m,p}$, H_β) Cy (PCy_2): 2.34 (br d, 1H, 12), 2.19-2.09 (m), 2.09-2.00 (m), 1.90 (br d, 2H, 12), 1.85-1.77 (br m, 19), 1.77-1.62 (om), 1.58-1.49 (br m, 25), 1.49-1.33 (om), 1.33-1.23 (om), 1.23-1.12 (om), 1.09-0.98 (om), 0.98-0.83 (om), 0.68 (br q, 1H, 13), 0.31 (br q, 1H, 13)

Table 4.4. 125.77 MHz ^{13}C NMR data for protonolysis product **10** at 300K: δ in ppm (multiplicity, J_{avg} or $\omega_{1/2}$ in Hz)

η^5 - C_9H_7							
C_6, C_5	C_7, C_4	C_{3a}, C_{7a}	$\Delta\delta(C_{3a,7a})^a$	C_2	C_3, C_1	PPh_3	Others
121.3 (s) 123.3 (s)	124.0 (s) 120.9 (s)	110.0 (s) 106.5 (s)	-22.5 (av)	92.3 (s)	70.3 (d, 10) 67.0 (d, 11)	C_i 138.5 (br d in baseline, 38) C_o 134.8 (d, 11) C_m 128.5 (s) C_p 127.2 (d, 10)	$H\underline{C}$=CH 174.2 (dd, 16, 35, C_α), 128.2 (s, C_β) PCy_2: PCH 40.3 (d, 18), 38.7 (d, 6) Others 32.4 (s), 30.3 (s), 29.3 (d, 8), 29.0 (s), 28.1 (d, 11), 27.8 (d, 11), 27.4 (d, 11), 27.2 (d, 7), 27.0 (s), 26.4 (s)

[a] *$\Delta\delta(C_{3a,7a}) = \delta(C_{3a,7a}(\eta^5\text{-indenyl complex})) - \delta(C_{3a,7a}(\eta\text{-sodium indenyl}))$. $\delta(C_{3a,7a})$ for sodium indenyl = 130.7 ppm*

4.7 References

(1) Crimmin, M. R.; Barrett, A. G. M.; Hill, M. S.; Hitchcock, P. B.; Procopiou, P. A. *Organometallics* **2007**, *26*, 2953.

(2) Motta, A.; Fragala, I. L.; Marks, T. J. *Organometallics* **2005**, *24*, 4995.

(3) Douglass, M. R.; Stern, C. L.; Marks, T. J. *J. Am. Chem. Soc.* **2001**, *123*, 10221.

(4) Shulyupin, M.; Trostyanskaya, I.; Kazankova, M.; Beletskaya, I. *Russ. J. Org. Chem.* **2006**, *42*, 17.

(5) Glueck, D. S. In *C-X Bond Formation*; Vigalok, A., Ed.; Springer Berlin Heidelberg: Berlin, Heidelberg, 2010; Vol. 31, p 65.

(6) Li, J.-N.; Liu, L.; Fu, Y.; Guo, Q.-X. *Tetrahedron* **2006**, *62*, 4453.

(7) Pantaztis, D. **2008** Unpublished results.

(8) McMurry, J. *Organic Chemistry*; 7 ed.; Cengage Learning, Brooks/Cole: Belmont, USA, 2009.

(9) Romero, P. E.; Piers, W. E. *J. Am. Chem. Soc.* **2005**, *127*, 5032.

(10) Piers, W. E.; Rowley, C. N.; van der Eide, E. F.; Woo, T. K. *Organometallics* **2008**, *27*, 6043.

Chapter 5 Future Work

5.1 Introduction

The research described in this thesis has focused on the formation of phosphorous-containing metallacycles from the [2+2] cycloaddition of unsaturated substrates to the Ru-P π-bond of [Ru(η^5-indenyl)(PCy$_2$)(PPh$_3$)] (**2**). The reagents, products, and by-products involved in the [2+2] cycloaddition, as well as their relationships with one another, were studied in detail. Rate and equilibrium constants for the isomerization of starting compound **2** were obtained, the ethylene coordination intermediate **6** was directly observed and identified by $^{31}P\{^1H\}$ NMR, and the facile cycloreversion of metallacycles **4a-e** was observed. Alkene substituent effects on the [2+2] cycloaddition were examined through computational DFT predictions (in collaboration with D. Pantazis of the Max Plank Institute for Bioinorganic Chemistry), metallacycle diastereomer distributions, rate constants, activation parameters, and a Hammett plot. The sensitivity of the [2+2] cycloaddition to electronic effects was found to decrease with decreasing electron-withdrawing ability of alkene substituents, allowing steric effects to play a greater role in the rates and selectivity of electron-rich alkene cycloadditions.

The following sections highlight ways in which the findings of this thesis can be studied in greater detail, expanded to include a wider range of substrates, and built upon to work towards a final goal of ruthenium-catalyzed hydrophosphination.

5.1.1 In-Depth Investigation: Metallacycle Diastereomer Epimerization

Diastereoselectivity in the [2+2] cycloaddition of terminal alkenes to give metallacycles **4b-e** was discussed in Chapter 3, Section 3.2. Understanding and exploiting this stereoselectivity is key in introducing chirality into a potential hydrophosphination product. Much of this thesis has focused on determining both initial, kinetic formation of metallacycle diastereomers and final thermodynamic distributions in order to establish the source of stereoselectivity. The process of diastereomer epimerization, however, remains largely unexplored. Greater control could be exerted in the stereoselective formation of chiral products if relative rates and mechanisms by which metallacycles convert from *syn* to *anti* isomers (or vice versa) were known.

There are a number of ways in which *syn* and *anti* isomers may interconvert, with two dissociative mechanisms appearing the most likely (Figure 5.1). In mechanism **A** (Figure 5.1), the metallacyclic phosphine –PCy_2– dissociates and re-associates on the opposite side of the Ru-C bond, thereby inverting the stereochemistry at the ruthenium centre and changing the orientation of the metallacyclic substituent relative to the coordinated indenyl ligand. In mechanism **B** (Figure 5.1), the triphenylphosphine ligand dissociates and the four-membered metallacycle inverts through a possibly strained, planar intermediate before triphenylphosphine reassociates on the opposite side of the ruthenium centre. This latter mechanism, inversion at a half-sandwich metal centre through a planar intermediate, has been examined in detail in similar, cyclic Ru complexes by Brunner[1,2].

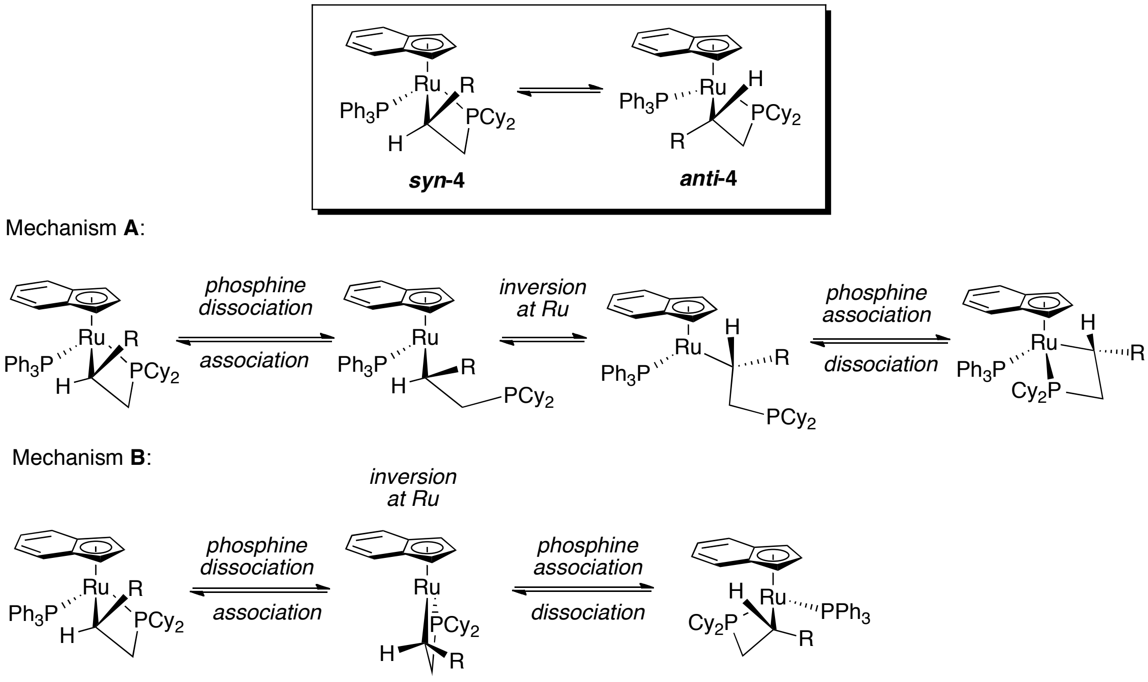

Figure 5.1. Possible mechanisms for metallacycle epimerization.

Future studies may be conducted on the metallacycles described in this thesis to distinguish these two mechanisms. First, rates of diastereomer epimerization may be determined by 2D-exchange spectroscopy (EXSY) NMR. Once standard rates of epimerization are determined, changes to rates of epimerization may be monitored in subsequent investigations. For example, the rate of metallacycle epimerization in the presence of excess triphenylphosphine could be determined. A decrease in the rate of epimerization would suggest that mechanism **B** was occurring, as excess triphenylphosphine would inhibit initial ligand dissociation.

5.1.2 Widening the Scope: Unsymmetrically-Substituted Phosphine Substrates

In addition to the more in-depth studies of metallacycle epimerization, the findings of this research can also be applied more broadly to widen the scope of the [2+2] cycloaddition to a variety of substrates, ultimately making a possible Ru hydrophosphination catalyst more versatile. One way to explore this area is by experimenting with unsymmetrically-substituted phosphine substrates. Unsymmetrically-substituted phosphines have the potential to form chiral-at-phosphorus compounds through stereoselective P-C bond formation.

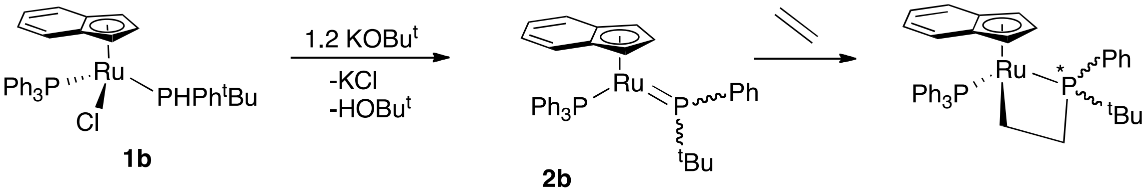

Scheme 5.1. Potential parallel route for secondary phosphine activation and [2+2] cycloaddition using an unsymmetrically-substituted phosphine.

A compound analogous to **1a** has been synthesized with an unsymmetrically-substituted secondary phosphine (**1b**) by a previous student, Greg Gibson[3]. Preliminary studies attempting the activation of the coordinated secondary phosphine of **1b** by the addition of base were conducted and recently published[3] (Scheme 5.1). Inequivalent distributions of isomer products **2b** were observed by $^{31}P\{^{1}H\}$ NMR for this reaction, which shows promise for further development with the possibility of stereoselective activation. The analogy to the symmetrically-substituted phosphine complexes could be extended and there may be potential for enantioselective metal-mediated P-C bond formation with unsaturated substrates resulting in chiral-at-phosphorus product phosphines.

5.1.3 Moving Forward: Promotion of Catalytic Turnover

As described in Chapter 4, preliminary studies were conducted to attempt the protonolysis of metallcycle complexes and subsequent regeneration of the active species **2**, thereby promoting putative catalytic turnover. Although protonolysis of the phenylacetylene adduct **5** was unsuccessful with secondary phosphines and triethylamine hydrochloride as proton sources, the protonolysis product **7d** was tentatively identified in a product mixture resulting from reaction with hydrochloric acid. Future work should focus on achieving effective protonolysis without by-product formation using a proton source less reactive than HCl (pK_a = -7)[4] and more reactive than $NEt_3\cdot HCl$ (pK_a = 11)[5], such as sodium bisulfate, $NaHSO_4$ (pK_a = 1.92)[6], or formic acid, HCO_2H (pK_a = 3.75)[6].

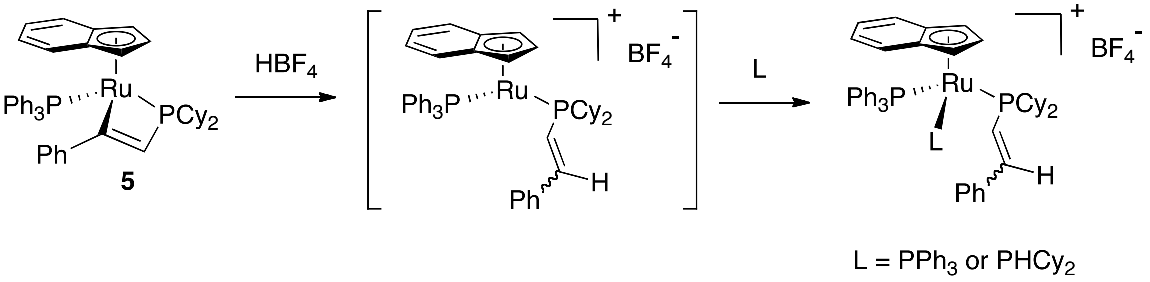

Scheme 5.2. Putative protonolysis of **5** with a proton source containing a non-coordinating anion.

In the full putative catalytic cycle, however, some problems may arise from these proton sources, namely competition for coordination to the metal centre between the corresponding anion and the phosphination substrate. Therefore, proton sources without coordinating anions, such as fluoroboric acid, HBF_4 (pK_a = -0.4)[7] are worth investigating (Scheme 5.2). Furthermore, the unsaturated, 5-coordinate product of this protonolysis is likely to be unstable and may be trapped by the addition of an L-type ligand, such as PPh_3 or $HPCy_2$ (Scheme 5.2), with smaller cone angle secondary phosphines likely coordinating more readily than the larger, tertiary phosphines. This outcome would accomplish the secondary phosphine coordination that is the necessary next step for achieving full catalytic turnover to **2**.

If protonolysis and subsequent catalytic turnover to active species **2** is unsuccessful, other methods of metallacycle opening may be explored that lead to stoichiometic tertiary phosphine formation. Addition of hydrogen or electrophiles (such as methyl iodide or $[Me_3O][BF_4]$) may result in Ru-C bond cleavage of **5** (Scheme 5.3), but would ultimately prove to be detrimental to catalysis. Methyl iodide or hydrogen would react to remove **2** from a catalytic process as has been shown previously by Derrah *et al*[8]. The nucleophilic phosphido would abstract the electrophile from each (CH_3^+ and H^+, respectively), leaving the corresponding anion to coordinate to the ruthenium centre (I^- and H^-), thereby removing any active species **2** from solution in a possible catalytic cycle.

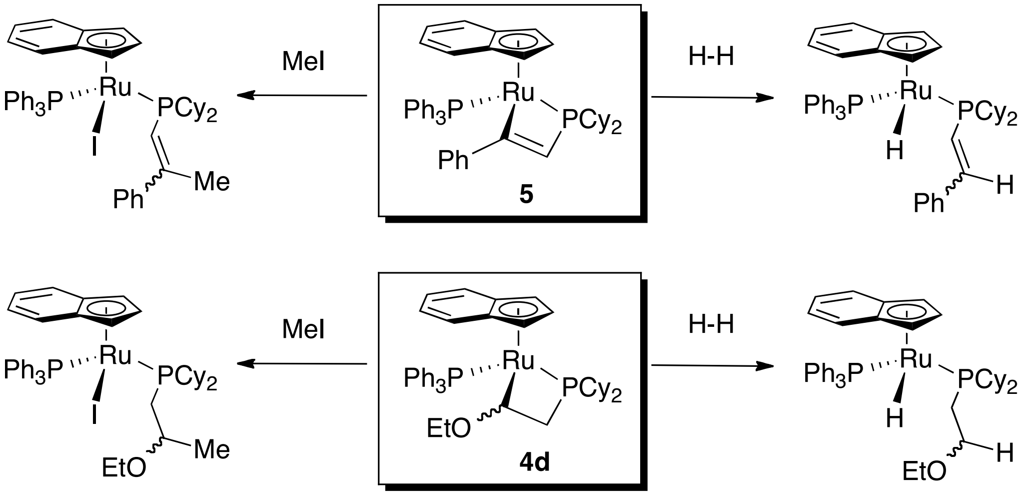

Scheme 5.3. Possible Ru-C bond cleavage of **4d** and/or **5** with hydrogen or electrophile MeI.

This method of Ru-C bond cleavage may also be suitable for the ethyl vinyl ether adduct **4d**. If **4d** did indeed undergo acid-catalyzed loss of ethanol as described in Chapter 4, Section 4.4.2 (which initial studies should first ascertain), then metallacycle protonolysis using the acids proposed for **5** previously is not likely to be successful. Thus, the viablitiy of stoichiometric hydrophosphination of ethyl vinyl ether should be examined using the non-protic methods of Ru-C bond cleavage (Scheme 5.3).

5.2 Summary

The findings described in this thesis explore the rich reactivity of [2+2] cycloadditions between unsaturated substrates and the terminal phosphido species [Ru(η^5-indenyl)(PCy_2)(PPh_3)] (**2**). The formation of phosphorus-containing metallacycles via this mechanism were investigated in detail: identification and analysis of reagents, intermediates, products, and byproducts involved; kinetic studies of transition-state alkene substituent effects on the [2+2] cycloaddition; and finally, preliminary attempts at the controlled release of phosphinated products from the phosphorus-containing metallacycles. However, the possibilities of this system extend far beyond the scope of this thesis. Questions answered by the previously-described findings raise many more interesting avenues of pursuit, including reactivity studies on new half-sandwich ruthenium complexes, kinetic and mechanistic studies on metallacycle diastereomer interconversion, as well as the possibility for the development of a complete, asymmetric, ruthenium-mediated hydrophosphination catalytic cycle.

5.3 References

(1) Brunner, H.; Muschiol, M.; Tsuno, T.; Takahashi, T.; Zabel, M. *Organometallics* **2008**, *27*, 3514.

(2) Brunner, H.; Tsuno, T. *Acc. Chem. Res.* **2009**, *42*, 1501.

(3) Gibson, G. L.; Morrow, K. M. E.; McDonald, R.; Rosenberg, L. *Inorg. Chim. Acta* **2011**, *369*, 133.

(4) McMurry, J. *Organic Chemistry*; 7 ed.; Cengage Learning, Brooks/Cole: Belmont, USA, 2009.

(5) Gordon, A. J.; Ford, R. A. *The Chemist's Companion: A Handbook of Practical Data, Techniques, and References*; John Wiley & Sons: New York, 1972.

(6) Anslyn, E. V.; Dougherty, D. A. *Modern Physical Organic Chemistry*; University Science Books: Sausalito, California, 2006.

(7) Housecroft, C. E.; Sharpe, A. G. *Inorganic Chemistry*; Pearson Prentice Hall: Edinburgh Gate, 2005.

(8) Derrah, E. J.; Pantazis, D. A.; McDonald, R.; Rosenberg, L. *Organometallics* **2007**, *26*, 1473.

Appendix A

X-Ray Crystallographic Structure Report for $[\mathrm{Ru}(\eta^5\text{-indenyl})(\kappa^2\text{-Ph}\underline{\mathrm{C}}\mathrm{HCH_2}\underline{\mathrm{P}}\mathrm{Cy_2})(\mathrm{PPh_3})]$ (4e)

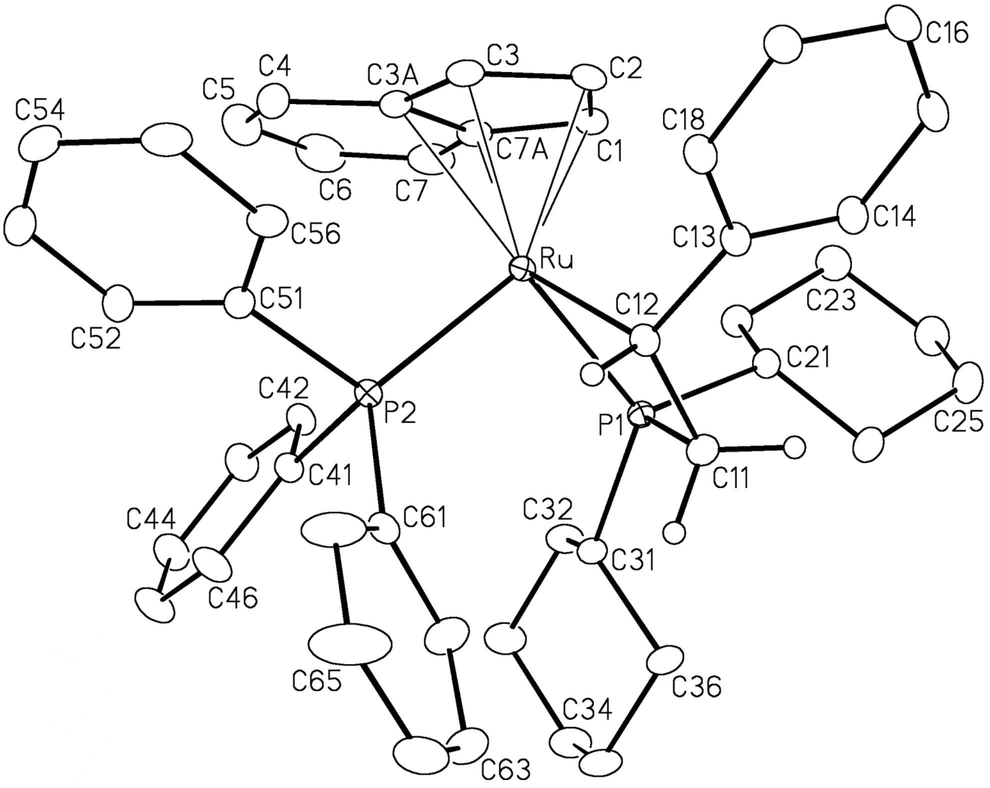

Figure A.1. Perspective view of the $[(\eta^5\text{–indenyl})\mathrm{Ru}(\kappa^2\text{–}\underline{\mathrm{P}}\mathrm{Cy_2CH_2}\underline{\mathrm{C}}\mathrm{HPh})(\mathrm{PPh_3})]$ (**4e**) molecule showing the atom labelling scheme. Non-hydrogen atoms are represented by Gaussian ellipsoids at the 20% probability level. The hydrogen atoms attached to C11 and C12 are shown with arbitrarily small thermal parameters; all other hydrogens are not shown.

This structure determination, as well as that of complex **10** (Appendix B), was carried out by Dr. Robert McDonald at the X-ray Crystallography Laboratory, Department of Chemistry, University of Alberta, Edmonton, Alberta, Canada T6G 2G2. Phone: 1 780 492 2485. Fax: 1 780 492 8231. E-mail: Bob.McDonald@ualberta.ca.

Table A.1. Crystallographic Experimental Details for [Ru(η^5-indenyl)(κ^2-Ph$\underline{\text{C}}$HCH$_2$$\underline{\text{P}}Cy_2$)(PPh$_3$)] (**4e**)

A. Crystal Data

formula	$C_{47}H_{52}P_2Ru$
formula weight	779.90
crystal dimensions (mm)	0.44 × 0.33 × 0.26
crystal system	monoclinic
space group	$P2_1/c$ (No. 14)
unit cell parameters[a]	
a (Å)	14.6811 (13)
b (Å)	13.3276 (12)
c (Å)	20.0712 (18)
β (deg)	99.3409 (12)
V (Å^3)	3875.1 (6)
Z	4
ρ_{calcd} (g cm^{-3})	1.337
μ (mm^{-1})	0.520

B. Data Collection and Refinement Conditions

diffractometer	Bruker PLATFORM/APEX II CCD[b]
radiation (λ [Å])	graphite-monochromated Mo Kα (0.71073)
temperature (°C)	–100
scan type	ω scans (0.3°) (15 s exposures)
data collection 2θ limit (deg)	55.02
total data collected	34530 ($-19 \le h \le 19$, $-17 \le k \le 17$, $-26 \le l \le 26$)
independent reflections	8912 ($R_{\text{int}} = 0.0169$)
number of observed reflections (*NO*)	8176 [$F_o^2 \ge 2\sigma(F_o^2)$]
structure solution method	Patterson/structure expansion (*DIRDIF–2008*[c])
refinement method	full-matrix least-squares on F^2 (*SHELXL–97*[d])
absorption correction method	Gaussian integration (face-indexed)
range of transmission factors	0.8772–0.8040
data/restraints/parameters	8912 / 0 / 451
goodness-of-fit (S)[e] [all data]	1.040
final R indices[f]	
R_1 [$F_o^2 \ge 2\sigma(F_o^2)$]	0.0207
wR_2 [all data]	0.0546
largest difference peak and hole	0.337 and –0.413 e Å^{-3}

(continued)

Table A.1. Crystallographic Experimental Details for [Ru(η^5-indenyl)(κ^2-PhCHCH$_2$PCy$_2$)(PPh$_3$)] (**4e**) (continued)

[a] Obtained from least-squares refinement of 9296 reflections with 4.42° < 2θ < 41.32°.

[b] Programs for diffractometer operation, data collection, data reduction and absorption correction were those supplied by Bruker.

[c] Beurskens, P. T.; Beurskens, G.; de Gelder, R.; Smits, J. M. M.; Garcia-Granda, S.; Gould, R. O. (2008). The *DIRDIF-2008* program system. Crystallography Laboratory, Radboud University Nijmegen, The Netherlands.

[d] Sheldrick, G. M. *Acta Crystallogr.* **2008**, *A64*, 112–122.

[e] $S = [\Sigma w(F_o^2 - F_c^2)^2/(n - p)]^{1/2}$ (n = number of data; p = number of parameters varied; $w = [\sigma^2(F_o^2) + (0.0228P)^2 + 1.8778P]^{-1}$ where $P = [\mathrm{Max}(F_o^2, 0) + 2F_c^2]/3$).

[f] $R_1 = \Sigma||F_o| - |F_c||/\Sigma|F_o|$; $wR_2 = [\Sigma w(F_o^2 - F_c^2)^2/\Sigma w(F_o^4)]^{1/2}$.

Table A.2. Atomic Coordinates and Equivalent Isotropic Displacement Parameters for [Ru(η^5-indenyl)(κ^2-PhCHCH$_2$PCy$_2$)(PPh$_3$)] (4e)

Atom	x	y	z	U_{eq}, Å^2
Ru	0.332941(7)	0.342649(7)	0.170132(5)	0.02100(3)*
P1	0.35302(2)	0.43034(2)	0.269716(16)	0.02204(7)*
P2	0.20474(2)	0.42616(2)	0.118841(16)	0.02233(7)*
C1	0.41133(11)	0.20538(11)	0.20641(8)	0.0354(3)*
C2	0.44127(10)	0.23739(11)	0.14678(8)	0.0360(3)*
C3	0.36695(10)	0.23064(11)	0.09240(7)	0.0330(3)*
C3A	0.29185(10)	0.18286(10)	0.11743(7)	0.0314(3)*
C4	0.20522(12)	0.14640(12)	0.08465(10)	0.0457(4)*
C5	0.14984(14)	0.09621(14)	0.12175(14)	0.0635(6)*
C6	0.17533(15)	0.08219(14)	0.19157(14)	0.0637(6)*
C7	0.25742(14)	0.11776(12)	0.22534(10)	0.0492(4)*
C7A	0.31857(11)	0.16705(10)	0.18861(8)	0.0329(3)*
C11	0.40753(10)	0.53142(10)	0.22831(7)	0.0284(3)*
C12	0.41426(9)	0.47803(10)	0.16120(6)	0.0253(3)*
C13	0.50894(9)	0.45380(10)	0.14826(7)	0.0268(3)*
C14	0.58483(9)	0.43864(11)	0.19909(7)	0.0322(3)*
C15	0.67001(10)	0.40948(12)	0.18374(8)	0.0374(3)*
C16	0.68295(10)	0.39690(12)	0.11765(8)	0.0373(3)*
C17	0.60917(10)	0.41372(12)	0.06622(8)	0.0364(3)*
C18	0.52398(10)	0.44143(12)	0.08162(7)	0.0323(3)*
C21	0.44554(9)	0.38479(10)	0.33715(7)	0.0274(3)*
C22	0.42190(10)	0.29125(11)	0.37567(7)	0.0339(3)*
C23	0.50905(12)	0.24782(13)	0.41803(9)	0.0449(4)*

Table A.2. Atomic Coordinates and Displacement Parameters for [Ru(η^5-indenyl)(κ^2-Ph$\underline{C}$HCH$_2$$\underline{P}Cy_2$)(PPh$_3$)] (**4e**) (continued)

Atom	*x*	*y*	*z*	U_{eq}, Å^2
C24	0.55735(13)	0.32578(14)	0.46701(9)	0.0502(4)*
C25	0.57809(12)	0.42091(14)	0.43033(9)	0.0475(4)*
C26	0.49043(11)	0.46363(12)	0.38784(8)	0.0379(3)*
C31	0.26103(9)	0.48817(10)	0.31056(7)	0.0261(3)*
C32	0.21913(11)	0.41918(11)	0.35831(8)	0.0371(3)*
C33	0.13037(12)	0.46477(13)	0.37619(10)	0.0485(4)*
C34	0.14886(13)	0.56837(14)	0.40760(10)	0.0501(4)*
C35	0.19297(13)	0.63680(13)	0.36110(10)	0.0473(4)*
C36	0.28128(11)	0.59154(12)	0.34334(9)	0.0389(3)*
C41	0.09907(9)	0.40773(10)	0.15551(7)	0.0270(3)*
C42	0.09429(10)	0.32468(11)	0.19635(8)	0.0315(3)*
C43	0.01324(10)	0.30270(13)	0.22092(8)	0.0400(4)*
C44	-0.06263(11)	0.36442(13)	0.20558(9)	0.0433(4)*
C45	-0.05868(11)	0.44740(13)	0.16563(10)	0.0461(4)*
C46	0.02142(10)	0.46917(12)	0.14010(9)	0.0398(4)*
C51	0.16812(10)	0.37970(11)	0.03237(7)	0.0300(3)*
C52	0.08100(12)	0.34080(12)	0.00887(9)	0.0414(4)*
C53	0.06009(14)	0.30419(14)	-0.05677(10)	0.0573(5)*
C54	0.12429(17)	0.30765(16)	-0.09903(10)	0.0654(7)*
C55	0.21099(15)	0.34668(14)	-0.07690(8)	0.0545(5)*
C56	0.23354(12)	0.38181(12)	-0.01110(7)	0.0373(3)*
C61	0.19909(9)	0.56390(10)	0.10309(7)	0.0267(3)*
C62	0.19779(14)	0.63025(13)	0.15586(8)	0.0490(4)*
C63	0.19659(14)	0.73360(13)	0.14660(10)	0.0522(5)*
C64	0.19563(13)	0.77332(13)	0.08420(11)	0.0512(5)*
C65	0.1945(2)	0.70928(15)	0.03075(12)	0.0755(8)*
C66	0.19685(15)	0.60565(13)	0.04009(9)	0.0542(5)*

Anisotropically-refined atoms are marked with an asterisk (*). The form of the anisotropic displacement parameter is: $\exp[-2\pi^2(h^2a^{*2}U_{11} + k^2b^{*2}U_{22} + l^2c^{*2}U_{33} + 2klb^*c^*U_{23} + 2hla^*c^*U_{13} + 2hka^*b^*U_{12})]$.

Table A.3. Selected Interatomic Distances (Å) for [Ru(η^5-indenyl)(κ^2-Ph$\underline{\mathrm{C}}$HCH$_2\underline{\mathrm{P}}$Cy$_2$)(PPh$_3$)] (**4e**)

Atom1	Atom2	Distance	Atom1	Atom2	Distance
Ru	P1	2.2927(4)	C17	C18	1.386(2)
Ru	P2	2.2830(4)	C21	C22	1.5360(19)
Ru	C1	2.2203(14)	C21	C26	1.5349(19)
Ru	C2	2.2269(14)	C22	C23	1.530(2)
Ru	C3	2.2726(14)	C23	C24	1.524(3)
Ru	C3A	2.4106(14)	C24	C25	1.521(3)
Ru	C7A	2.3842(14)	C25	C26	1.534(2)
Ru	C12	2.1869(13)	C31	C32	1.5276(19)
P1	C11	1.8336(13)	C31	C36	1.5348(19)
P1	C21	1.8571(13)	C32	C33	1.532(2)
P1	C31	1.8573(13)	C33	C34	1.524(2)
P2	C41	1.8383(13)	C34	C35	1.522(3)
P2	C51	1.8389(14)	C35	C36	1.524(2)
P2	C61	1.8623(14)	C41	C42	1.3859(19)
C1	C2	1.407(2)	C41	C46	1.3969(19)
C1	C7A	1.444(2)	C42	C43	1.391(2)
C2	C3	1.415(2)	C43	C44	1.379(2)
C3	C3A	1.433(2)	C44	C45	1.373(2)
C3A	C4	1.419(2)	C45	C46	1.387(2)
C3A	C7A	1.434(2)	C51	C52	1.390(2)
C4	C5	1.364(3)	C51	C56	1.399(2)
C5	C6	1.403(3)	C52	C53	1.392(2)
C6	C7	1.368(3)	C53	C54	1.367(3)
C7	C7A	1.413(2)	C54	C55	1.380(3)
C11	C12	1.5407(18)	C55	C56	1.390(2)
C12	C13	1.4903(17)	C61	C62	1.382(2)
C13	C14	1.3979(19)	C61	C66	1.377(2)
C13	C18	1.4003(19)	C62	C63	1.390(2)
C14	C15	1.391(2)	C63	C64	1.358(3)
C15	C16	1.380(2)	C64	C65	1.369(3)
C16	C17	1.388(2)	C65	C66	1.393(3)

Table A.4. Selected Interatomic Angles (°) for [Ru(η^5-indenyl)(κ^2-Ph$\underline{C}$HCH$_2\underline{P}$Cy$_2$)(PPh$_3$)] (**4e**)

Atom1	Atom2	Atom3	Angle	Atom1	Atom2	Atom3	Angle
P1	Ru	P2	97.154(13)	Ru	C1	C2	71.82(8)
P1	Ru	C1	98.49(4)	Ru	C1	C7A	78.02(8)
P1	Ru	C2	120.63(4)	C2	C1	C7A	108.00(13)
P1	Ru	C3	157.20(4)	Ru	C2	C1	71.31(8)
P1	Ru	C3A	145.13(4)	Ru	C2	C3	73.43(8)
P1	Ru	C7A	111.52(4)	C1	C2	C3	109.19(13)
P1	Ru	C12	69.90(4)	Ru	C3	C2	69.92(8)
P2	Ru	C1	153.52(4)	Ru	C3	C3A	77.52(8)
P2	Ru	C2	140.97(4)	C2	C3	C3A	107.37(13)
P2	Ru	C3	105.52(4)	Ru	C3A	C3	67.00(8)
P2	Ru	C3A	95.94(4)	Ru	C3A	C4	130.35(10)
P2	Ru	C7A	117.47(4)	Ru	C3A	C7A	71.59(8)
P2	Ru	C12	88.96(4)	C3	C3A	C4	132.24(15)
C1	Ru	C2	36.88(6)	C3	C3A	C7A	108.23(13)
C1	Ru	C3	61.57(5)	C4	C3A	C7A	119.40(15)
C1	Ru	C3A	59.70(5)	C3A	C4	C5	118.93(18)
C1	Ru	C7A	36.34(5)	C4	C5	C6	121.64(18)
C1	Ru	C12	116.48(5)	C5	C6	C7	121.30(18)
C2	Ru	C3	36.65(5)	C6	C7	C7A	119.06(18)
C2	Ru	C3A	59.17(5)	Ru	C7A	C1	65.64(8)
C2	Ru	C7A	59.91(6)	Ru	C7A	C3A	73.60(8)
C2	Ru	C12	94.85(5)	Ru	C7A	C7	128.13(11)
C3	Ru	C3A	35.48(5)	C1	C7A	C3A	106.80(13)
C3	Ru	C7A	59.79(5)	C1	C7A	C7	133.54(16)
C3	Ru	C12	107.57(5)	C3A	C7A	C7	119.60(15)
C3A	Ru	C7A	34.81(5)	P1	C11	C12	98.72(9)
C3A	Ru	C12	142.56(5)	Ru	C12	C11	101.30(8)
C7A	Ru	C12	152.36(5)	Ru	C12	C13	111.87(9)
Ru	P1	C11	89.04(4)	C11	C12	C13	116.51(11)
Ru	P1	C21	116.37(5)	C12	C13	C14	124.03(12)
Ru	P1	C31	126.63(4)	C12	C13	C18	119.21(12)
C11	P1	C21	104.42(6)	C14	C13	C18	116.72(12)
C11	P1	C31	107.30(6)	C13	C14	C15	121.15(14)
C21	P1	C31	108.19(6)	C14	C15	C16	121.05(14)
Ru	P2	C41	116.22(5)	C15	C16	C17	118.85(13)
Ru	P2	C51	110.78(5)	C16	C17	C18	120.05(14)
Ru	P2	C61	124.60(4)	C13	C18	C17	122.15(13)
C41	P2	C51	101.33(6)	P1	C21	C22	115.71(9)
C41	P2	C61	100.51(6)	P1	C21	C26	116.35(10)
C51	P2	C61	100.00(6)	C22	C21	C26	109.25(11)

Table A.4. Selected Interatomic Angles for [Ru(η^5-indenyl)(κ^2-Ph<u>C</u>HCH$_2$<u>P</u>Cy$_2$)(PPh$_3$)] (**4e**) (continued)

Atom1	Atom2	Atom3	Angle	Atom1	Atom2	Atom3	Angle
C21	C22	C23	110.48(13)	C44	C45	C46	120.19(15)
C22	C23	C24	111.10(14)	C41	C46	C45	120.38(14)
C23	C24	C25	111.39(14)	P2	C51	C52	123.91(12)
C24	C25	C26	111.27(14)	P2	C51	C56	117.18(11)
C21	C26	C25	110.23(13)	C52	C51	C56	118.88(14)
P1	C31	C32	115.01(9)	C51	C52	C53	120.11(18)
P1	C31	C36	117.23(10)	C52	C53	C54	120.46(19)
C32	C31	C36	109.95(12)	C53	C54	C55	120.39(16)
C31	C32	C33	110.65(13)	C54	C55	C56	119.86(19)
C32	C33	C34	110.80(14)	C51	C56	C55	120.28(17)
C33	C34	C35	110.74(14)	P2	C61	C62	120.42(11)
C34	C35	C36	111.66(15)	P2	C61	C66	123.23(12)
C31	C36	C35	110.04(13)	C62	C61	C66	116.35(14)
P2	C41	C42	118.07(10)	C61	C62	C63	122.22(16)
P2	C41	C46	122.99(11)	C62	C63	C64	120.52(17)
C42	C41	C46	118.77(13)	C63	C64	C65	118.48(16)
C41	C42	C43	120.41(13)	C64	C65	C66	121.04(18)
C42	C43	C44	120.11(15)	C61	C66	C65	121.36(17)
C43	C44	C45	120.13(14)				

Table A.5. Torsional Angles (deg) for $[Ru(\eta^5\text{-indenyl})(\kappa^2\text{-Ph}\underline{C}HCH_2\underline{P}Cy_2)(PPh_3)]$ (**4e**)

Atom1	Atom2	Atom3	Atom4	Angle
P2	Ru	P1	C11	-80.02(5)
P2	Ru	P1	C21	174.33(5)
P2	Ru	P1	C31	30.96(5)
C1	Ru	P1	C11	121.41(6)
C1	Ru	P1	C21	15.76(7)
C1	Ru	P1	C31	-127.61(7)
C2	Ru	P1	C11	89.79(7)
C2	Ru	P1	C21	-15.86(7)
C2	Ru	P1	C31	-159.23(7)
C3	Ru	P1	C11	93.88(11)
C3	Ru	P1	C21	-11.76(12)
C3	Ru	P1	C31	-155.14(11)
C3A	Ru	P1	C11	168.72(7)
C3A	Ru	P1	C21	63.07(8)
C3A	Ru	P1	C31	-80.30(8)
C7A	Ru	P1	C11	156.66(6)
C7A	Ru	P1	C21	51.01(6)
C7A	Ru	P1	C31	-92.36(7)
C12	Ru	P1	C11	6.23(6)
C12	Ru	P1	C21	-99.42(6)
C12	Ru	P1	C31	117.21(7)
P1	Ru	P2	C41	-67.64(5)
P1	Ru	P2	C51	177.45(5)
P1	Ru	P2	C61	58.29(6)
C1	Ru	P2	C41	58.21(11)
C1	Ru	P2	C51	-56.70(11)
C1	Ru	P2	C61	-175.86(10)
C2	Ru	P2	C41	126.35(8)
C2	Ru	P2	C51	11.44(9)
C2	Ru	P2	C61	-107.72(8)
C3	Ru	P2	C41	114.80(6)
C3	Ru	P2	C51	-0.10(7)
C3	Ru	P2	C61	-119.26(7)
C3A	Ru	P2	C41	79.97(6)
C3A	Ru	P2	C51	-34.94(6)
C3A	Ru	P2	C61	-154.10(7)
C7A	Ru	P2	C41	51.17(7)
C7A	Ru	P2	C51	-63.73(7)
C7A	Ru	P2	C61	177.11(7)
C12	Ru	P2	C41	-137.23(6)
C12	Ru	P2	C51	107.86(6)
C12	Ru	P2	C61	-11.30(6)
P1	Ru	C1	C2	-131.25(8)
P1	Ru	C1	C7A	115.03(8)
P2	Ru	C1	C2	103.15(12)
P2	Ru	C1	C7A	-10.57(15)
C2	Ru	C1	C7A	-113.72(13)
C3	Ru	C1	C2	36.99(9)
C3	Ru	C1	C7A	-76.73(9)
C3A	Ru	C1	C2	77.87(9)
C3A	Ru	C1	C7A	-35.85(8)
C7A	Ru	C1	C2	113.72(13)
C12	Ru	C1	C2	-59.55(10)
C12	Ru	C1	C7A	-173.27(8)
P1	Ru	C2	C1	59.78(10)
P1	Ru	C2	C3	177.34(7)
P2	Ru	C2	C1	-136.40(8)
P2	Ru	C2	C3	-18.84(12)
C1	Ru	C2	C3	117.56(13)
C3	Ru	C2	C1	-117.56(13)
C3A	Ru	C2	C1	-79.42(10)
C3A	Ru	C2	C3	38.14(9)
C7A	Ru	C2	C1	-38.83(9)
C7A	Ru	C2	C3	78.74(10)
C12	Ru	C2	C1	129.25(9)
C12	Ru	C2	C3	-113.18(9)
P1	Ru	C3	C2	-5.91(16)
P1	Ru	C3	C3A	108.08(11)
P2	Ru	C3	C2	167.82(8)
P2	Ru	C3	C3A	-78.20(8)
C1	Ru	C3	C2	-37.22(9)
C1	Ru	C3	C3A	76.76(9)
C2	Ru	C3	C3A	113.98(13)
C3A	Ru	C3	C2	-113.98(13)
C7A	Ru	C3	C2	-79.08(10)
C7A	Ru	C3	C3A	34.90(8)
C12	Ru	C3	C2	73.90(10)
C12	Ru	C3	C3A	-172.11(8)
P1	Ru	C3A	C3	-139.87(8)
P1	Ru	C3A	C4	93.43(16)

Table A.5. Torsional Angles for $[Ru(\eta^5\text{-indenyl})(\kappa^2\text{-Ph}\underline{C}HCH_2\underline{P}Cy_2)(PPh_3)]$ (**4e**) (continued)

Atom1	Atom2	Atom3	Atom4	Angle
P1	Ru	C3A	C7A	-19.91(12)
P2	Ru	C3A	C3	108.51(8)
P2	Ru	C3A	C4	-18.19(16)
P2	Ru	C3A	C7A	-131.52(8)
C1	Ru	C3A	C3	-82.53(10)
C1	Ru	C3A	C4	150.78(18)
C1	Ru	C3A	C7A	37.44(9)
C2	Ru	C3A	C3	-39.43(9)
C2	Ru	C3A	C4	-166.12(18)
C2	Ru	C3A	C7A	80.54(10)
C3	Ru	C3A	C4	-126.70(19)
C3	Ru	C3A	C7A	119.97(12)
C7A	Ru	C3A	C3	-119.97(12)
C7A	Ru	C3A	C4	113.34(19)
C12	Ru	C3A	C3	12.43(13)
C12	Ru	C3A	C4	-114.27(16)
C12	Ru	C3A	C7A	132.40(10)
P1	Ru	C7A	C1	-74.44(9)
P1	Ru	C7A	C3A	167.92(7)
P1	Ru	C7A	C7	52.86(17)
P2	Ru	C7A	C1	174.71(7)
P2	Ru	C7A	C3A	57.07(9)
P2	Ru	C7A	C7	-57.99(17)
C1	Ru	C7A	C3A	-117.64(13)
C1	Ru	C7A	C7	127.3(2)
C2	Ru	C7A	C1	39.42(9)
C2	Ru	C7A	C3A	-78.22(9)
C2	Ru	C7A	C7	166.72(18)
C3	Ru	C7A	C1	82.06(10)
C3	Ru	C7A	C3A	-35.58(8)
C3	Ru	C7A	C7	-150.64(18)
C3A	Ru	C7A	C1	117.64(13)
C3A	Ru	C7A	C7	-115.06(19)
C12	Ru	C7A	C1	13.08(16)
C12	Ru	C7A	C3A	-104.56(12)
C12	Ru	C7A	C7	140.38(15)
P1	Ru	C12	C11	-7.57(7)
P1	Ru	C12	C13	117.23(9)
P2	Ru	C12	C11	90.44(8)
P2	Ru	C12	C13	-144.76(9)
C1	Ru	C12	C11	-97.19(9)
C1	Ru	C12	C13	27.61(11)
C2	Ru	C12	C11	-128.46(9)
C2	Ru	C12	C13	-3.66(10)
C3	Ru	C12	C11	-163.60(8)
C3	Ru	C12	C13	-38.80(10)
C3A	Ru	C12	C11	-171.13(8)
C3A	Ru	C12	C13	-46.33(13)
C7A	Ru	C12	C11	-105.80(12)
C7A	Ru	C12	C13	19.00(16)
Ru	P1	C11	C12	-8.42(8)
C21	P1	C11	C12	108.60(9)
C31	P1	C11	C12	-136.71(8)
Ru	P1	C21	C22	-77.47(11)
Ru	P1	C21	C26	152.22(10)
C11	P1	C21	C22	-173.68(10)
C11	P1	C21	C26	56.01(12)
C31	P1	C21	C22	72.27(12)
C31	P1	C21	C26	-58.04(12)
Ru	P1	C31	C32	88.42(11)
Ru	P1	C31	C36	-140.01(10)
C11	P1	C31	C32	-169.49(11)
C11	P1	C31	C36	-37.92(13)
C21	P1	C31	C32	-57.34(12)
C21	P1	C31	C36	74.23(12)
Ru	P2	C41	C42	-19.36(13)
Ru	P2	C41	C46	165.50(12)
C51	P2	C41	C42	100.77(12)
C51	P2	C41	C46	-74.37(14)
C61	P2	C41	C42	-156.68(11)
C61	P2	C41	C46	28.18(14)
Ru	P2	C51	C52	122.71(12)
Ru	P2	C51	C56	-55.57(12)
C41	P2	C51	C52	-1.21(14)
C41	P2	C51	C56	-179.49(11)
C61	P2	C51	C52	-104.17(13)
C61	P2	C51	C56	77.55(12)
Ru	P2	C61	C62	-72.94(14)
Ru	P2	C61	C66	106.45(14)
C41	P2	C61	C62	59.43(14)

Table A.5. Torsional Angles for [Ru(η^5-indenyl)(κ^2-Ph$\underline{C}$HCH$_2\underline{P}$Cy$_2$)(PPh$_3$)] (**4e**) (continued)

Atom1	Atom2	Atom3	Atom4	Angle	Atom1	Atom2	Atom3	Atom4	Angle
C41	P2	C61	C66	-121.18(15)	C11	C12	C13	C14	26.34(19)
C51	P2	C61	C62	163.06(14)	C11	C12	C13	C18	-156.10(13)
C51	P2	C61	C66	-17.55(16)	C12	C13	C14	C15	175.55(14)
Ru	C1	C2	C3	-64.12(10)	C18	C13	C14	C15	-2.1(2)
C7A	C1	C2	Ru	70.34(10)	C12	C13	C18	C17	-176.56(14)
C7A	C1	C2	C3	6.22(16)	C14	C13	C18	C17	1.2(2)
Ru	C1	C7A	C3A	62.59(10)	C13	C14	C15	C16	1.6(2)
Ru	C1	C7A	C7	-120.31(17)	C14	C15	C16	C17	-0.1(2)
C2	C1	C7A	Ru	-66.15(10)	C15	C16	C17	C18	-0.8(2)
C2	C1	C7A	C3A	-3.56(15)	C16	C17	C18	C13	0.2(2)
C2	C1	C7A	C7	173.54(16)	P1	C21	C22	C23	167.32(11)
Ru	C2	C3	C3A	-69.18(10)	C26	C21	C22	C23	-59.04(16)
C1	C2	C3	Ru	62.77(10)	P1	C21	C26	C25	-167.79(11)
C1	C2	C3	C3A	-6.41(16)	C22	C21	C26	C25	58.91(17)
Ru	C3	C3A	C4	124.37(16)	C21	C22	C23	C24	57.15(19)
Ru	C3	C3A	C7A	-59.93(10)	C22	C23	C24	C25	-54.8(2)
C2	C3	C3A	Ru	64.04(9)	C23	C24	C25	C26	54.9(2)
C2	C3	C3A	C4	-171.58(15)	C24	C25	C26	C21	-57.24(19)
C2	C3	C3A	C7A	4.11(15)	P1	C31	C32	C33	-166.86(12)
Ru	C3A	C4	C5	-90.82(19)	C36	C31	C32	C33	58.18(17)
C3	C3A	C4	C5	174.67(16)	P1	C31	C36	C35	168.32(12)
C7A	C3A	C4	C5	-0.6(2)	C32	C31	C36	C35	-57.84(18)
Ru	C3A	C7A	C1	-57.46(9)	C31	C32	C33	C34	-57.2(2)
Ru	C3A	C7A	C7	124.96(13)	C32	C33	C34	C35	55.6(2)
C3	C3A	C7A	Ru	57.10(9)	C33	C34	C35	C36	-56.1(2)
C3	C3A	C7A	C1	-0.36(15)	C34	C35	C36	C31	57.2(2)
C3	C3A	C7A	C7	-177.95(13)	P2	C41	C42	C43	-174.77(12)
C4	C3A	C7A	Ru	-126.56(13)	C46	C41	C42	C43	0.6(2)
C4	C3A	C7A	C1	175.98(13)	P2	C41	C46	C45	175.44(14)
C4	C3A	C7A	C7	-1.6(2)	C42	C41	C46	C45	0.3(2)
C3A	C4	C5	C6	1.7(3)	C41	C42	C43	C44	-1.0(3)
C4	C5	C6	C7	-0.5(3)	C42	C43	C44	C45	0.4(3)
C5	C6	C7	C7A	-1.8(3)	C43	C44	C45	C46	0.5(3)
C6	C7	C7A	Ru	94.69(19)	C44	C45	C46	C41	-0.9(3)
C6	C7	C7A	C1	-174.01(16)	P2	C51	C52	C53	-177.86(13)
C6	C7	C7A	C3A	2.8(2)	C56	C51	C52	C53	0.4(2)
P1	C11	C12	Ru	9.00(8)	P2	C51	C56	C55	179.19(12)
P1	C11	C12	C13	-112.61(11)	C52	C51	C56	C55	0.8(2)
Ru	C12	C13	C14	-89.52(14)	C51	C52	C53	C54	-1.1(3)
Ru	C12	C13	C18	88.04(14)	C52	C53	C54	C55	0.6(3)

Table A.5. Torsional Angles for $[\mathrm{Ru}(\eta^5\text{-indenyl})(\kappa^2\text{-Ph}\underline{\mathrm{C}}\mathrm{HCH_2}\underline{\mathrm{P}}\mathrm{Cy_2})(\mathrm{PPh_3})]$ (**4e**) (continued)

Atom1	Atom2	Atom3	Atom4	Angle	Atom1	Atom2	Atom3	Atom4	Angle
C53	C54	C55	C56	0.6(3)	C62	C61	C66	C65	0.8(3)
C54	C55	C56	C51	-1.3(2)	C61	C62	C63	C64	0.7(3)
P2	C61	C62	C63	177.89(15)	C62	C63	C64	C65	0.9(3)
C66	C61	C62	C63	-1.5(3)	C63	C64	C65	C66	-1.7(4)
P2	C61	C66	C65	-178.66(18)	C64	C65	C66	C61	0.8(4)

Table A.6. Least-Squares Planes for $[\mathrm{Ru}(\eta^5\text{-indenyl})(\kappa^2\text{-Ph}\underline{\mathrm{C}}\mathrm{HCH_2}\underline{\mathrm{P}}\mathrm{Cy_2})(\mathrm{PPh_3})]$ (**4e**)

Plane	Coefficients[a]				Defining Atoms with Deviations (Å)[b]			
1	-5.525(10)	12.109(4)	4.816(14)	1.180(4)				
					C1	0.0282(9)	C2	-0.0367(9)
					C3	0.0303(9)	C3A	-0.0128(9)
					C7A	-0.0091(9)		
					$\underline{\mathrm{Ru}}$	1.9489(6)		

Distance: Ru–C_{cent} = 1.959 Å (C_{cent} = C1–C2–C3–C3A–C7A centroid)

Angles: C_{cent}–Ru–P1 = 130.9°, C_{cent}–Ru–P2 = 125.4°, C_{cent}–Ru–C12 = 127.0°

2	-4.42(2)	12.489(9)	4.487(19)	1.675(13)				
					C1	C2	C3	
					$\underline{\mathrm{Ru}}$	1.8979(15)		
3	-5.918(13)	11.951(6)	4.931(14)	1.039(6)				
					C1	-0.0012(5)	C3	0.0012(5)
					C3A	-0.0020(8)	C7A	0.0019(8)
					$\underline{\mathrm{Ru}}$	1.9244(9)		
4	-6.830(9)	11.573(5)	4.920(13)	0.699(3)				
					C3A	0.0017(10)	C4	0.0101(12)
					C5	-0.0098(13)	C6	-0.0027(13)
					C7	0.0144(12)	C7A	-0.0136(10)
					$\underline{\mathrm{Ru}}$	1.8295(17)		

Dihedral angle between planes 2 and 3: 6.31(15)°
Dihedral angle between planes 3 and 4: 3.97(10)°

[a] Coefficients are for the form $ax+by+cz = d$ where x, y and z are crystallographic coordinates.

[b] Underlined atoms were not included in the definition of the plane.

Table A.7. Anisotropic Displacement Parameters (U_{ij}, Å^2) for [Ru(η^5-indenyl)(κ^2-Ph$\underline{C}$HCH$_2\underline{P}$Cy$_2$)(PPh$_3$)] (**4e**)

Atom	U_{11}	U_{22}	U_{33}	U_{23}	U_{13}	U_{12}
Ru	0.02015(5)	0.02108(6)	0.02185(5)	-0.00106(4)	0.00360(4)	0.00226(3)
P1	0.02332(15)	0.02151(15)	0.02164(15)	-0.00016(12)	0.00466(12)	-0.00028(12)
P2	0.02061(15)	0.02312(15)	0.02323(15)	0.00060(12)	0.00349(12)	0.00129(12)
C1	0.0390(8)	0.0271(7)	0.0370(8)	-0.0043(6)	-0.0032(6)	0.0134(6)
C2	0.0292(7)	0.0285(7)	0.0511(9)	-0.0075(6)	0.0092(6)	0.0080(6)
C3	0.0407(8)	0.0284(7)	0.0317(7)	-0.0046(6)	0.0109(6)	0.0071(6)
C3A	0.0355(7)	0.0221(6)	0.0357(7)	-0.0039(5)	0.0030(6)	0.0050(5)
C4	0.0429(9)	0.0292(8)	0.0597(11)	-0.0084(7)	-0.0078(8)	0.0015(7)
C5	0.0410(10)	0.0324(9)	0.1136(19)	-0.0041(10)	0.0021(11)	-0.0076(7)
C6	0.0589(12)	0.0313(9)	0.1084(19)	0.0134(10)	0.0361(12)	-0.0030(8)
C7	0.0689(12)	0.0275(8)	0.0568(10)	0.0109(7)	0.0271(9)	0.0093(8)
C7A	0.0411(8)	0.0223(6)	0.0358(7)	0.0008(5)	0.0079(6)	0.0076(6)
C11	0.0306(7)	0.0257(6)	0.0303(7)	-0.0009(5)	0.0094(5)	-0.0040(5)
C12	0.0228(6)	0.0282(6)	0.0256(6)	0.0026(5)	0.0056(5)	-0.0007(5)
C13	0.0233(6)	0.0279(6)	0.0295(6)	0.0017(5)	0.0057(5)	-0.0026(5)
C14	0.0265(7)	0.0400(8)	0.0297(7)	0.0005(6)	0.0034(5)	-0.0037(6)
C15	0.0240(7)	0.0430(8)	0.0433(8)	0.0012(7)	-0.0006(6)	0.0000(6)
C16	0.0243(7)	0.0392(8)	0.0499(9)	-0.0042(7)	0.0108(6)	0.0005(6)
C17	0.0312(7)	0.0448(9)	0.0357(8)	-0.0054(6)	0.0124(6)	-0.0028(6)
C18	0.0251(6)	0.0425(8)	0.0294(7)	0.0007(6)	0.0051(5)	-0.0014(6)
C21	0.0272(6)	0.0290(7)	0.0249(6)	0.0007(5)	0.0011(5)	0.0011(5)
C22	0.0377(8)	0.0318(7)	0.0308(7)	0.0056(6)	0.0018(6)	0.0011(6)
C23	0.0496(10)	0.0394(9)	0.0423(9)	0.0103(7)	-0.0030(7)	0.0084(7)
C24	0.0506(10)	0.0556(11)	0.0383(9)	0.0068(8)	-0.0106(7)	0.0066(8)
C25	0.0429(9)	0.0531(10)	0.0403(9)	-0.0006(8)	-0.0120(7)	-0.0049(8)
C26	0.0431(8)	0.0346(8)	0.0321(7)	-0.0013(6)	-0.0060(6)	-0.0026(6)
C31	0.0290(6)	0.0245(6)	0.0258(6)	-0.0016(5)	0.0076(5)	0.0014(5)
C32	0.0432(8)	0.0311(7)	0.0419(8)	0.0029(6)	0.0216(7)	0.0017(6)
C33	0.0462(9)	0.0429(9)	0.0646(11)	-0.0033(8)	0.0333(9)	-0.0016(7)
C34	0.0514(10)	0.0494(10)	0.0560(11)	-0.0113(8)	0.0287(9)	0.0060(8)
C35	0.0557(10)	0.0335(8)	0.0573(11)	-0.0122(7)	0.0232(9)	0.0051(7)
C36	0.0438(9)	0.0309(7)	0.0453(9)	-0.0118(6)	0.0173(7)	-0.0041(6)
C41	0.0220(6)	0.0282(6)	0.0312(7)	0.0003(5)	0.0054(5)	0.0003(5)
C42	0.0243(6)	0.0315(7)	0.0381(7)	0.0043(6)	0.0036(6)	0.0004(5)
C43	0.0317(7)	0.0415(9)	0.0475(9)	0.0118(7)	0.0083(7)	-0.0054(6)
C44	0.0269(7)	0.0486(9)	0.0574(10)	0.0048(8)	0.0160(7)	-0.0027(7)
C45	0.0272(7)	0.0448(9)	0.0689(12)	0.0090(8)	0.0153(7)	0.0090(7)
C46	0.0299(7)	0.0363(8)	0.0551(10)	0.0134(7)	0.0127(7)	0.0080(6)
C51	0.0330(7)	0.0278(7)	0.0269(6)	-0.0014(5)	-0.0024(5)	0.0050(5)

Table A.7. Anisotropic Displacement Parameters for $[\mathrm{Ru}(\eta^5\text{-indenyl})(\kappa^2\text{-Ph}\underline{\mathrm{C}}\mathrm{HCH_2}\underline{\mathrm{P}}\mathrm{Cy_2})(\mathrm{PPh_3})]$ (**4e**) (continued)

Atom	U_{11}	U_{22}	U_{33}	U_{23}	U_{13}	U_{12}
C52	0.0390(8)	0.0343(8)	0.0450(9)	-0.0044(7)	-0.0108(7)	0.0042(6)
C53	0.0604(12)	0.0410(10)	0.0577(11)	-0.0162(8)	-0.0291(10)	0.0146(9)
C54	0.0923(16)	0.0541(11)	0.0378(9)	-0.0192(8)	-0.0258(10)	0.0393(11)
C55	0.0773(14)	0.0559(11)	0.0288(8)	-0.0033(7)	0.0046(8)	0.0358(10)
C56	0.0461(9)	0.0376(8)	0.0280(7)	-0.0006(6)	0.0052(6)	0.0135(7)
C61	0.0210(6)	0.0255(6)	0.0334(7)	0.0038(5)	0.0043(5)	0.0022(5)
C62	0.0792(13)	0.0307(8)	0.0315(8)	0.0011(6)	-0.0084(8)	0.0088(8)
C63	0.0679(12)	0.0296(8)	0.0520(10)	-0.0065(7)	-0.0111(9)	0.0070(8)
C64	0.0535(10)	0.0264(8)	0.0786(13)	0.0116(8)	0.0256(9)	0.0046(7)
C65	0.135(2)	0.0389(10)	0.0687(13)	0.0243(10)	0.0652(15)	0.0242(12)
C66	0.0919(15)	0.0340(9)	0.0464(10)	0.0099(7)	0.0405(10)	0.0163(9)

The form of the anisotropic displacement parameter is:

$$\exp[-2\pi^2(h^2a^{*2}U_{11} + k^2b^{*2}U_{22} + l^2c^{*2}U_{33} + 2klb^*c^*U_{23} + 2hla^*c^*U_{13} + 2hka^*b^*U_{12})]$$

Table A.8. Derived Atomic Coordinates and Displacement Parameters for Hydrogen Atoms for $[\mathrm{Ru}(\eta^5\text{-indenyl})(\kappa^2\text{-Ph}\underline{\mathrm{C}}\mathrm{HCH_2}\underline{\mathrm{P}}\mathrm{Cy_2})(\mathrm{PPh_3})]$ (**4e**)

Atom	x	y	z	U_{eq}, Å^2
H1	0.4515	0.1975	0.2514	0.042
H2	0.5060	0.2564	0.1428	0.043
H3	0.3700	0.2455	0.0440	0.040
H4	0.1861	0.1568	0.0376	0.055
H5	0.0926	0.0701	0.0998	0.076
H6	0.1348	0.0473	0.2159	0.076
H7	0.2731	0.1094	0.2728	0.059
H11A	0.3682	0.5921	0.2215	0.034
H11B	0.4691	0.5493	0.2535	0.034
H12	0.3821	0.5197	0.1230	0.030
H14	0.5781	0.4484	0.2449	0.039
H15	0.7201	0.3980	0.2193	0.045
H16	0.7414	0.3771	0.1075	0.045
H17	0.6171	0.4062	0.0204	0.044
H18	0.4742	0.4524	0.0458	0.039
H21	0.4962	0.3626	0.3127	0.033
H22A	0.3770	0.3093	0.4055	0.041
H22B	0.3931	0.2401	0.3432	0.041
H23A	0.4923	0.1891	0.4437	0.054
H23B	0.5518	0.2248	0.3878	0.054

Table A.8. Derived Atomic Coordinates and Displacement Parameters for Hydrogen Atoms for [Ru(η^5-indenyl)(κ^2-Ph$\underline{C}$HCH$_2\underline{P}$Cy$_2$)(PPh$_3$)] (**4e**) (continued)

Atom	*x*	*y*	*z*	U_{eq}, Å^2
H24A	0.5176	0.3425	0.5009	0.060
H24B	0.6158	0.2974	0.4913	0.060
H25A	0.6240	0.4059	0.4006	0.057
H25B	0.6052	0.4717	0.4638	0.057
H26A	0.5062	0.5240	0.3633	0.046
H26B	0.4463	0.4838	0.4178	0.046
H31	0.2094	0.5007	0.2725	0.031
H32A	0.2642	0.4087	0.4001	0.044
H32B	0.2052	0.3531	0.3365	0.044
H33A	0.0836	0.4702	0.3349	0.058
H33B	0.1054	0.4202	0.4084	0.058
H34A	0.0901	0.5982	0.4161	0.060
H34B	0.1904	0.5621	0.4515	0.060
H35A	0.2073	0.7024	0.3835	0.057
H35B	0.1486	0.6486	0.3191	0.057
H36A	0.3277	0.5847	0.3847	0.047
H36B	0.3069	0.6365	0.3117	0.047
H42	0.1467	0.2825	0.2076	0.038
H43	0.0102	0.2451	0.2483	0.048
H44	-0.1177	0.3495	0.2227	0.052
H45	-0.1109	0.4900	0.1554	0.055
H46	0.0235	0.5262	0.1120	0.048
H52	0.0356	0.3392	0.0377	0.050
H53	0.0008	0.2766	-0.0723	0.069
H54	0.1091	0.2831	-0.1439	0.079
H55	0.2552	0.3495	-0.1066	0.065
H56	0.2936	0.4074	0.0044	0.045
H62	0.1977	0.6043	0.1999	0.059
H63	0.1964	0.7768	0.1842	0.063
H64	0.1957	0.8439	0.0778	0.061
H65	0.1922	0.7359	-0.0134	0.091
H66	0.1969	0.5629	0.0022	0.065

Appendix B

X-Ray Crystallographic Structure Report for [Ru(η^5-indenyl)(κ^2-$\underline{C}$HCH$\underline{P}$Cy$_2$)(PPh$_3$)] (10)

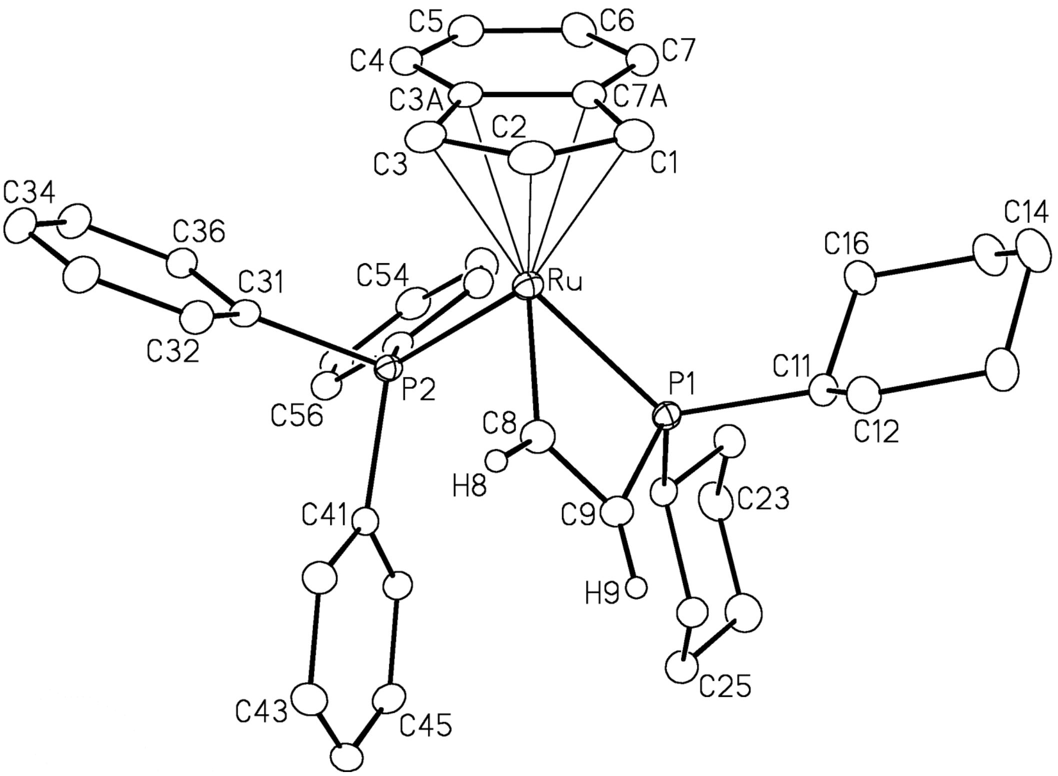

Figure B.1. Perspective view of the [(η^5–indenyl)Ru(κ^2–H$\underline{C}$CH$\underline{P}$Cy$_2$)(PPh$_3$)] (**10**) molecule showing the atom labelling scheme. Non-hydrogen atoms are represented by Gaussian ellipsoids at the 20% probability level. The hydrogen atoms attached to C8 and C9 are shown with arbitrarily small thermal parameters; these hydrogens were located and their coordinates and thermal parameters were freely refined. All other hydrogens are not shown.

This structure determination, as well as that of complex **4e** (Appendix A), was carried out by Dr. Robert McDonald at the X-ray Crystallography Laboratory, Department of Chemistry, University of Alberta, Edmonton, Alberta, Canada T6G 2G2. Phone: 1 780 492 2485. Fax: 1 780 492 8231. E-mail: Bob.McDonald@ualberta.ca.

Table B.1. Crystallographic Experimental Details for $[(\eta^5\text{–indenyl})Ru(\kappa^2\text{–H}\underline{C}CH\underline{P}Cy_2)(PPh_3)]$ (**10**)

A. Crystal Data	
formula	$C_{41}H_{46}P_2Ru$
formula weight	701.79
crystal dimensions (mm)	0.22 × 0.07 × 0.05
crystal system	triclinic
space group	$P\bar{1}$ (No. 2)
unit cell parameters[a]	
a (Å)	10.0731 (3)
b (Å)	12.3036 (4)
c (Å)	15.8279 (5)
α (deg)	71.003 (2)
β (deg)	88.926 (2)
γ (deg)	68.5986 (19)
V (Å^3)	1715.72 (9)
Z	2
ρ_{calcd} (g cm^{-3})	1.358
μ (mm^{-1})	4.777
B. Data Collection and Refinement Conditions	
diffractometer	Bruker D8/APEX II CCD[b]
radiation (λ [Å])	graphite-monochromated Cu Kα (1.54178)
temperature (°C)	–100
scan type	ω scans (0.8°) (5 s exposures)
data collection 2θ limit (deg)	136.00
total data collected	11330 ($-12 \leq h \leq 12$, $-14 \leq k \leq 14$, $-19 \leq l \leq 19$)
independent reflections	5926 ($R_{\text{int}} = 0.0313$)
number of observed reflections (*NO*)	5282 [$F_o^2 \geq 2\sigma(F_o^2)$]
structure solution method	Patterson/structure expansion (*DIRDIF–2008*[c])
refinement method	full-matrix least-squares on F^2 (*SHELXL–97*[d])
absorption correction method	Gaussian integration (face-indexed)
range of transmission factors	0.8102–0.4210
data/restraints/parameters	5926 / 0 / 405
goodness-of-fit (*S*)[e] [all data]	1.114
final *R* indices[f]	
R_1 [$F_o^2 \geq 2\sigma(F_o^2)$]	0.0376
wR_2 [all data]	0.1022
largest difference peak and hole	1.289 and –0.454 e Å^{-3}

(continued)

Table B.1. Crystallographic Experimental Details for [(η^5–indenyl)Ru(κ^2–H$\underline{C}$CH$\underline{P}$Cy$_2$)(PPh$_3$)] (**10**) (continued)

[a] Obtained from least-squares refinement of 9857 reflections with 8.22° < 2θ < 138.82°.

[b] Programs for diffractometer operation, data collection, data reduction and absorption correction were those supplied by Bruker.

[c] Beurskens, P. T.; Beurskens, G.; de Gelder, R.; Smits, J. M. M.; Garcia-Granda, S.; Gould, R. O. (2008). The *DIRDIF-2008* program system. Crystallography Laboratory, Radboud University Nijmegen, The Netherlands.

[d] Sheldrick, G. M. *Acta Crystallogr.* **2008**, *A64*, 112–122.

[e] $S = [\Sigma w(F_o^2 - F_c^2)^2/(n - p)]^{1/2}$ (n = number of data; p = number of parameters varied; $w = [\sigma^2(F_o^2) + (0.0571P)^2 + 0.9789P]^{-1}$ where $P = [\mathrm{Max}(F_o^2, 0) + 2F_c^2]/3$).

[f] $R_1 = \Sigma||F_o| - |F_c||/\Sigma|F_o|$; $wR_2 = [\Sigma w(F_o^2 - F_c^2)^2/\Sigma w(F_o^4)]^{1/2}$.

Table B.2. Atomic Coordinates and Equivalent Isotropic Displacement Parameters for [(η^5–indenyl)Ru(κ^2–H$\underline{C}$CH$\underline{P}$Cy$_2$)(PPh$_3$)] (**10**)

Atom	x	y	z	U_{eq}, Å^2
Ru	0.24640(2)	0.14341(2)	0.329626(15)	0.02814(10)*
P1	0.42389(8)	0.20756(7)	0.26085(5)	0.02681(17)*
P2	0.24154(8)	0.03116(7)	0.24123(5)	0.02707(17)*
C1	0.1604(4)	0.2652(4)	0.4129(2)	0.0410(8)*
C2	0.1776(4)	0.1416(4)	0.4627(2)	0.0438(8)*
C3	0.0862(4)	0.1048(4)	0.4216(2)	0.0421(8)*
C3A	0.0005(3)	0.2122(3)	0.3463(2)	0.0365(7)*
C4	-0.1106(4)	0.2311(4)	0.2827(3)	0.0409(8)*
C5	-0.1713(4)	0.3454(4)	0.2168(3)	0.0462(9)*
C6	-0.1270(4)	0.4429(4)	0.2112(3)	0.0486(9)*
C7	-0.0200(4)	0.4280(3)	0.2709(3)	0.0434(8)*
C7A	0.0470(4)	0.3113(3)	0.3404(2)	0.0372(7)*
C8	0.4523(3)	0.0218(3)	0.3816(2)	0.0319(7)*
C9	0.5479(3)	0.0607(3)	0.3342(2)	0.0312(7)*
C11	0.4672(3)	0.3299(3)	0.2856(2)	0.0320(7)*
C12	0.5307(4)	0.2866(3)	0.3838(2)	0.0376(7)*
C13	0.5636(4)	0.3875(4)	0.4051(3)	0.0442(8)*
C14	0.4312(5)	0.5074(4)	0.3823(3)	0.0470(9)*
C15	0.3723(5)	0.5532(4)	0.2838(3)	0.0473(9)*
C16	0.3363(4)	0.4531(3)	0.2623(2)	0.0382(7)*
C21	0.4664(3)	0.2261(3)	0.1435(2)	0.0287(6)*
C22	0.4027(4)	0.3598(3)	0.0772(2)	0.0382(8)*
C23	0.4380(5)	0.3641(4)	-0.0186(2)	0.0486(9)*

Table B.2. Atomic Coordinates and Displacement Parameters for [(η^5–indenyl)Ru(κ^2–H$\underline{C}$CH$\underline{P}$Cy$_2$)(PPh$_3$)] (**10**) (continued)

Atom	*x*	*y*	*z*	U_{eq}, Å^2
C24	0.5985(5)	0.3065(4)	-0.0224(3)	0.0529(10)*
C25	0.6620(4)	0.1747(4)	0.0434(2)	0.0428(8)*
C26	0.6277(3)	0.1673(3)	0.1389(2)	0.0348(7)*
C31	0.1390(3)	-0.0694(3)	0.2848(2)	0.0316(7)*
C32	0.1775(4)	-0.1536(3)	0.3734(2)	0.0370(7)*
C33	0.1050(4)	-0.2309(3)	0.4102(3)	0.0433(8)*
C34	-0.0116(4)	-0.2238(4)	0.3599(3)	0.0451(9)*
C35	-0.0543(4)	-0.1388(4)	0.2740(3)	0.0433(8)*
C36	0.0198(4)	-0.0619(3)	0.2367(2)	0.0351(7)*
C41	0.4117(3)	-0.0806(3)	0.2232(2)	0.0308(6)*
C42	0.4921(4)	-0.1873(3)	0.2951(3)	0.0410(8)*
C43	0.6259(4)	-0.2675(3)	0.2851(3)	0.0489(10)*
C44	0.6822(4)	-0.2421(3)	0.2044(3)	0.0474(9)*
C45	0.6051(4)	-0.1385(4)	0.1334(3)	0.0434(8)*
C46	0.4707(3)	-0.0582(3)	0.1419(2)	0.0353(7)*
C51	0.1542(3)	0.1192(3)	0.1250(2)	0.0314(7)*
C52	0.0925(4)	0.2490(3)	0.0983(2)	0.0363(7)*
C53	0.0203(4)	0.3186(4)	0.0122(3)	0.0468(9)*
C54	0.0081(4)	0.2625(4)	-0.0474(2)	0.0451(9)*
C55	0.0699(4)	0.1330(4)	-0.0217(2)	0.0419(8)*
C56	0.1423(4)	0.0623(3)	0.0633(2)	0.0361(7)*
H8	0.488(4)	-0.054(3)	0.434(3)	0.033(9)
H9	0.644(5)	0.025(4)	0.338(3)	0.042(11)

Anisotropically-refined atoms are marked with an asterisk (*). The form of the anisotropic displacement parameter is: $\exp[-2\pi^2(h^2a^{*2}U_{11} + k^2b^{*2}U_{22} + l^2c^{*2}U_{33} + 2klb^*c^*U_{23} + 2hla^*c^*U_{13} + 2hka^*b^*U_{12})]$.

Table B.3. Selected Interatomic Distances (Å) for $[(\eta^5\text{–indenyl})\text{Ru}(\kappa^2\text{–H}\underline{\text{C}}\text{CH}\underline{\text{P}}\text{Cy}_2)(\text{PPh}_3)]$ (**10**)

Atom1	Atom2	Distance
Ru	P1	2.3242(8)
Ru	P2	2.2753(8)
Ru	C1	2.243(4)
Ru	C2	2.201(3)
Ru	C3	2.229(3)
Ru	C3A	2.347(3)
Ru	C7A	2.349(3)
Ru	C8	2.053(3)
Ru	C9	2.823(3)[a]
P1	C9	1.793(3)
P1	C11	1.865(3)
P1	C21	1.858(3)
P2	C31	1.851(3)
P2	C41	1.852(3)
P2	C51	1.843(3)
C1	C2	1.413(6)
C1	C7A	1.447(5)
C2	C3	1.413(6)
C3	C3A	1.446(5)
C3A	C4	1.421(5)
C3A	C7A	1.435(5)
C4	C5	1.371(6)
C5	C6	1.403(6)
C6	C7	1.367(6)
C7	C7A	1.421(5)
C8	C9	1.339(5)
C8	H8	0.98(4)
C9	H9	0.90(4)
C11	C12	1.537(4)
C11	C16	1.539(4)
C12	C13	1.529(5)
C13	C14	1.524(6)
C14	C15	1.523(5)
C15	C16	1.537(5)
C21	C22	1.533(4)
C21	C26	1.530(4)
C22	C23	1.539(5)
C23	C24	1.519(6)
C24	C25	1.513(5)
C25	C26	1.525(5)
C31	C32	1.404(5)
C31	C36	1.391(5)
C32	C33	1.382(5)
C33	C34	1.390(6)
C34	C35	1.377(5)
C35	C36	1.391(5)
C41	C42	1.400(5)
C41	C46	1.394(5)
C42	C43	1.392(5)
C43	C44	1.377(6)
C44	C45	1.366(6)
C45	C46	1.390(5)
C51	C52	1.400(5)
C51	C56	1.404(5)
C52	C53	1.393(5)
C53	C54	1.368(6)
C54	C55	1.399(6)
C55	C56	1.382(5)

[a] Nonbonded distance.

Table B.4. Selected Interatomic Angles (°) for [(η^5–indenyl)Ru(κ^2–H$\underline{C}$CH$\underline{P}$Cy$_2$)(PPh$_3$)] (**10**)

Atom1	Atom2	Atom3	Angle	Atom1	Atom2	Atom3	Angle
P1	Ru	P2	95.27(3)	Ru	C1	C2	69.9(2)
P1	Ru	C1	103.34(10)	Ru	C1	C7A	75.7(2)
P1	Ru	C2	127.72(11)	C2	C1	C7A	107.1(3)
P1	Ru	C3	164.61(11)	Ru	C2	C1	73.1(2)
P1	Ru	C3A	143.42(9)	Ru	C2	C3	72.5(2)
P1	Ru	C7A	111.68(9)	C1	C2	C3	110.2(3)
P1	Ru	C8	65.48(9)	Ru	C3	C2	70.3(2)
P2	Ru	C1	157.53(10)	Ru	C3	C3A	76.07(19)
P2	Ru	C2	133.60(12)	C2	C3	C3A	107.0(3)
P2	Ru	C3	99.94(11)	Ru	C3A	C3	67.20(18)
P2	Ru	C3A	96.69(9)	Ru	C3A	C4	125.4(2)
P2	Ru	C7A	123.93(9)	Ru	C3A	C7A	72.28(18)
P2	Ru	C8	89.37(10)	C3	C3A	C4	132.1(4)
C1	Ru	C2	37.08(15)	C3	C3A	C7A	107.9(3)
C1	Ru	C3	62.43(15)	C4	C3A	C7A	120.0(3)
C1	Ru	C3A	60.84(13)	C3A	C4	C5	118.4(3)
C1	Ru	C7A	36.65(13)	C4	C5	C6	121.8(4)
C1	Ru	C8	109.68(13)	C5	C6	C7	121.4(4)
C2	Ru	C3	37.19(15)	C6	C7	C7A	119.2(4)
C2	Ru	C3A	60.61(13)	Ru	C7A	C1	67.67(19)
C2	Ru	C7A	60.68(14)	Ru	C7A	C3A	72.14(18)
C2	Ru	C8	93.43(14)	Ru	C7A	C7	125.8(3)
C3	Ru	C3A	36.73(13)	C1	C7A	C3A	107.6(3)
C3	Ru	C7A	61.10(13)	C1	C7A	C7	133.2(4)
C3	Ru	C8	112.11(13)	C3A	C7A	C7	119.1(3)
C3A	Ru	C7A	35.57(12)	Ru	C8	C9	110.9(2)
C3A	Ru	C8	148.83(13)	Ru	C8	H8	131(2)
C7A	Ru	C8	146.25(13)	C9	C8	H8	118(2)
Ru	P1	C9	85.55(11)	P1	C9	C8	97.7(2)
Ru	P1	C11	120.82(11)	P1	C9	H9	131(3)
Ru	P1	C21	127.19(10)	C8	C9	H9	131(3)
C9	P1	C11	106.76(15)	P1	C11	C12	111.8(2)
C9	P1	C21	108.71(15)	P1	C11	C16	112.1(2)
C11	P1	C21	103.67(15)	C12	C11	C16	110.4(3)
Ru	P2	C31	112.57(11)	C11	C12	C13	112.1(3)
Ru	P2	C41	119.70(11)	C12	C13	C14	111.4(3)
Ru	P2	C51	116.97(11)	C13	C14	C15	110.7(3)
C31	P2	C41	101.57(14)	C14	C15	C16	110.5(3)
C31	P2	C51	101.89(15)	C11	C16	C15	111.9(3)
C41	P2	C51	101.57(15)	P1	C21	C22	114.8(2)

Table B.4. Selected Interatomic Angles for $[(\eta^5\text{–indenyl})Ru(\kappa^2\text{–H}\underline{C}CH\underline{P}Cy_2)(PPh_3)]$ (**10**) (continued)

Atom1	Atom2	Atom3	Angle
P1	C21	C26	112.0(2)
C22	C21	C26	110.8(3)
C21	C22	C23	110.6(3)
C22	C23	C24	111.9(3)
C23	C24	C25	110.9(3)
C24	C25	C26	112.0(3)
C21	C26	C25	112.0(3)
P2	C31	C32	118.6(2)
P2	C31	C36	123.9(3)
C32	C31	C36	117.4(3)
C31	C32	C33	121.5(3)
C32	C33	C34	119.8(3)
C33	C34	C35	119.5(3)
C34	C35	C36	120.5(3)
C31	C36	C35	121.1(3)
P2	C41	C42	119.7(3)
P2	C41	C46	122.5(2)
C42	C41	C46	117.5(3)
C41	C42	C43	120.8(4)
C42	C43	C44	120.3(4)
C43	C44	C45	119.7(3)
C44	C45	C46	120.7(4)
C41	C46	C45	120.9(3)
P2	C51	C52	118.2(3)
P2	C51	C56	123.2(3)
C52	C51	C56	118.6(3)
C51	C52	C53	119.9(3)
C52	C53	C54	121.2(4)
C53	C54	C55	119.4(3)
C54	C55	C56	120.2(4)
C51	C56	C55	120.6(3)

Table B.5. Torsional Angles (deg) for [(η^5–indenyl)Ru(κ^2–H$\underline{C}$CH$\underline{P}$Cy$_2$)(PPh$_3$)] (**10**)

Atom1	Atom2	Atom3	Atom4	Angle
P2	Ru	P1	C9	-83.63(11)
P2	Ru	P1	C11	169.50(12)
P2	Ru	P1	C21	26.54(13)
C1	Ru	P1	C9	109.06(15)
C1	Ru	P1	C11	2.19(15)
C1	Ru	P1	C21	-140.77(16)
C2	Ru	P1	C9	77.62(17)
C2	Ru	P1	C11	-29.26(18)
C2	Ru	P1	C21	-172.21(18)
C3	Ru	P1	C9	87.6(4)
C3	Ru	P1	C11	-19.3(4)
C3	Ru	P1	C21	-162.2(4)
C3A	Ru	P1	C9	167.69(19)
C3A	Ru	P1	C11	60.8(2)
C3A	Ru	P1	C21	-82.1(2)
C7A	Ru	P1	C9	146.59(15)
C7A	Ru	P1	C11	39.72(15)
C7A	Ru	P1	C21	-103.24(16)
C8	Ru	P1	C9	3.26(15)
C8	Ru	P1	C11	-103.61(16)
C8	Ru	P1	C21	113.43(17)
P1	Ru	P2	C31	167.97(11)
P1	Ru	P2	C41	48.81(12)
P1	Ru	P2	C51	-74.51(11)
C1	Ru	P2	C31	-46.0(3)
C1	Ru	P2	C41	-165.2(3)
C1	Ru	P2	C51	71.5(3)
C2	Ru	P2	C31	8.54(18)
C2	Ru	P2	C41	-110.62(18)
C2	Ru	P2	C51	126.05(17)
C3	Ru	P2	C31	-9.67(14)
C3	Ru	P2	C41	-128.83(15)
C3	Ru	P2	C51	107.84(15)
C3A	Ru	P2	C31	-46.67(14)
C3A	Ru	P2	C41	-165.83(15)
C3A	Ru	P2	C51	70.85(14)
C7A	Ru	P2	C31	-71.42(15)
C7A	Ru	P2	C41	169.42(16)
C7A	Ru	P2	C51	46.09(16)
C8	Ru	P2	C31	102.67(14)
C8	Ru	P2	C41	-16.48(15)
C8	Ru	P2	C51	-139.81(14)
P1	Ru	C1	C2	-136.8(2)
P1	Ru	C1	C7A	108.5(2)
P2	Ru	C1	C2	78.1(3)
P2	Ru	C1	C7A	-36.6(4)
C2	Ru	C1	C7A	-114.7(3)
C3	Ru	C1	C2	36.9(2)
C3	Ru	C1	C7A	-77.8(2)
C3A	Ru	C1	C2	78.8(2)
C3A	Ru	C1	C7A	-35.9(2)
C7A	Ru	C1	C2	114.7(3)
C8	Ru	C1	C2	-68.4(2)
C8	Ru	C1	C7A	176.9(2)
P1	Ru	C2	C1	57.3(2)
P1	Ru	C2	C3	175.63(17)
P2	Ru	C2	C1	-148.90(18)
P2	Ru	C2	C3	-30.6(3)
C1	Ru	C2	C3	118.3(3)
C3	Ru	C2	C1	-118.3(3)
C3A	Ru	C2	C1	-79.5(2)
C3A	Ru	C2	C3	38.8(2)
C7A	Ru	C2	C1	-38.5(2)
C7A	Ru	C2	C3	79.8(2)
C8	Ru	C2	C1	118.7(2)
C8	Ru	C2	C3	-123.0(2)
P1	Ru	C3	C2	-13.1(5)
P1	Ru	C3	C3A	101.0(4)
P2	Ru	C3	C2	158.0(2)
P2	Ru	C3	C3A	-87.9(2)
C1	Ru	C3	C2	-36.8(2)
C1	Ru	C3	C3A	77.3(2)
C2	Ru	C3	C3A	114.1(3)
C3A	Ru	C3	C2	-114.1(3)
C7A	Ru	C3	C2	-78.6(2)
C7A	Ru	C3	C3A	35.5(2)
C8	Ru	C3	C2	64.6(3)
C8	Ru	C3	C3A	178.7(2)
P1	Ru	C3A	C3	-154.1(2)
P1	Ru	C3A	C4	79.5(4)

Table B.5. Torsional Angles for [(η^5–indenyl)Ru(κ^2–HCCHPCy$_2$)(PPh$_3$)] (**10**) (continued)

Atom1	Atom2	Atom3	Atom4	Angle
P1	Ru	C3A	C7A	-35.1(3)
P2	Ru	C3A	C3	97.7(2)
P2	Ru	C3A	C4	-28.7(3)
P2	Ru	C3A	C7A	-143.3(2)
C1	Ru	C3A	C3	-82.0(2)
C1	Ru	C3A	C4	151.6(4)
C1	Ru	C3A	C7A	37.0(2)
C2	Ru	C3A	C3	-39.3(2)
C2	Ru	C3A	C4	-165.7(4)
C2	Ru	C3A	C7A	79.7(2)
C3	Ru	C3A	C4	-126.4(4)
C3	Ru	C3A	C7A	119.0(3)
C7A	Ru	C3A	C3	-119.0(3)
C7A	Ru	C3A	C4	114.6(4)
C8	Ru	C3A	C3	-2.2(4)
C8	Ru	C3A	C4	-128.6(3)
C8	Ru	C3A	C7A	116.7(3)
P1	Ru	C7A	C1	-83.2(2)
P1	Ru	C7A	C3A	158.37(18)
P1	Ru	C7A	C7	44.9(3)
P2	Ru	C7A	C1	164.05(18)
P2	Ru	C7A	C3A	45.6(2)
P2	Ru	C7A	C7	-67.9(3)
C1	Ru	C7A	C3A	-118.4(3)
C1	Ru	C7A	C7	128.1(4)
C2	Ru	C7A	C1	38.9(2)
C2	Ru	C7A	C3A	-79.5(2)
C2	Ru	C7A	C7	167.0(4)
C3	Ru	C7A	C1	81.7(2)
C3	Ru	C7A	C3A	-36.7(2)
C3	Ru	C7A	C7	-150.2(4)
C3A	Ru	C7A	C1	118.4(3)
C3A	Ru	C7A	C7	-113.5(4)
C8	Ru	C7A	C1	-5.3(3)
C8	Ru	C7A	C3A	-123.7(3)
C8	Ru	C7A	C7	122.8(3)
P1	Ru	C8	C9	-4.7(2)
P2	Ru	C8	C9	91.4(2)
C1	Ru	C8	C9	-100.8(3)
C2	Ru	C8	C9	-134.9(3)
C3	Ru	C8	C9	-168.1(2)
C3A	Ru	C8	C9	-166.7(2)
C7A	Ru	C8	C9	-97.4(3)
Ru	P1	C9	C8	-4.6(2)
C11	P1	C9	C8	116.3(2)
C21	P1	C9	C8	-132.5(2)
Ru	P1	C11	C12	65.4(3)
Ru	P1	C11	C16	-59.2(3)
C9	P1	C11	C12	-29.5(3)
C9	P1	C11	C16	-154.1(2)
C21	P1	C11	C12	-144.2(2)
C21	P1	C11	C16	91.2(3)
Ru	P1	C21	C22	99.0(2)
Ru	P1	C21	C26	-133.5(2)
C9	P1	C21	C22	-162.1(2)
C9	P1	C21	C26	-34.6(3)
C11	P1	C21	C22	-48.8(3)
C11	P1	C21	C26	78.7(3)
Ru	P2	C31	C32	-55.0(3)
Ru	P2	C31	C36	121.1(3)
C41	P2	C31	C32	74.2(3)
C41	P2	C31	C36	-109.6(3)
C51	P2	C31	C32	178.9(3)
C51	P2	C31	C36	-5.0(3)
Ru	P2	C41	C42	67.4(3)
Ru	P2	C41	C46	-107.0(3)
C31	P2	C41	C42	-57.2(3)
C31	P2	C41	C46	128.4(3)
C51	P2	C41	C42	-162.1(3)
C51	P2	C41	C46	23.5(3)
Ru	P2	C51	C52	-1.7(3)
Ru	P2	C51	C56	-179.5(2)
C31	P2	C51	C52	121.4(3)
C31	P2	C51	C56	-56.3(3)
C41	P2	C51	C52	-133.9(3)
C41	P2	C51	C56	48.3(3)
Ru	C1	C2	C3	-63.5(3)
C7A	C1	C2	Ru	67.1(2)
C7A	C1	C2	C3	3.6(4)
Ru	C1	C7A	C3A	61.4(2)

Table B.5. Torsional Angles for [(η^5–indenyl)Ru(κ^2–H$\underline{C}$CH$\underline{P}$Cy$_2$)(PPh$_3$)] (**10**) (continued)

Atom1	Atom2	Atom3	Atom4	Angle
Ru	C1	C7A	C7	-118.8(4)
C2	C1	C7A	Ru	-63.2(2)
C2	C1	C7A	C3A	-1.8(4)
C2	C1	C7A	C7	178.0(4)
Ru	C2	C3	C3A	-67.9(2)
C1	C2	C3	Ru	63.8(3)
C1	C2	C3	C3A	-4.0(4)
Ru	C3	C3A	C4	117.8(4)
Ru	C3	C3A	C7A	-61.1(2)
C2	C3	C3A	Ru	64.0(2)
C2	C3	C3A	C4	-178.2(4)
C2	C3	C3A	C7A	2.8(4)
Ru	C3A	C4	C5	-89.0(4)
C3	C3A	C4	C5	-179.1(4)
C7A	C3A	C4	C5	-0.2(5)
Ru	C3A	C7A	C1	-58.6(2)
Ru	C3A	C7A	C7	121.6(3)
C3	C3A	C7A	Ru	57.9(2)
C3	C3A	C7A	C1	-0.7(4)
C3	C3A	C7A	C7	179.5(3)
C4	C3A	C7A	Ru	-121.2(3)
C4	C3A	C7A	C1	-179.8(3)
C4	C3A	C7A	C7	0.4(5)
C3A	C4	C5	C6	-0.3(6)
C4	C5	C6	C7	0.6(7)
C5	C6	C7	C7A	-0.4(6)
C6	C7	C7A	Ru	88.1(4)
C6	C7	C7A	C1	-179.9(4)
C6	C7	C7A	C3A	-0.1(5)
Ru	C8	C9	P1	5.6(3)
P1	C11	C12	C13	-178.8(2)
C16	C11	C12	C13	-53.2(4)
P1	C11	C16	C15	179.4(2)
C12	C11	C16	C15	54.0(4)
C11	C12	C13	C14	55.3(4)
C12	C13	C14	C15	-57.0(4)
C13	C14	C15	C16	57.4(4)
C14	C15	C16	C11	-56.5(4)
P1	C21	C22	C23	-177.3(2)
C26	C21	C22	C23	54.6(4)
P1	C21	C26	C25	176.2(2)
C22	C21	C26	C25	-54.3(4)
C21	C22	C23	C24	-56.0(4)
C22	C23	C24	C25	55.7(5)
C23	C24	C25	C26	-54.7(5)
C24	C25	C26	C21	54.5(4)
P2	C31	C32	C33	179.7(3)
C36	C31	C32	C33	3.3(5)
P2	C31	C36	C35	-178.8(3)
C32	C31	C36	C35	-2.6(5)
C31	C32	C33	C34	-1.8(6)
C32	C33	C34	C35	-0.5(6)
C33	C34	C35	C36	1.2(6)
C34	C35	C36	C31	0.4(6)
P2	C41	C42	C43	-174.8(3)
C46	C41	C42	C43	-0.1(5)
P2	C41	C46	C45	173.8(3)
C42	C41	C46	C45	-0.7(5)
C41	C42	C43	C44	1.0(6)
C42	C43	C44	C45	-1.2(6)
C43	C44	C45	C46	0.4(6)
C44	C45	C46	C41	0.5(6)
P2	C51	C52	C53	-177.3(3)
C56	C51	C52	C53	0.5(5)
P2	C51	C56	C55	177.1(3)
C52	C51	C56	C55	-0.7(5)
C51	C52	C53	C54	0.0(6)
C52	C53	C54	C55	-0.3(6)
C53	C54	C55	C56	0.2(6)
C54	C55	C56	C51	0.3(5)

Table B.6. Least-Squares Planes for [(η^5–indenyl)Ru(κ^2–HCCHPCy$_2$)(PPh$_3$)] (**10**)

Plane	Coefficients[a]				Defining Atoms with Deviations (Å)[b]			
1	-6.088(14)	3.46(2)	11.463(19)	4.691(11)				
					C1	-0.016(2)	C2	0.022(2)
					C3	-0.020(2)	C3A	0.010(2)
					C7A	0.003(2)		
					Ru	-1.9155(15)		

Distance: Ru–C_{cent} = 1.922 Å (C_{cent} = C1–C2–C3–C3A–C7A centroid)

Angles: C_{cent}–Ru–P1 = 134.8°, C_{cent}–Ru–P2 = 125.4°, C_{cent}–Ru–C8 = 126.3°

2	-6.33(2)	3.52(2)	10.93(5)	4.43(2)				
					C1	C2	C3	
					Ru	-1.884(4)		
3	-6.001(16)	3.43(2)	11.64(2)	4.753(12)				
					C1	0.0022(12)	C3	-0.0022(12)
					C3A	0.004(2)	C7A	-0.004(2)
					Ru	-1.902(2)		
4	-6.019(12)	3.463(18)	11.590(16)	4.742(7)				
					C3A	0.002(2)	C4	-0.000(3)
					C5	-0.003(3)	C6	0.003(3)
					C7	-0.001(3)	C7A	-0.002(2)
					Ru	-1.908(4)		

Dihedral angle between planes 2 and 3: 3.9(5)°

Dihedral angle between planes 3 and 4: 0.3(3)°

[a] Coefficients are for the form $ax+by+cz = d$ where x, y and z are crystallographic coordinates.

[b] Underlined atoms were not included in the definition of the plane.

Table B.7. Anisotropic Displacement Parameters (U_{ij}, Å^2) for [(η^5–indenyl)Ru(κ^2–H$\underline{C}$CH$\underline{P}$Cy$_2$)(PPh$_3$)] (**10**)

Atom	U_{11}	U_{22}	U_{33}	U_{23}	U_{13}	U_{12}
Ru	0.02399(13)	0.03170(14)	0.02825(14)	-0.01080(10)	0.00251(8)	-0.00954(9)
P1	0.0243(4)	0.0279(4)	0.0275(4)	-0.0089(3)	0.0002(3)	-0.0094(3)
P2	0.0229(3)	0.0277(4)	0.0295(4)	-0.0090(3)	0.0025(3)	-0.0090(3)
C1	0.0363(18)	0.052(2)	0.0395(18)	-0.0248(17)	0.0071(14)	-0.0146(15)
C2	0.0385(18)	0.058(2)	0.0306(16)	-0.0164(16)	0.0107(14)	-0.0135(16)
C3	0.0359(18)	0.0451(19)	0.0399(18)	-0.0105(16)	0.0157(15)	-0.0134(15)
C3A	0.0274(16)	0.0402(18)	0.0458(19)	-0.0214(16)	0.0146(14)	-0.0118(13)
C4	0.0270(16)	0.0447(19)	0.060(2)	-0.0279(18)	0.0100(15)	-0.0147(14)
C5	0.0264(16)	0.049(2)	0.063(2)	-0.0236(19)	-0.0003(16)	-0.0097(15)
C6	0.0333(18)	0.0356(18)	0.068(3)	-0.0180(19)	-0.0072(17)	-0.0025(14)
C7	0.0323(17)	0.0370(18)	0.063(2)	-0.0225(18)	0.0024(16)	-0.0100(14)
C7A	0.0289(16)	0.0436(18)	0.0460(19)	-0.0259(16)	0.0096(14)	-0.0124(14)
C8	0.0302(15)	0.0314(15)	0.0287(15)	-0.0070(13)	-0.0024(12)	-0.0083(12)
C9	0.0251(15)	0.0310(15)	0.0324(16)	-0.0081(13)	-0.0023(12)	-0.0069(12)
C11	0.0312(16)	0.0346(16)	0.0339(16)	-0.0143(14)	0.0010(12)	-0.0142(13)
C12	0.0390(18)	0.0412(18)	0.0350(17)	-0.0164(15)	-0.0008(14)	-0.0145(14)
C13	0.052(2)	0.049(2)	0.0414(19)	-0.0223(17)	0.0002(16)	-0.0242(17)
C14	0.064(2)	0.0421(19)	0.0418(19)	-0.0209(17)	0.0053(17)	-0.0227(18)
C15	0.064(2)	0.0364(18)	0.044(2)	-0.0163(17)	0.0036(18)	-0.0196(17)
C16	0.0383(18)	0.0330(16)	0.0423(18)	-0.0149(15)	-0.0013(14)	-0.0104(14)
C21	0.0289(15)	0.0317(15)	0.0270(14)	-0.0102(13)	0.0015(11)	-0.0131(12)
C22	0.0410(18)	0.0320(16)	0.0354(17)	-0.0065(14)	-0.0040(14)	-0.0109(14)
C23	0.064(3)	0.0411(19)	0.0325(18)	-0.0048(16)	-0.0070(17)	-0.0164(18)
C24	0.070(3)	0.053(2)	0.0360(19)	-0.0109(18)	0.0156(18)	-0.028(2)
C25	0.045(2)	0.047(2)	0.0422(19)	-0.0185(17)	0.0137(16)	-0.0208(16)
C26	0.0328(16)	0.0359(16)	0.0349(16)	-0.0117(14)	0.0038(13)	-0.0127(13)
C31	0.0251(14)	0.0335(15)	0.0360(16)	-0.0132(14)	0.0057(12)	-0.0097(12)
C32	0.0331(16)	0.0373(17)	0.0402(18)	-0.0117(15)	0.0048(14)	-0.0143(14)
C33	0.0395(19)	0.0414(18)	0.0435(19)	-0.0067(16)	0.0091(15)	-0.0165(15)
C34	0.0411(19)	0.046(2)	0.056(2)	-0.0187(18)	0.0170(17)	-0.0254(16)
C35	0.0356(18)	0.053(2)	0.049(2)	-0.0205(18)	0.0063(15)	-0.0228(16)
C36	0.0314(16)	0.0391(17)	0.0391(17)	-0.0174(15)	0.0056(13)	-0.0149(13)
C41	0.0262(15)	0.0283(15)	0.0409(17)	-0.0150(14)	0.0033(13)	-0.0110(12)
C42	0.0342(17)	0.0334(17)	0.050(2)	-0.0102(16)	0.0050(15)	-0.0102(14)
C43	0.0323(18)	0.0327(17)	0.071(3)	-0.0123(18)	-0.0015(17)	-0.0051(14)
C44	0.0300(17)	0.0403(19)	0.080(3)	-0.034(2)	0.0106(18)	-0.0110(14)
C45	0.0331(17)	0.053(2)	0.056(2)	-0.0298(19)	0.0133(16)	-0.0200(16)
C46	0.0287(16)	0.0363(16)	0.0449(18)	-0.0179(15)	0.0058(14)	-0.0133(13)
C51	0.0235(14)	0.0389(17)	0.0292(15)	-0.0081(13)	0.0022(12)	-0.0122(12)

Table B.7. Anisotropic Displacement Parameters for $[(\eta^5\text{–indenyl})Ru(\kappa^2\text{–H}\underline{C}CH\underline{P}Cy_2)(PPh_3)]$ (**10**) (continued)

Atom	U_{11}	U_{22}	U_{33}	U_{23}	U_{13}	U_{12}
C52	0.0318(16)	0.0350(16)	0.0393(17)	-0.0094(14)	-0.0012(13)	-0.0121(13)
C53	0.044(2)	0.0357(18)	0.048(2)	-0.0031(17)	-0.0061(16)	-0.0102(15)
C54	0.0368(18)	0.056(2)	0.0352(18)	-0.0074(17)	-0.0036(14)	-0.0163(16)
C55	0.0392(18)	0.057(2)	0.0340(17)	-0.0185(17)	0.0061(14)	-0.0213(16)
C56	0.0323(16)	0.0419(18)	0.0369(17)	-0.0159(15)	0.0057(13)	-0.0149(14)

The form of the anisotropic displacement parameter is:

$$\exp[-2\pi^2(h^2a^{*2}U_{11} + k^2b^{*2}U_{22} + l^2c^{*2}U_{33} + 2klb^*c^*U_{23} + 2hla^*c^*U_{13} + 2hka^*b^*U_{12})]$$

Table B.8. Derived Atomic Coordinates and Displacement Parameters for Hydrogen Atoms for $[(\eta^5\text{–indenyl})Ru(\kappa^2\text{–H}\underline{C}CH\underline{P}Cy_2)(PPh_3)]$ (**10**)

Atom	x	y	z	U_{eq}, Å^2
H1	0.2078	0.3152	0.4296	0.049
H2	0.2397	0.0900	0.5212	0.053
H3	0.0723	0.0242	0.4457	0.051
H4	-0.1421	0.1661	0.2858	0.049
H5	-0.2453	0.3589	0.1738	0.055
H6	-0.1722	0.5210	0.1649	0.058
H7	0.0092	0.4948	0.2659	0.052
H11	0.5420	0.3461	0.2466	0.038
H12A	0.4620	0.2630	0.4241	0.045
H12B	0.6202	0.2120	0.3957	0.045
H13A	0.5980	0.3578	0.4698	0.053
H13B	0.6409	0.4039	0.3702	0.053
H14A	0.3565	0.4929	0.4208	0.056
H14B	0.4565	0.5718	0.3945	0.056
H15A	0.4443	0.5738	0.2452	0.057
H15B	0.2847	0.6296	0.2707	0.057
H16A	0.3022	0.4833	0.1975	0.046
H16B	0.2578	0.4387	0.2968	0.046
H21	0.4216	0.1780	0.1220	0.034
H22A	0.4422	0.4121	0.0962	0.046
H22B	0.2973	0.3937	0.0777	0.046
H23A	0.3897	0.3190	-0.0397	0.058
H23B	0.4003	0.4516	-0.0595	0.058
H24A	0.6165	0.3064	-0.0840	0.063
H24B	0.6459	0.3570	-0.0078	0.063
H25A	0.7674	0.1417	0.0428	0.051

Table B.8. Derived Atomic Coordinates and Displacement Parameters for [(η^5–indenyl)Ru(κ^2–H$\underline{C}$CH$\underline{P}$Cy$_2$)(PPh$_3$)] (**10**) (continued)

Atom	*x*	*y*	*z*	U_{eq}, Å^2
H25B	0.6237	0.1221	0.0239	0.051
H26A	0.6772	0.2104	0.1614	0.042
H26B	0.6645	0.0791	0.1785	0.042
H32	0.2553	-0.1575	0.4089	0.044
H33	0.1346	-0.2888	0.4697	0.052
H34	-0.0613	-0.2772	0.3847	0.054
H35	-0.1350	-0.1326	0.2399	0.052
H36	-0.0114	-0.0034	0.1775	0.042
H42	0.4549	-0.2051	0.3514	0.049
H43	0.6785	-0.3402	0.3342	0.059
H44	0.7743	-0.2962	0.1981	0.057
H45	0.6438	-0.1213	0.0776	0.052
H46	0.4183	0.0129	0.0917	0.042
H52	0.0999	0.2896	0.1388	0.044
H53	-0.0213	0.4066	-0.0054	0.056
H54	-0.0419	0.3111	-0.1058	0.054
H55	0.0622	0.0934	-0.0629	0.050
H56	0.1844	-0.0256	0.0801	0.043

Appendix C

NMR Spectra for the Characterization of [Ru(η^5-indenyl)(κ^2-Ph$\underline{C}$HCH$_2\underline{P}$Cy$_2$)(PPh$_3$)] (4e)

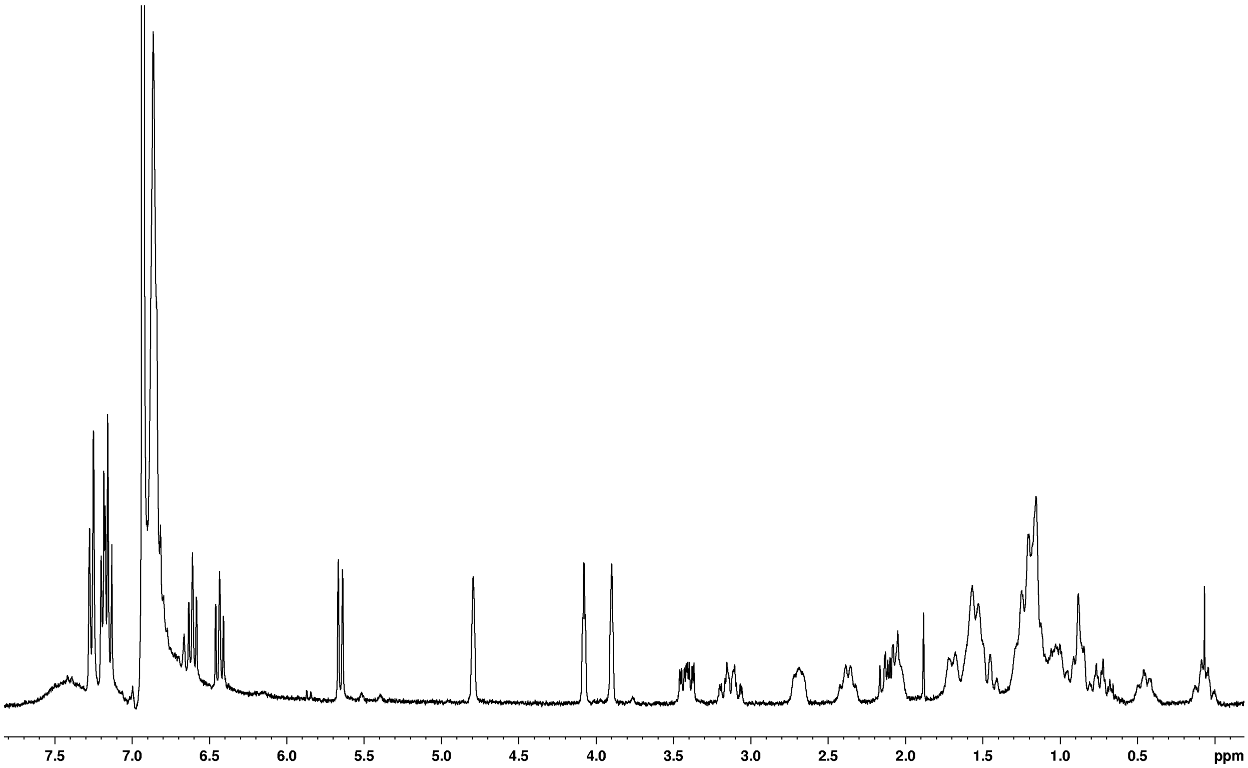

Figure C.1. ^{1}H NMR spectrum of [Ru(η^5-indenyl)(κ^2-Ph$\underline{C}$HCH$\underline{P}$Cy$_2$)(PPh$_3$)] (**4e**). (500.13 MHz, *d*$_6$-benzene)

Appendix C- NMR Spectra for the Characterization of [Ru(η^5-indenyl)(κ^2-Ph$\underline{C}$HCH$_2\underline{P}$Cy$_2$)(PPh$_3$)] (4e)

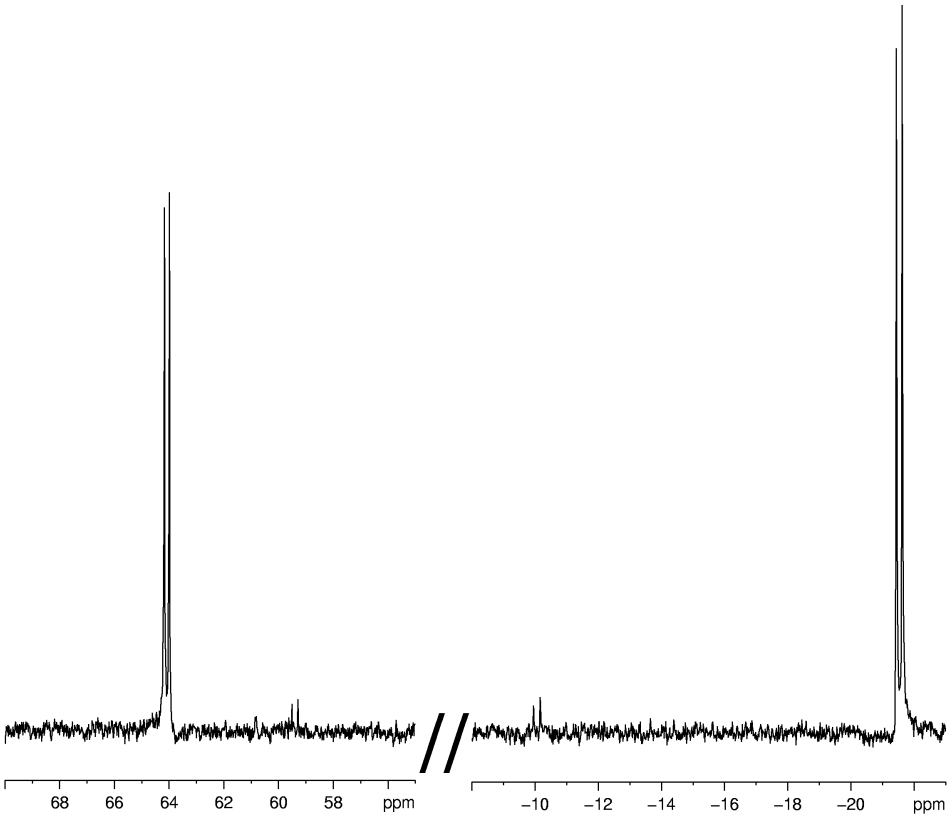

Figure C.2. ^{31}P{^{1}H} NMR spectrum of [Ru(η^5-indenyl)(κ^2-Ph$\underline{C}$HCH$\underline{P}$Cy$_2$)(PPh$_3$)] (**4e**). (202.46 MHz, d_6-benzene)

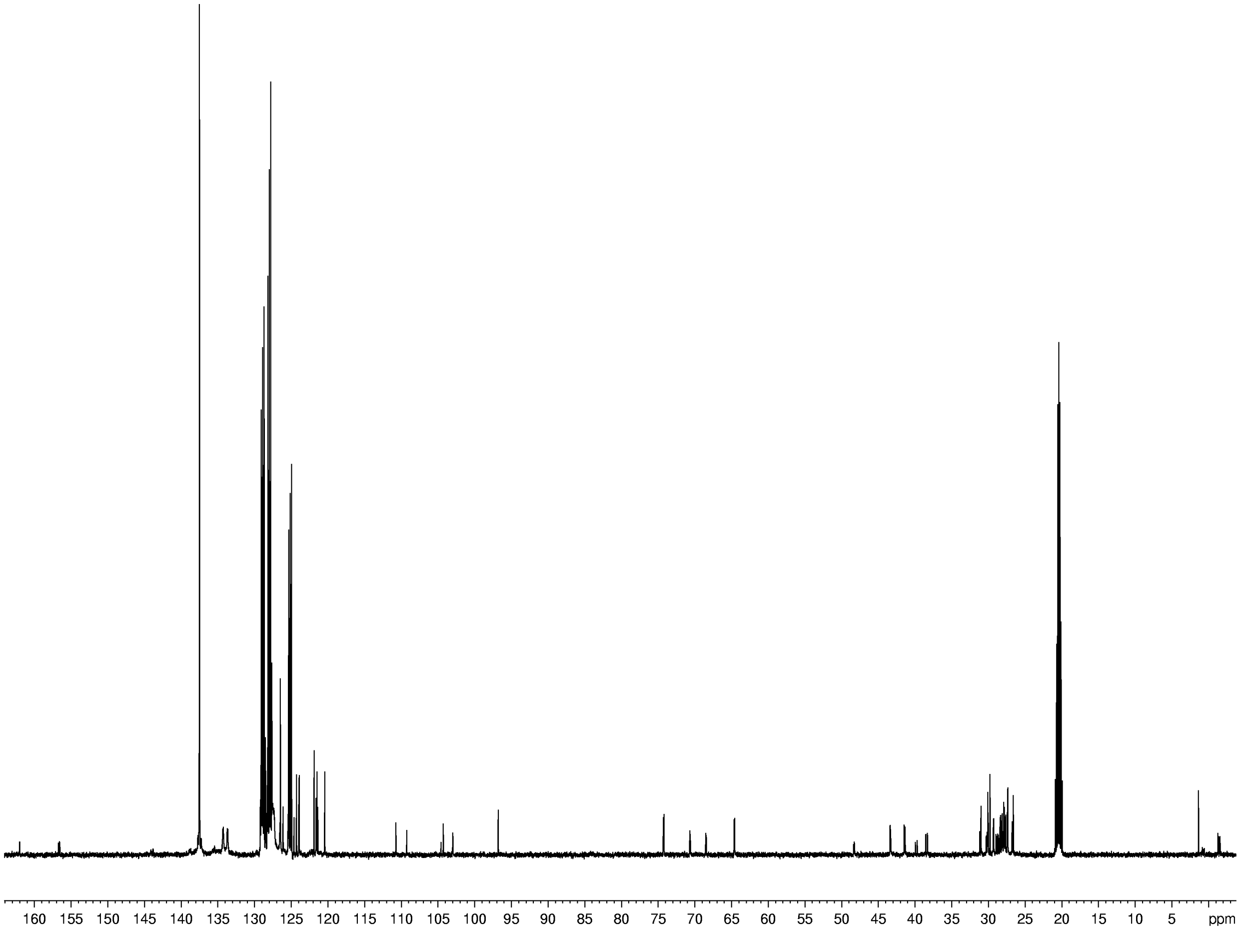

Figure C.3. ^{13}C NMR spectrum of [Ru(η^5-indenyl)(κ^2-Ph<u>C</u>HCH<u>P</u>Cy$_2$)(PPh$_3$)] (**4e**). (125.77 MHz, *d*$_6$-benzene)

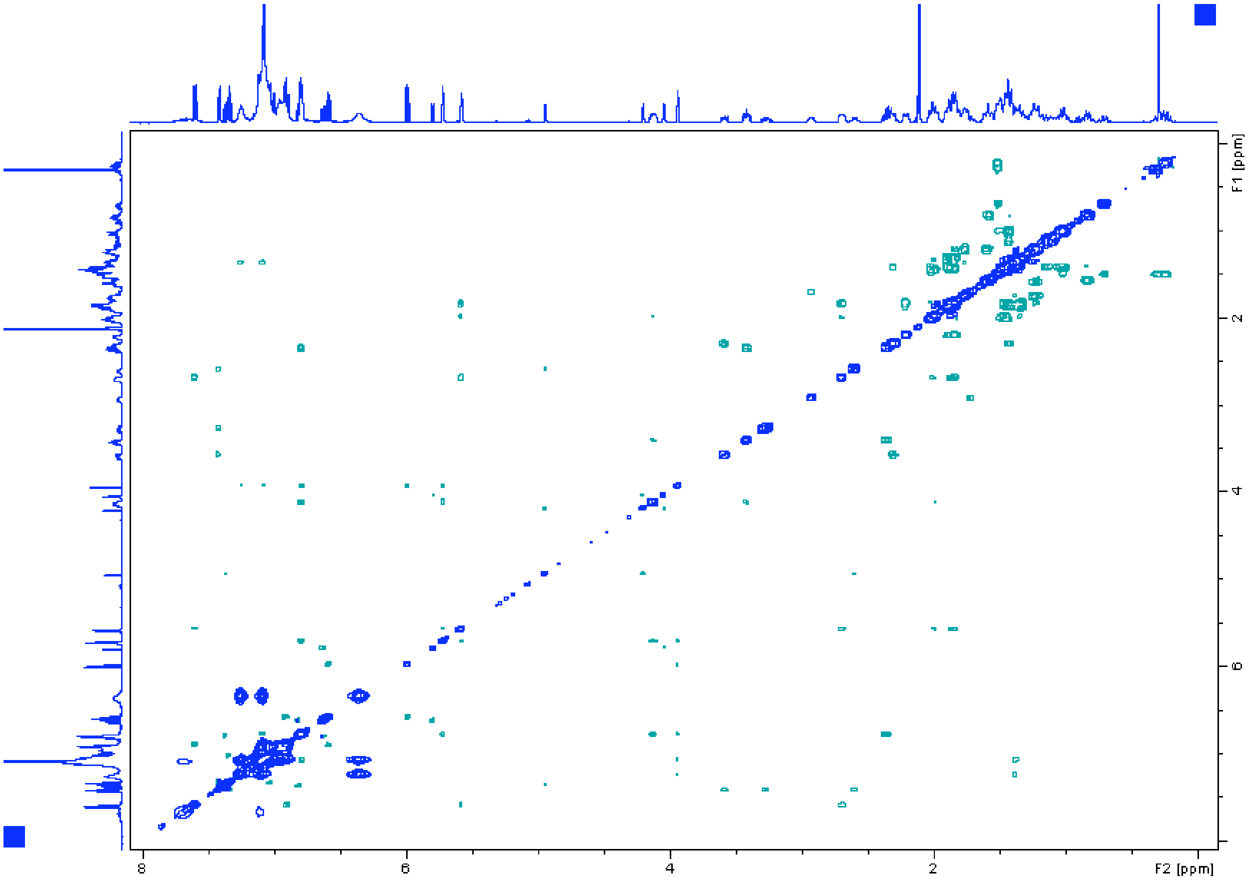

Figure C.4. ^{1}H-NOESY 2D NMR spectrum of [Ru(η^5-indenyl)(κ^2-Ph$\underline{C}$HCH$\underline{P}$Cy$_2$)(PPh$_3$)] (**4e**). (500.13 MHz, d_6-benzene)

Appendix D

NMR Spectra for the Characterization of [Ru(η^5-indenyl)(κ^2-$\underline{C}$HCH$\underline{P}$Cy$_2$)(PPh$_3$)] (10)

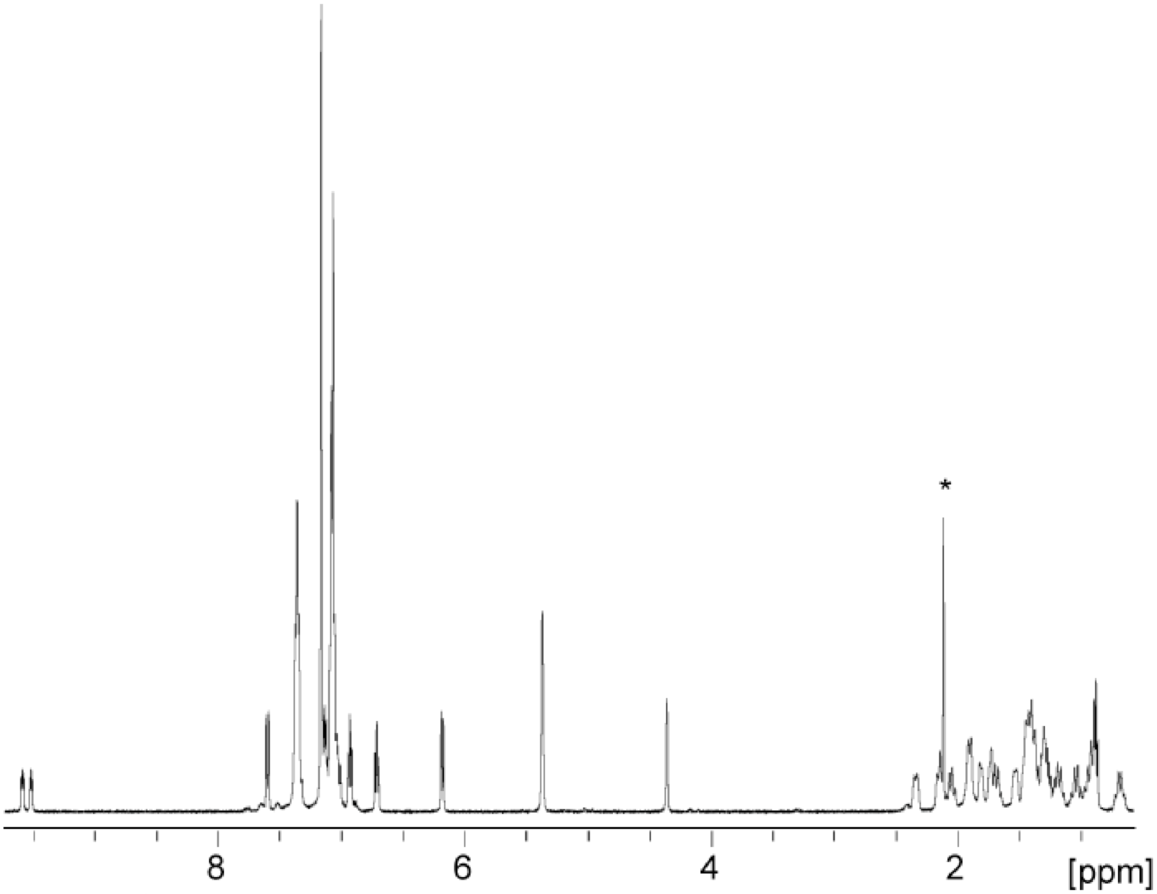

Figure D.1. ^{1}H NMR spectrum of [Ru(η^5-indenyl)(κ^2-H$\underline{C}$=CH$\underline{P}$Cy$_2$)(PPh$_3$)] (**10**), residual solvent toluene indicated by (*). (500.13 MHz, d_6-benzene)

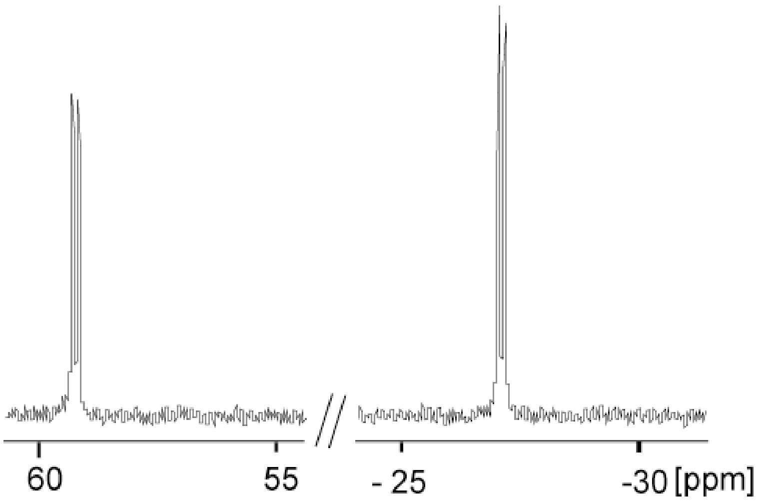

Figure D.2. ^{31}P{^{1}H} NMR spectrum of [Ru(η^5-indenyl)(κ^2-H<u>C</u>=CH<u>P</u>Cy$_2$)(PPh$_3$)] (**10**). (202.46 MHz, d_6-benzene)

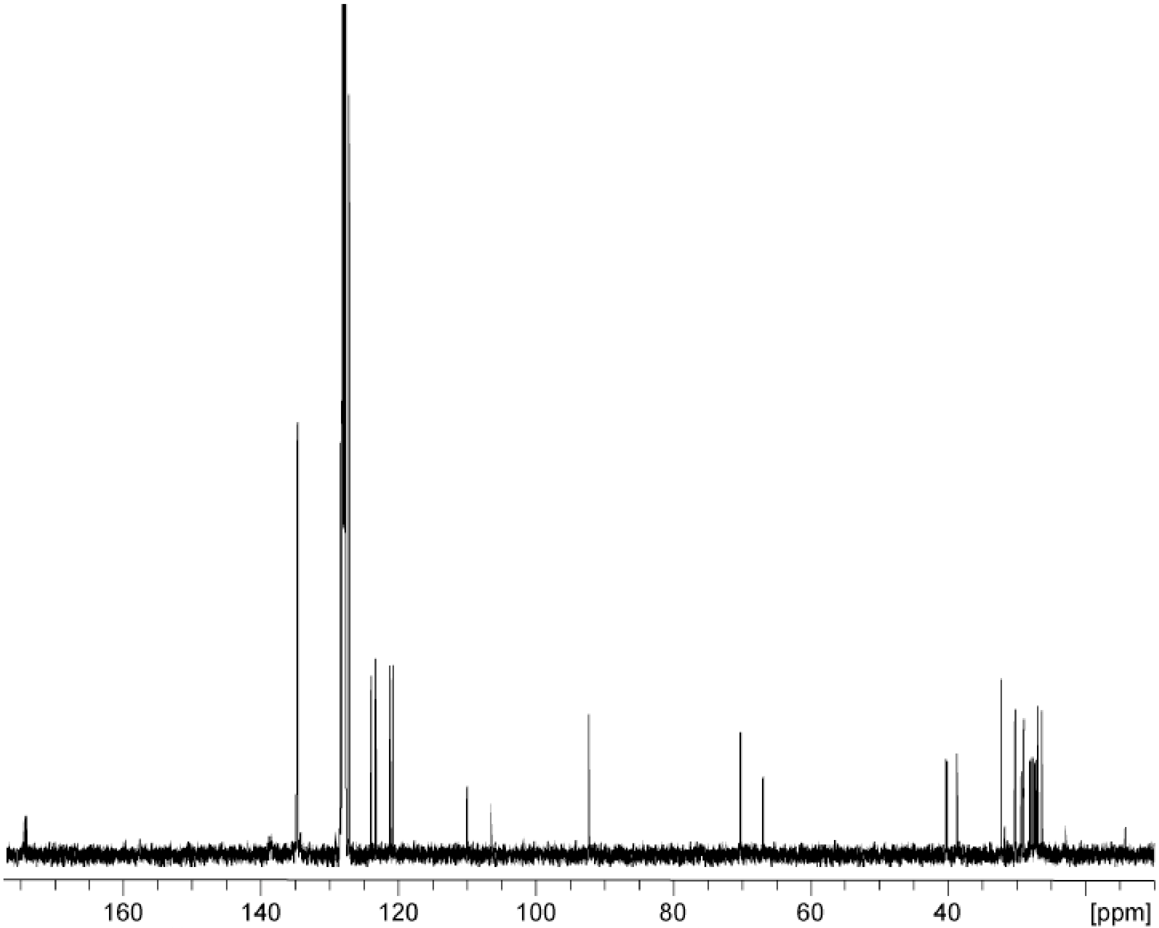

Figure D.3. ^{13}C NMR spectrum of [Ru(η^5-indenyl)(κ^2-H<u>C</u>=CH<u>P</u>Cy$_2$)(PPh$_3$)] (**10**). (125.77 MHz, d_6-benzene)

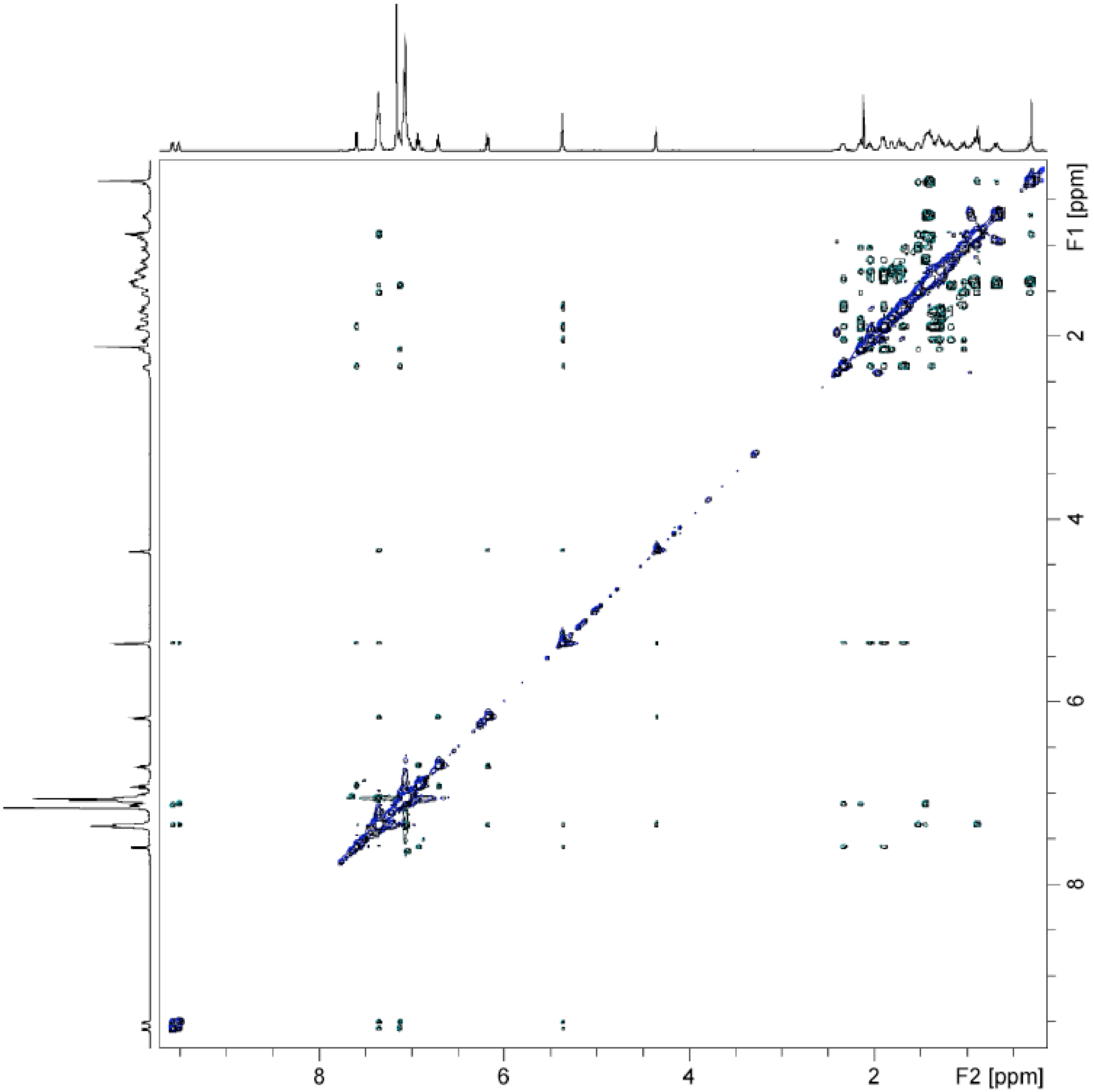

Figure D.4. ^{1}H-NOESY 2D NMR spectrum of [Ru(η^5-indenyl)(κ^2-H$\underline{C}$=CH$\underline{P}$Cy$_2$)(PPh$_3$)] (**10**) demonstrating Hα ↔ H_1, H_3, H_O and Hβ ↔ H_{Cy} correlations used to distinguish between Hα and Hβ. (500.13 MHz, d_6-benzene)

Appendix E

Second Order Rate Constant Determination Plots for the [2+2]-Cycloaddition of Terminal Alkenes to [Ru(η^5-indenyl)(PCy_2)(PPh_3)] (2)

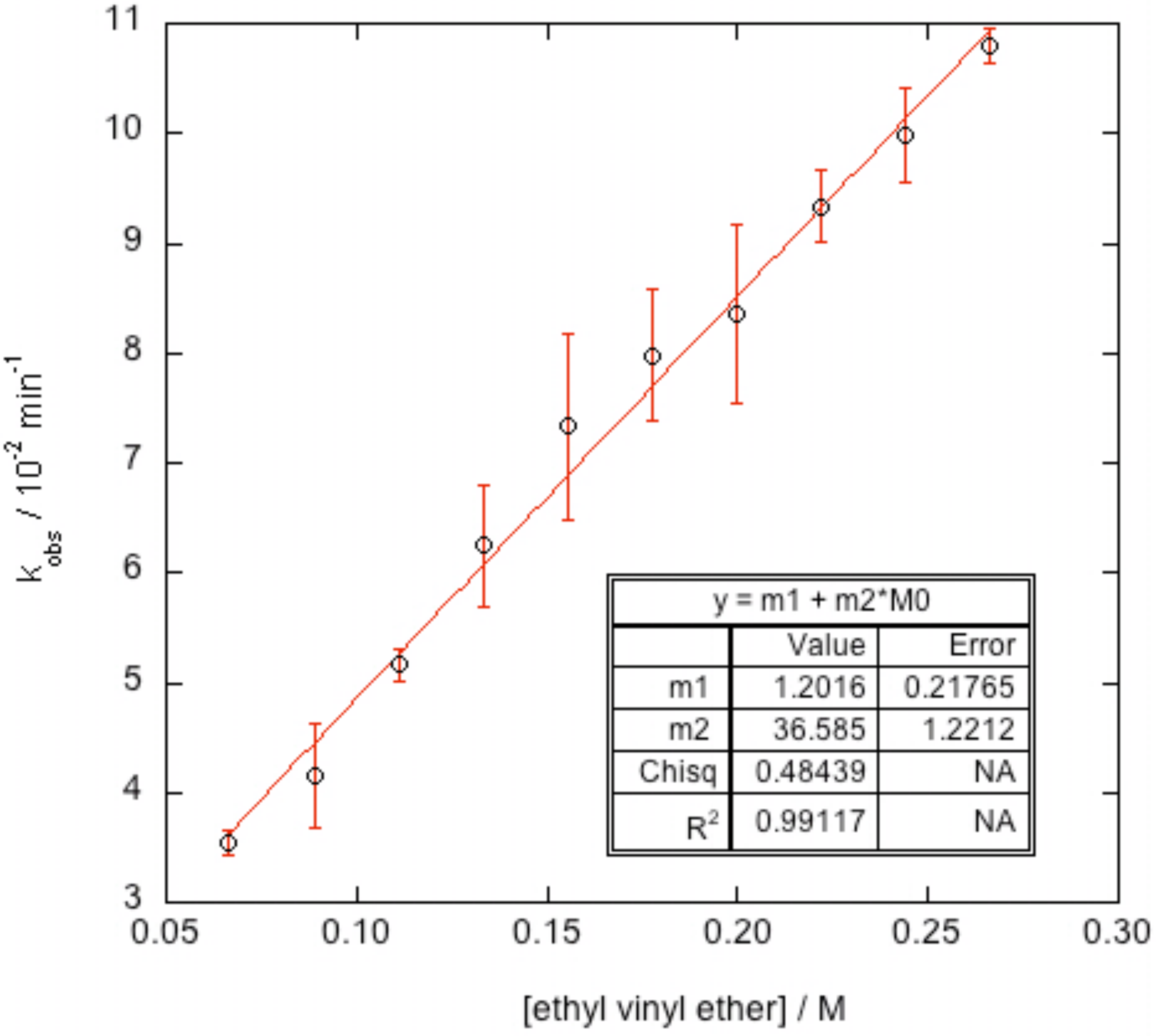

	Value	Error
m1	1.2016	0.21765
m2	36.585	1.2212
Chisq	0.48439	NA
R^2	0.99117	NA

Figure E.1. Determination of second order rate constant for the cycloaddition of ethyl vinyl ether to **2** at 25°C in toluene. Determined from UV-Vis monitoring at λ = 590 nm

*Appendix E- Second Order Rate Constant Determination Plots for the [2+2]-Cycloaddition of Terminal Alkenes to [Ru(η^5-indenyl)(PCy_2)(PPh_3)] (**2**)*

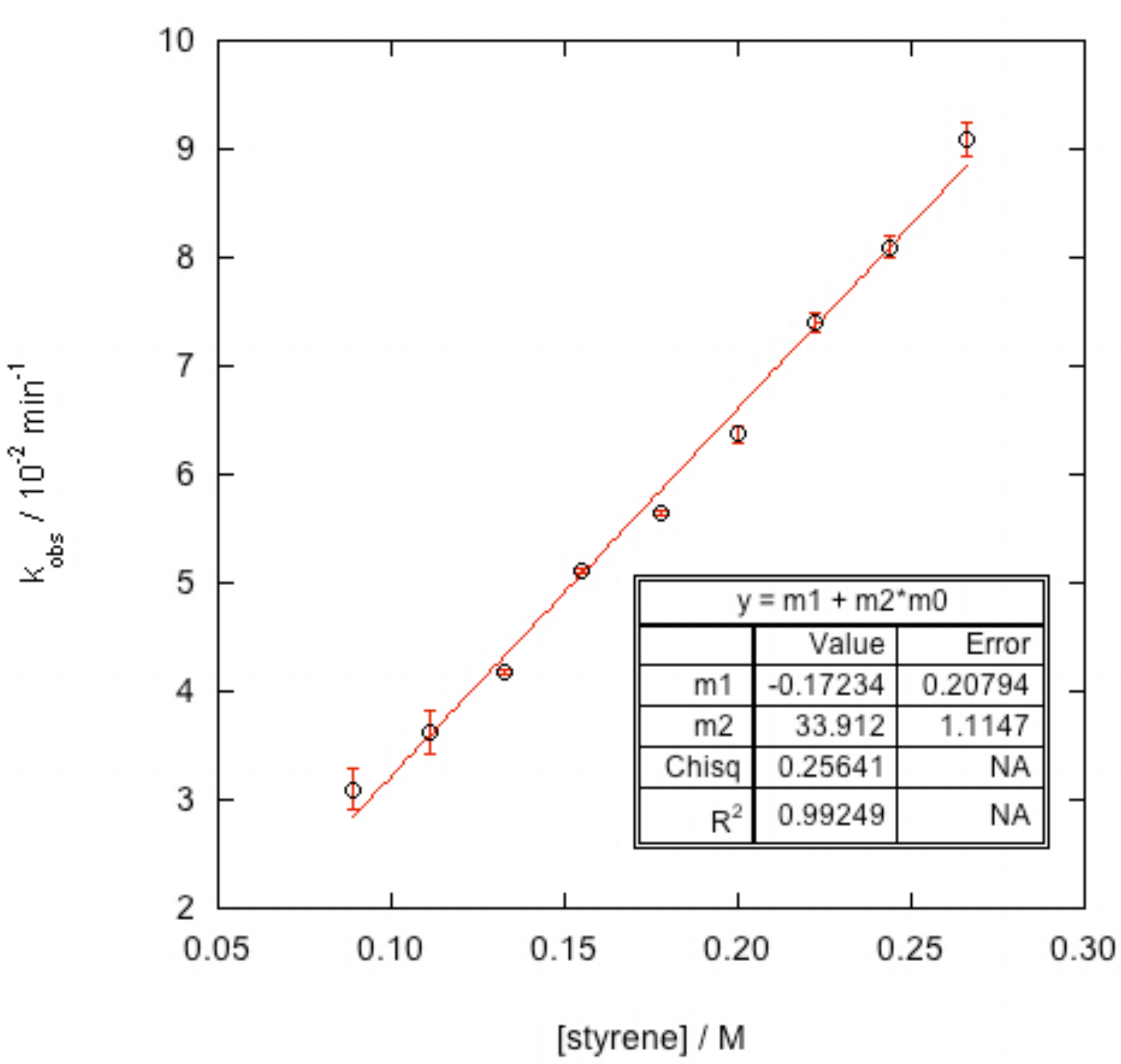

Figure E.2. Determination of second order rate constant for the cycloaddition of styrene to **2** at 25°C in toluene. Determined from UV-Vis monitoring at λ = 590 nm

Appendix F

Eyring Plots for the [2+2] Cycloaddition of Terminal Alkenes to [Ru(η^5-indenyl)(PCy$_2$)(PPh$_3$)] (2)

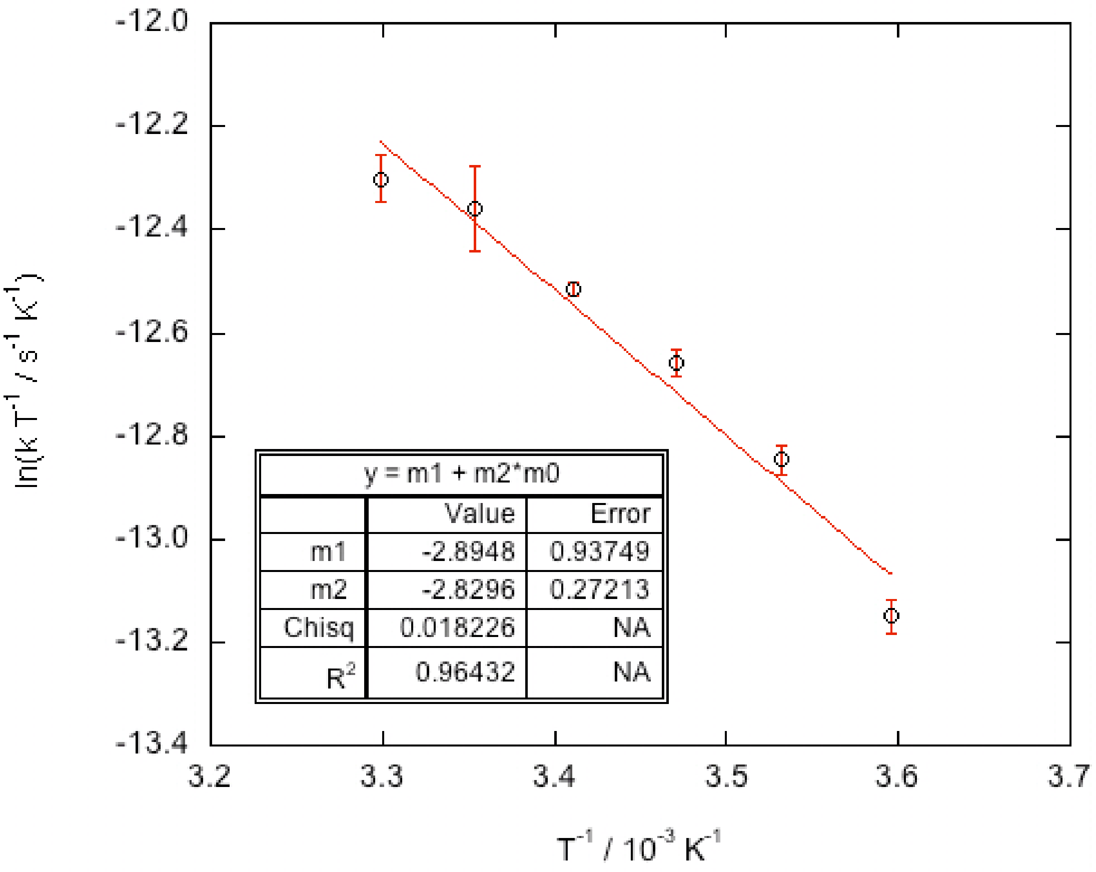

	Value	Error
m1	-2.8948	0.93749
m2	-2.8296	0.27213
Chisq	0.018226	NA
R^2	0.96432	NA

Figure F.1. Eyring relationship for the [2+2] cycloaddition of ethyl vinyl ether to **2**. Pseudo first order rate constants obtained for 500 equiv ethyl vinyl ether.

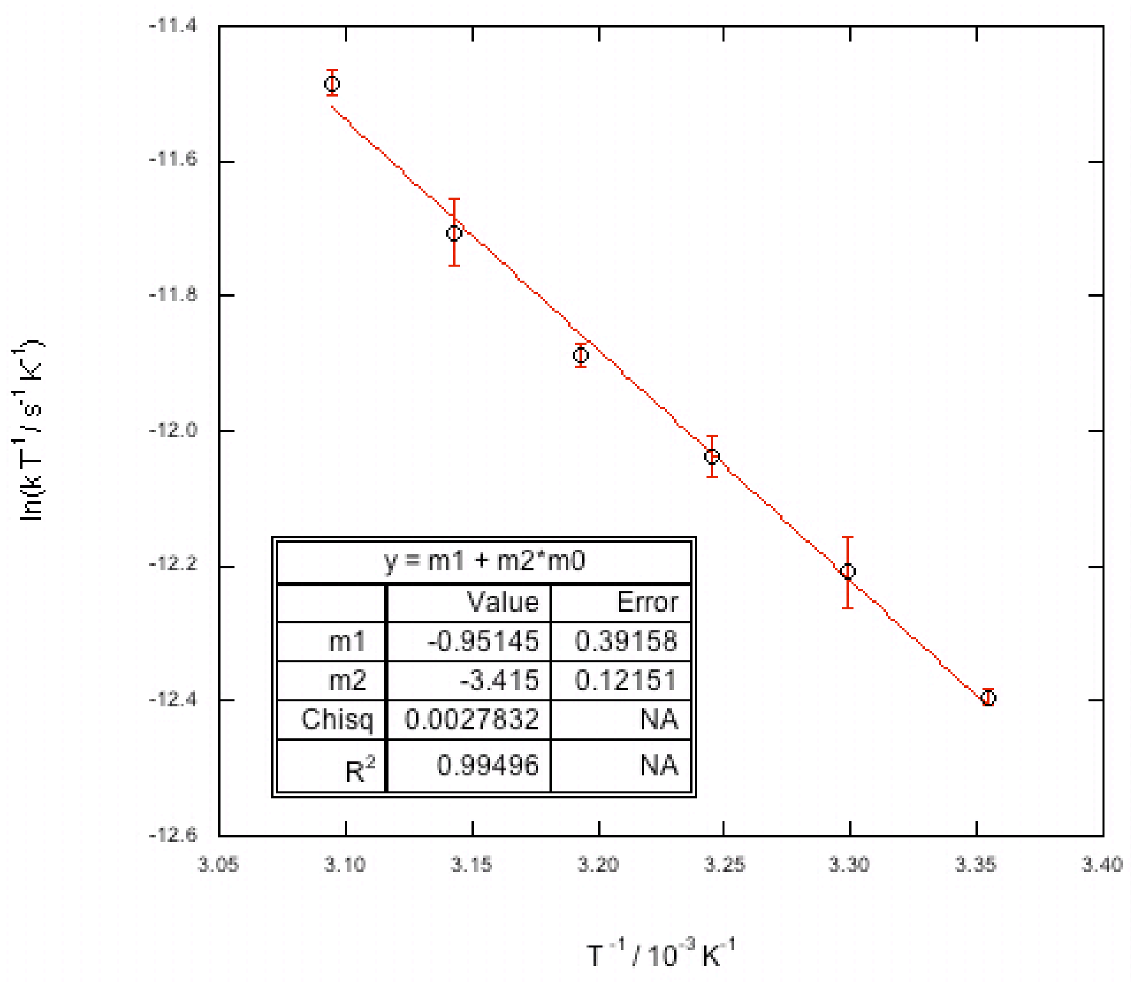

y = m1 + m2*m0

	Value	Error
m1	-0.95145	0.39158
m2	-3.415	0.12151
Chisq	0.0027832	NA
R^2	0.99496	NA

Figure F.2. Eyring relationship for the [2+2] cycloaddition of styrene to **2**. Pseudo first order rate constants obtained for 500 equiv styrene.